VTRC
Virginia Transportation
RESEARCH Council

We Bring Innovation to Transportation

Corrosion-Resistant Stainless Steel Strands for Prestressed Bridge Piles in Marine Atmospheric Environments

http://www.virginiadot.org/vtrc/main/online_reports/pdf/20-r2.pdf

BRENDY C. RINCON TROCONIS, Ph.D.
Assistant Professor, Mechanical Engineering Department
University of Texas at San Antonio

STEPHEN R. SHARP, Ph.D., P.E.
Senior Research Scientist
Virginia Transportation Research Council

H. CELIK OZYILDIRIM, Ph.D., P.E.
Principal Research Scientist
Virginia Transportation Research Council

CHARLES R. DEMAREST
Graduate Research Assistant, Center for Electrochemical Science and Engineering
University of Virginia

JACOB WRIGHT
Research Assistant, Center for Electrochemical Science and Engineering
University of Virginia

JOHN R. SCULLY, Ph.D.
Charles Henderson Chaired Professor of Materials Science and Engineering
University of Virginia

Final Report VTRC 20-R2

Standard Title Page - Report on Federally Funded Project

1. Report No.: FHWA/VTRC 20-R2	2. Government Accession No.:	3. Recipient's Catalog No.:
4. Title and Subtitle: Corrosion-Resistant Stainless Steel Strands for Prestressed Bridge Piles in Marine Atmospheric Environments		5. Report Date: March 2020
		6. Performing Organization Code:
7. Author(s): B.C. Rincon Troconis, Ph.D., Stephen R. Sharp, Ph.D., P.E., H. Celik Ozyildirim, Ph.D., P.E., Charles R. Demarest, Jacob Wright, and John R. Scully, Ph.D.		8. Performing Organization Report No.: VTRC 20-R2
9. Performing Organization and Address: Virginia Transportation Research Council 530 Edgemont Road Charlottesville, VA 22903		10. Work Unit No. (TRAIS):
		11. Contract or Grant No.: 105169
12. Sponsoring Agencies' Name and Address: Virginia Department of Transportation Federal Highway Administration 1401 E. Broad Street 400 North 8th Street, Room 750 Richmond, VA 23219 Richmond, VA 23219-4825		13. Type of Report and Period Covered: Final
		14. Sponsoring Agency Code:

15. Supplementary Notes:
This is an SPR-B report.

16. Abstract:

   This study demonstrated that Type 2205 stainless steel strand can be used as a replacement for conventional ASTM A416 steel strands where an increase in service life is required. The benefit and practicality of using Type 2205 stainless steel strand in prestressed piles were determined from two tasks performed in this study.

   First, a corrosion assessment was performed on stranded cold worked AISI 1080 carbon steel (hereinafter "SCW1080 steel") (equivalent to conventional steel strands); cold worked austenitic stainless steel Type 201 modified (hereinafter "CW201 steel"); and stranded heavily cold worked Type 2205 duplex stainless steel (hereinafter "SCW2205 steel"), a currently available duplex stainless steel strand product.   Second, the fabrication and placement of several prestressed piles reinforced with SCW2205 steel, which are now part of Virginia bridge structures, were observed.

   Laboratory corrosion testing under different exposure conditions was conducted on SCW1080 steel (as a baseline); CW201 steel (with some limited testing on non-cold worked Type 201 modified stainless steel to evaluate cold working effects); and SCW2205 steel. The laboratory studies were augmented with four-point bend and U-bend tests of specimens exposed to field conditions for 295 days.

   This study showed that in pore solution (strands embedded in quality concrete with no chloride), in concrete exposed to artificial seawater (strands embedded in concrete with the chloride concentration slowly increasing in pore solution), and in direct contact with artificial seawater (concrete damaged and strand exposed to artificial seawater), the SCW2205 steel outperformed the other steels tested. Based on the corrosion test results, it is expected that SCW2205 steel strand will provide a considerably more corrosion-resistant reinforcement option in prestressed concrete products as compared to conventional strand.

   Design, fabrication, and driving of concrete piles reinforced with SCW2205 steel strands and Type 304 stainless steel spirals were documented for three bridges; a fourth structure is currently under construction. Selected mechanical properties and estimated baseline costs were also determined for conventional ASTM A416 steel strands, SCW2205 steel strands, and carbon fiber reinforced polymer strands to facilitate lifecycle cost analysis by others.

   Based on this study, the Virginia Department of Transportation can implement the use of a corrosion-resistant strand in bridge elements in competition with carbon fiber reinforced polymer where corrosion is a concern, such as concrete elements exposed to brackish water, saltwater, or deicing salts.

17 Key Words: concrete, corrosion, pile, pitting, prestressed, SCC, stainless steel, SCC, and stress	18. Distribution Statement: No restrictions. This document is available to the public through NTIS, Springfield, VA 22161.		
19. Security Classif. (of this report): Unclassified	20. Security Classif. (of this page): Unclassified	21. No. of Pages: 83	22. Price:

Form DOT F 1700.7 (8-72)   Reproduction of completed page authorized

FINAL REPORT

CORROSION-RESISTANT STAINLESS STEEL STRANDS FOR PRESTRESSED BRIDGE PILES IN MARINE ATMOSPHERIC ENVIRONMENTS

Brendy C. Rincon Troconis, Ph.D.
Assistant Professor
Mechanical Engineering Department
University of Texas at San Antonio

Stephen R. Sharp, Ph.D., P.E.
Senior Research Scientist
Virginia Transportation Research Council

H. Celik Ozyildirim, Ph.D., P.E.
Principal Research Scientist
Virginia Transportation Research Council

Charles R. Demarest
Graduate Research Assistant
Center for Electrochemical Science and Engineering
University of Virginia

Jacob Wright
Research Assistant
Center for Electrochemical Science and Engineering
University of Virginia

John R. Scully, Ph.D.
Charles Henderson Chaired Professor of Materials Science and Engineering
University of Virginia

DISCLAIMER

The contents of this report reflect the views of the authors, who are responsible for the facts and the accuracy of the data presented herein. The contents do not necessarily reflect the official views or policies of the Virginia Department of Transportation, the Commonwealth Transportation Board, or the Federal Highway Administration. This report does not constitute a standard, specification, or regulation. Any inclusion of manufacturer names, trade names, or trademarks is for identification purposes only and is not to be considered an endorsement.

ABSTRACT

This study demonstrated that Type 2205 stainless steel strand can be used as a replacement for conventional ASTM A416 steel strands where an increase in service life is required. The benefit and practicality of using Type 2205 stainless steel strand in prestressed piles were determined from two tasks performed in this study.

First, a corrosion assessment was performed on stranded cold worked AISI 1080 carbon steel (hereinafter "SCW1080 steel") (equivalent to conventional steel strands); cold worked austenitic stainless steel Type 201 modified (hereinafter "CW201 steel"); and stranded heavily cold worked Type 2205 duplex stainless steel (hereinafter "SCW2205 steel"), a currently available duplex stainless steel strand product. Second, the fabrication and placement of several prestressed piles reinforced with SCW2205 steel, which are now part of Virginia bridge structures, were observed.

Laboratory corrosion testing under different exposure conditions was conducted on SCW1080 steel (as a baseline); CW201 steel (with some limited testing on non-cold worked Type 201 modified stainless steel to evaluate cold working effects); and SCW2205 steel. The laboratory studies were augmented with four-point bend and U-bend tests of specimens exposed to field conditions for 295 days.

This study showed that in pore solution (strands embedded in quality concrete with no chloride), in concrete exposed to artificial seawater (strands embedded in concrete with the chloride concentration slowly increasing in pore solution), and in direct contact with artificial seawater (concrete damaged and strand exposed to artificial seawater), the SCW2205 steel outperformed the other steels tested. Based on the corrosion test results, it is expected that SCW2205 steel strand will provide a considerably more corrosion-resistant reinforcement option in prestressed concrete products as compared to conventional strand.

Design, fabrication, and driving of concrete piles reinforced with SCW2205 steel strands and Type 304 stainless steel spirals were documented for three bridges; a fourth structure is currently under construction. Selected mechanical properties and estimated baseline costs were also determined for conventional ASTM A416 steel strands, SCW2205 steel strands, and carbon fiber reinforced polymer strands to facilitate lifecycle cost analysis by others.

Based on this study, the Virginia Department of Transportation can implement the use of a corrosion-resistant strand in bridge elements in competition with carbon fiber reinforced polymer where corrosion is a concern, such as concrete elements exposed to brackish water, saltwater, or deicing salts.

TABLE OF CONTENTS

FINAL REPORT

CORROSION-RESISTANT STAINLESS STEEL STRANDS FOR PRESTRESSED BRIDGE PILES IN MARINE ATMOSPHERIC ENVIRONMENTS

Brendy C. Rincon Troconis, Ph.D.
Assistant Professor
Mechanical Engineering Department
University of Texas at San Antonio

Stephen R. Sharp, Ph.D., P.E.
Senior Research Scientist
Virginia Transportation Research Council

H. Celik Ozyildirim, Ph.D., P.E.
Principal Research Scientist
Virginia Transportation Research Council

Charles R. Demarest
Graduate Research Assistant
Center for Electrochemical Science and Engineering
University of Virginia

Jacob Wright
Research Assistant
Center for Electrochemical Science and Engineering
University of Virginia

John R. Scully, Ph.D.
Charles Henderson Chaired Professor of Materials Science and Engineering
University of Virginia

INTRODUCTION

The Virginia Department of Transportation (VDOT) has transitioned from the use of epoxy-coated reinforcing bars in bridge deck construction to corrosion-resistant reinforcement (CRR) because of the escalating maintenance costs associated with corrosion in bridge decks. This change demonstrated that one of the primary factors for selecting reinforcing materials should be life cycle costs analysis (Sharp et al., 2019). Minor changes in initial material costs are anticipated to reduce future corrosion significantly, an important cost factor associated with maintenance operations (Sharp et al., 2019).

VDOT's research to date has addressed conventional reinforcement in bridge structures, including conventional CRR. However, the use of corrosion-resistant prestressing strands in bridge elements has not been addressed. Relatively speaking, prestressing strands are used in

small quantities in bridge structures but are subjected to greater stress than conventional deck reinforcement. This is because strands are used to compress concrete and prevent cracking whereas conventional reinforcement is used to transmit tension and control, but not prevent, cracking.

Corrosion is more critical in strands because they are under higher stress conditions than conventional reinforcing steel bars. Wires can fracture even though section loss attributable to corrosion is small because of the combination of the high stress in each wire and the change in stress intensity created by sharp features, such as pits, in the area of corrosion. As corrosion progresses and individual wire(s) fractures, the remaining wires in the strand can become overloaded and result in an unexpected rapid failure of the structural steel strand.

Corrosion-related damage to prestressed and post-tensioned strands has been observed in the field. Examples of corrosion in conventional reinforcement, pre-tensioning and post-tensioned high-strength steel strands, leading to concrete damage and loss of reinforcement continuity, are shown in Figure 1.
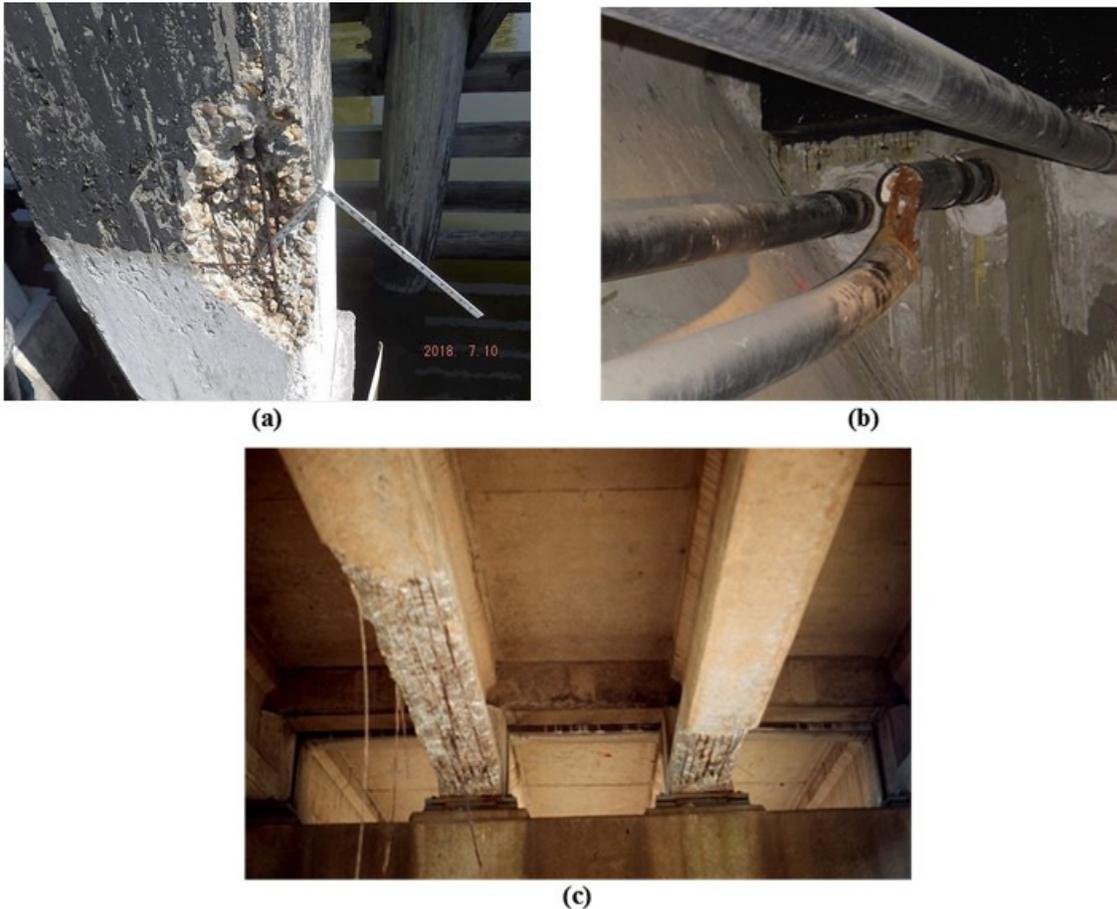

Figure 1. Corrosive Attack in Virginia: (a) reinforcing steel in concrete bridge pile leading to exposure of prestressing strand; (b) steel strands in external tendon resulting in tendon failure in post-tensioned box girder portion of bridge; (c) corroded prestressing strands along bottom of prestressed concrete beam with several failed strands

Since corrosion shortens the service life of structures and VDOT seeks to extend service lives to 75- to 100-year designs, corrosion-resistant materials are becoming more prevalent in bridges. Although this change can increase initial costs, repairs to elements with strands are costly and difficult since these elements are generally load-carrying members that support the deck. Further, since corrosion in prestressed elements reduces or eliminates precompression, a true repair may involve post-tensioning, which is very expensive. In addition to structural concerns, in some cases traffic must be interrupted, causing inconvenience and safety concerns related to work zones. Therefore, it is evident that repair cycles can be reduced by using materials that are more durable, which can also provide long-term cost savings.

Further, although it has not received the widespread publicity of CRR, research on alternative (corrosion-resistant) high-strength strand materials has been progressing. Earlier work with carbon fiber reinforced polymer (CFRP) strands for reinforcing concrete piles has shown promising results when they are used as a corrosion-free high-strength prestressing reinforcement (Sharp et al., 2019). Following the success of CFRP strands, another strand material, heavily cold worked and stranded Type 2205 duplex stainless steel (hereinafter "SCW2205 steel"), was proposed as high-strength reinforcement for prestressed concrete to increase the durability of structures when exposed to marine environments (Moser et al., 2012).

Since this study focused on two different areas of engineering, corrosion testing and precast concrete element fabrication, it is important to clarify at this point in the report the use of the acronym "SCC," which traditionally has two very different meanings. With concrete-related applications, the acronym is commonly used to mean "self-consolidating concrete," which is associated with a concrete that exhibits a very useful material behavior, i.e., high workability. However, in this report, which predominantly focuses on corrosion, "SCC" is used as an acronym for "stress corrosion cracking," which is an unfavorable material response when the material is subjected to certain conditions.

It has been suggested that SCW2205 steel can resist localized corrosion in the presence of chlorides (Sandvik, 2013) and room temperature SCC, specifically in a solution in a heat-treated and slightly cold worked condition (Hinds and Turnbull, 2008). However, this susceptibility changes, for example, when the material is heavily cold worked, coupled to carbon steel, and exposed to H_2S (Griffiths and Turnbull, 1997), resulting in hydrogen controlled SCC. SCC depends on the exact strength level and hydrogen uptake scenario, which determines the dissolved hydrogen content.

The reinforcement material used in prestressed concrete applications can be exposed to an environment characterized by several sets of conditions, which can range from concrete pore solution to atmospheric exposure with salt deposition because of concrete cover loss. Cold worked SCW2205 steel has been found to exhibit a high pitting potential (indicating also a high resistance to pitting of the metal) in alkaline-diluted chlorine solutions (Moser et al., 2012). However, the atmospheric exposure can create cyclic wet/dry conditions, resulting in the deposition of saturated or highly concentrated $MgCl_2$, NaCl, or $CaCl_2$ solutions on metallic surfaces (Baker, 1987; Hinds and Turnbull, 2008; Masuda, 2007; Sanchez et al., 2009; Shoji and Ohnaka, 1989). Under these situations, 300 series austenitic and duplex stainless steel have undergone or been susceptible to localized corrosion in the form of pitting (Baker, 1987; Hinds

and Turnbull, 2008; Masuda, 2007; Sanchez et al., 2009; Shoji and Ohnaka, 1989); and in some cases, SCC has occurred (Prosek et al., 2009; Shiwa et al., 2012a, 2012b, 2012c; Turnbull et al., 2008). Different SCC susceptibility maps, indicating temperature-Cl$^-$ levels that produce SCC, are currently available for non-cold worked 300 series austenitic stainless steel and non-cold worked duplex stainless steel (Prosek et al., 2009; Shoji and Ohnaka, 1989). These maps depend on different parameters, such as relative humidity (RH), molecular identity of chloride species, chloride concentration, exposure time, and pitting resistance equivalent number (PREN). SCC was also not found in the non-cold worked duplex material under the atmospheric exposure conditions previously tested (Prosek et al., 2009). However, heavily cold worked materials have not been tested. Therefore, an unresolved question is whether highly alloyed and heavily cold worked duplex stainless steels, specifically Type 2205, pit under wetting and drying conditions.

PURPOSE AND SCOPE

The purpose of this study was to evaluate the corrosion resistance of SCW2205 steel and determine if corrosion-resistant prestressing strand in prestressed concrete elements can be effectively employed in Virginia for bridge structures at high risk for corrosion.

The scope of this study included laboratory and field segments. For the laboratory segment, the relative corrosion susceptibility was determined for stranded cold worked AISI 1080 carbon steel (hereinafter "SCW1080 steel"); non-stranded cold worked austenitic type 201 stainless steel (hereinafter "CW201 steel"); and SCW2205 steel under different exposure conditions. The field segment included observing and gathering data from the strand producer, precast concrete product producers, and several construction sites. All of the stainless steel–reinforced concrete piles that were included in the field segment of this study are functioning elements in actual highway bridges.

METHODS

Corrosion Testing

The corrosion testing determined the intrinsic susceptibility of high-strength steel prestressing materials to SCC in the pretensioned marine exposure environment. This was accomplished by first characterizing the sample materials that were received from a precaster. These materials were then subjected to materials characterization evaluations, electrochemical experiments, pitting resistance experiments, four-point bend tests (FPBTs), and outdoor exposure testing of U-bend environmental exposure samples and then non-destructive testing on these samples.

Materials

Three different types of steels were tested in this study. The first two were cold worked and stranded (seven-wire strand) materials. One was SCW1080 steel, 7/16-in rod diameter for ½-in strand, and the other was SCW2205 steel, in a hot finished pickled condition that was then

cold worked and stranded (0.163-in diameter, 82% reduction in area [% RA]). A third material, SS201 high-manganese, nitrogen (N)-strengthened austenitic stainless steel that was tested in a cold worked condition (CW201 steel) and in some instances in a non-cold worked (non-CW201 steel) condition. This material was provided with a diameter of 0.172 in for CW201 steel (76% RA) and a diameter of 0.280 in for non-CW201 steel (0% RA).

The SCW1080 carbon steel was used as a control material, which would provide a relative measure of the improved corrosion resistance of the stainless alloys as compared to the SCW1080 steel. The CW201 steel was also of interest since it is an austenitic stainless steel that was expected to have a corrosion resistance between those of the SCW1080 and SCW2205 steels. The SCW2205 streel was studied since it is the most promising material for use as prestressed strand for reinforced concrete.

Materials Characterization

To characterize the microstructure of the test materials, samples were prepared by grinding with silicon carbide paper up to 1200 grit and then polishing using a diamond paste with a particle size of 5 and then 3 µm. A final polish was done using a silica suspension, for a final finish of 0.02 µm. The microstructure was then evaluated using a scanning electron microscope (SEM) with energy dispersive spectroscopy (EDS) capability at an accelerating voltage of 15 kV. The SCW2205 steel was further analyzed using transmission electron microscopy to determine if martensite was present in the microstructure. Chemical composition analysis was performed using inductively coupled plasma optical emission spectroscopy (ICP-OES) in accordance with ASTM E2594 (ASTM, 2014a).

The hardness of the materials studied was measured using Vickers hardness testing by applying a load of 1 kg for 15 seconds. At least five measurements were taken for each material, with the testing being performed in accordance with ASTM E384 (ASTM, 2011d). To evaluate the microstructure and determine the crystal structure of the material, X-ray diffraction (XRD) was performed using a diffractometer with Θ-Θ geometry, 2Θ range of $10°$ to $140°$ and a Cu-Kα X-ray wavelength of 1.5406 Å.

Laboratory Test Solutions

During laboratory testing, the test solutions were prepared using deionized water with a resistivity of 18.2 MΩcm and reagent grade chemicals. The test solutions used in this study are listed in Table 1. Depending on the condition needed for the electrochemical, pitting resistance, and FPBT experiments, the appropriate solutions in Table 1 were prepared. These solutions provided an accelerated mechanism for creating the different environments to which the strands might be subjected so that the corrosion susceptibility of each material could be determined. It is important to highlight for clarity, that simplified ocean water (SOW) and artificial seawater test solutions are different solutions

Table 1. Description of Electrolytes Used for Laboratory Testing of Prestressing Strand Materials

Name	Composition	Simulated Condition
0.9 M NaCl	0.9 M NaCl	Marine exposure
5.3 M NaCl	5.3 M NaCl	Marine exposure
0.6 M $MgCl_2$	0.6 M $MgCl_2$	Marine exposure
2.37 M $MgCl_2$	2.37 M $MgCl_2$	Marine exposure
5.4 M $MgCl_2$	5.4 M $MgCl_2$	Marine exposure
Simplified Ocean Water, or SOW	55 mM $MgCl_2$ + 420 mM NaCl	Marine exposure
Artificial Seawater	ASTM D1141 (ASTM, 2013) without heavy metals	Marine exposure
Inland Atmospheric, or Inland	5.1 mg $(NH_4)_2SO_4$ + 6.4 mg NaCl in 1 L water	Inland atmospheric exposure
$FeCl_3$ + NaCl	0.411 M $FeCl_3$ + 4.07 M NaCl	Oxidizing exposure with NaCl present
$FeCl_3$ + $MgCl_2$	0.411 M $FeCl_3$ + 4.78 M $MgCl_2$	Oxidizing exposure with $MgCl_2$ present
Pore Solution + NaCl or Pore + NaCl	1.5 g $Ca(OH)_2$ + 8.33 g NaOH + 23.3 g KOH + 180 g NaCl in 1 L water	Exposure inside concrete with NaCl present
Pore Solution + $MgCl_2$ or Pore + $MgCl_2$	1.5 g $Ca(OH)_2$ + 8.33 g NaOH + 23.3 g KOH + 28 g $MgCl_2$ in 1 L water	Exposure inside concrete with $MgCl_2$ present

Electrochemical Experiments

The electrochemical experiments were performed using a standard three-electrode setup and a horizontal cell. The counter and reference electrodes used were a platinum mesh and a saturated calomel electrode (SCE), respectively. Research grade potentiostats were used to control these experiments. The rods were ground along their periphery using silicon carbide paper up to 1200 grit to enhance the bonding in the epoxy/metal interface and to avoid crevice corrosion. The rod was then cut, producing a surface perpendicular to the drawing direction. This surface was ground up to 1200 grit, rinsed with deionized water, ultrasonically cleaned in ethanol, and dried with compressed air. Cyclic polarization was performed at a rate of 0.167 mV/s in accordance with ASTM G5 (ASTM, 2014b), with the scan being reversed when the current density achieved 1 mA/cm^2.

It is important to point out that the concentrations were selected for some testing to represent the cases of both low and high RH and were based on OLI Systems, Inc. (OLI), modelling software. The OLI modelling software was used to assess the effect of RH on salt concentration for salts such as $MgCl_2$ and NaCl. The solutions used during this testing included the following:

- 0.9 M NaCl, 5.3 M NaCl, 0.6 M $MgCl_2$, 2.7 M $MgCl_2$, or 5.4 M $MgCl_2$ solutions to simulate diluted and concentrated marine exposure conditions

- SOW to simulate marine exposure when both NaCl and $MgCl_2$ are present in the solution

- saltwater or artificial seawater to simulate marine exposure, but the solution did not include the heavy metals or organic matter that would be found in actual seawater

- inland atmospheric solution (hereinafter "inland") to simulate inland atmospheric exposure conditions

- $FeCl_3$ + NaCl and $FeCl_3$ + $MgCl_2$ solutions to simulate oxidizing conditions with salt present

- Pore + NaCl and Pore + $MgCl_2$ solutions to simulate strand embedded in concrete with salt present.

Pitting Resistance Experiments

Pitting resistance experiments were performed on non-CW201 steel, CW201 steel, and SCW2205 steel samples by placing 3 droplets (each 0.1 µL) with the electrolyte placement on a surface parallel to the drawing direction of the wires. Prior to the droplets being placed, the surfaces were prepared in accordance with the same protocol described previously for the electrochemical experiments.

Characterization was performed in two different sets of samples/condition arrangements. The first set of experiments was part of a preliminary stage of this test, whereas the second set included some of the samples/condition combinations in the first set plus other conditions that simulate field exposure and other extreme conditions.

For the first set of experiments, the concentration of the droplets depended on the salt used. For these experiments, OLI software was used to model the dependence of salt concentration on RH to avoid droplet size change during the experiment when simulating the different stages of wet and dry conditions during atmospheric exposure. This approach allowed for the testing of dilute and concentrated conditions. The RH was controlled in a sealed environment by using concentrated solutions in accordance with ASTM E104 (ASTM, 2012), with the samples being kept in the simulated atmospheric environment for 32 days. The RH/droplet chemistry combination used for the first set of data were as follows:

- 97 % RH controlled using deionized water and droplet chemistries of 0.9 M NaCl, 0.6 M $MgCl_2$, or SOW

- 80 % RH using saturated potassium chloride (KCl) to control RH: 5.3 M NaCl, 2.37 M $MgCl_2$, and SOW

- 38 % RH using saturated sodium iodide (NaI) to control RH: 5.4 M $MgCl_2$, and SOW.

The second set of experiments focused on SCW2205 steel samples, which were examined in detail to document pitting damage after exposure. These samples were tested using droplet electrolytes that were made in bulk and then placed at various temperatures on the test surfaces. The test temperatures used for the following electrolytes were 25, 35, 55, 75, and 95 °C.
- 5.3 M NaCl
- 5.4 M $MgCl_2$

- artificial seawater
- inland
- $FeCl_3$ + NaCl
- $FeCl_3$ + $MgCl_2$
- Pore + NaCl
- Pore + $MgCl_2$.

The environments of interest were those ranging from pore solution, SOW, and very oxidizing $MgCl_2$, which might form from salt spray with an atmospheric oxidizer. They ranged from inland low chloride environments to environments containing chlorides of various types such as NaCl and $MgCl_2$ and environments such as $FeCl_3$ and $MgCl_2$, which contain strong oxidizers and have a chloride concentration of 1.2 M.

For both sets of experiments, after testing, the sample surfaces were rinsed with deionized water thoroughly and the droplet region was marked using microhardness indents followed by cleaning of the corrosion products in accordance with ASTM G1 (ASTM, 2011a). The pitting resistance was evaluated through the observation of the corrosion morphology after exposure using an advanced optical profiler that incorporated a three-dimensional surface structure analyzer providing graphic images and high-resolution numerical analysis to characterize the surface structure of samples accurately.

FPBT

The FPBT was performed on both laboratory and field samples. To create test samples, SCW1080, CW201, and SCW2205 steel samples were machined to obtain a flat reproducible surface to deposit droplets and equal dimensions for all the specimens (75 mm x 2 mm x 3.3 mm).

The FPBT frame was made of lacquer-coated carbon steel with ceramic rods in the pressure points to avoid galvanic coupling with the specimen. It was designed in accordance with ASTM G39 (ASTM, 2011b) as shown in Figure 2 a-c to suit the specimen dimensions. The frame makes contact at four points, which is shown in Figure 2, with the distance between the two outermost points (H) being 60 mm and the distance between an outer and an inner contact point (A) being 15 mm, in accordance with the rule A = H/4. The test fixture is symmetric along an axis oriented along the center of the bolt's longest dimension, so the distance between the other outer and inner contact points on the test frame is also 15 mm. When an approximate Young's modulus (E) of 200 GPa and a specimen thickness (t) of 2 mm is taken into consideration, then the required maximum deflection of the specimen (y) to achieve a stress of approximately 965 MPa is 2 mm when the following equation in ASTM G39 is used:

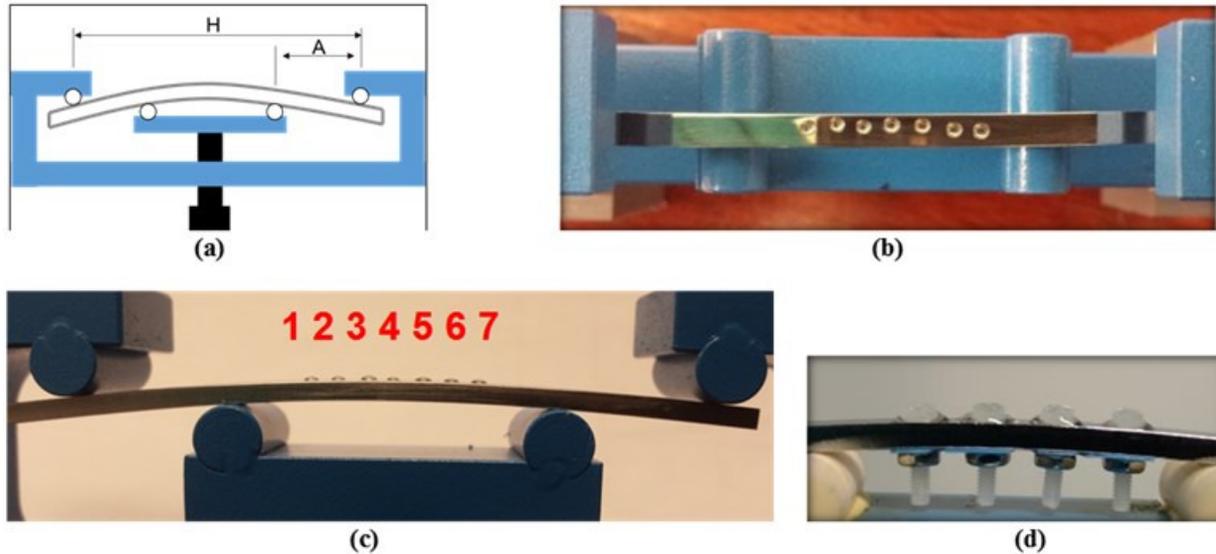$$\sigma = \frac{12Ety}{(3H^2 - 4A^2)}$$

Figure 2. Four-Point Bend Test Design Based on ASTM G39: (a) schematic showing distance between outer pressure points (H) and the distance between the outer and the inner pressure points (A); (b) top view; (c) side view after droplet (0.1 μL per droplet) deposition; (d) side view of specimen under creviced condition

For the laboratory study, it was decided that CW201 and SCW2205 steel samples would be evaluated. After the specimens were stressed, 7 droplets of 5.4 M MgCl2 were deposited on top of the surface and the specimen was exposed to a control RH of 38% RH using a saturated NaI solution. The RH and temperature were measured during exposure using a RH/temperature data logger. To increase the corrosiveness of the exposure, crevice formers were introduced in the specimen configuration for the FPBTs (Figure 2d), with four holes of 1.50 mm in diameter spaced at 8.1 mm from hole center to hole center for this purpose. The crevice formers consisted of a No. 0-80 Teflon screw and an 18-8 nut; a plastic shim was used as an insulator between the specimen and the nut to avoid galvanic coupling. In order to analyze the results of this test, the samples had to be sectioned normal to the z-axis at several locations to look for evidence of SCC, as shown in Figure 3.

The FPBT frames were also used for environmental exposure in the field. For the field study, it was decided that SCW1080, CW201, and SCW2205 steel samples would be evaluated. The samples were exposed for 295 days in Covington, Hampton Roads, and Harrisonburg, which represents different environments of interest to VDOT.
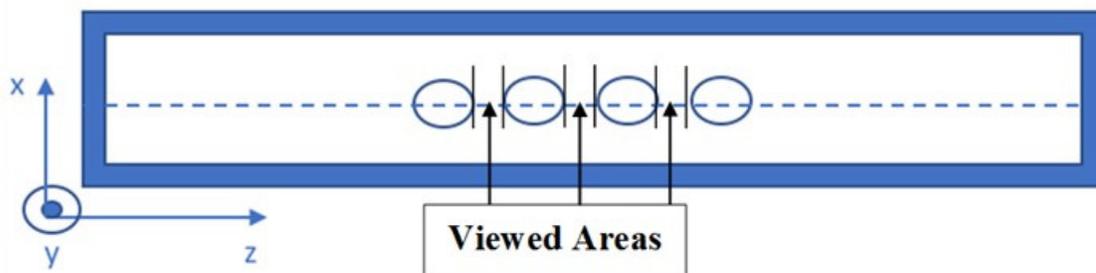

Figure 3. Top View of Bar. Dotted line shows cut axis.

Outdoor Exposure of U-bend Environmental Exposure and Non-destructive Testing

Specimens were bent in a U shape and were exposed for 295 days at the three outdoor exposure sites in Covington, Hampton Roads, and Harrisonburg. Atmospheric contaminant analysis was performed to characterize each site. The techniques used for characterizing the sites and the results of the characterization work are provided in Appendix A.

After the specimens were exposed for 295 days, a dye penetration test was performed on the surface of the specimens. Dye penetration permits a rapid, qualitative assessment of surface cracks on specimens. The sample preparation for this test consisted of cleaning by wiping with acetone followed by spraying with a dye penetrant. Then, at least 20 minutes were allowed for the chemical to penetrate into any cracks formed. The dyed surface was wiped down gently with acetone to ensure that wicking of the penetrated area did not occur, and a dye-sensitive developer was applied on the cleaned surface. Finally, following a wait time of about 10 minutes, the surface was inspected using an optical microscope.

Field Demonstration

The field demonstration focused on documenting the use of stainless steel conventional and high-strength reinforcement in precast concrete piles. This included recording any differences in production or installation processes between the corrosion-resistant and conventional prestressed piles. Lessons learned during the fabrication and construction of three bridges in Virginia were documented. The first bridge to use stainless steel reinforcement in prestressed concrete piles in Virginia was the Nimmo Parkway Bridge over West Neck Creek in Virginia Beach. This construction project was completed in September 2014; it also included CFRP prestressed piles (Sharp et al., 2019). For the stainless steel reinforced piles, the strands used were SCW2205 steel, and the spiral was made from Type 304 stainless steel. The next two bridges were the Route 621 Bridge over Passenger Swamp, and the Route 680 Bridge over Stallings Creek, both in Isle of Wight County. These two bridges were completed by December 30, 2016. A fourth structure that will use SCW2205 steel piles, the High Rise Bridge in Chesapeake, is currently under construction. Available information about the fabrication and driving of these piles is included in this report.

Materials of Construction

The materials used to manufacture the piles and any other incidental observations were documented. With a potential galvanic cell, it was important to minimize contact between SCW2205 and carbon steel. Documentation included a detailed drawing of the connection, minimizing contact, and feedback from the pile manufacturer and contractor about the pile detail and ease of implementation. For the initial set of piles for the Nimmo Parkway Bridge, the fabricated piles were inspected.

Field Evaluation of SCW2205 Steel Pile

Piles were inspected for damage after the driving was completed. For the initial set of test piles at the Nimmo Parkway Bridge, the condition of the piles after driving was documented.

Comparing Properties and Initial Costs of Conventional and Corrosion-Resistant Strands

Comparing the four materials tested in this study, SCW1080, SCW2205, SS2205, and CW201 steel, was a challenge since the material properties are different and thus the designs will be different. New or unfamiliar technologies holding promise for reduced maintenance costs over the service live often have higher initial material and installation costs than are expected in the longer run. SCW2205 and CW201 steels are expected to follow this trend; therefore, the material properties and estimated initial unit cost of each material are reported to allow lifecycle cost analysis (LCCA) for projects using these materials.

RESULTS AND DISCUSSION

Corrosion Testing

Materials

The materials evaluated included conventional steel strand; SCW1080 steel, CW201 steel; and stranded duplex stainless steel, SCW2205. The duplex stainless steel is a widely used stainless steel product that has roughly an even mixture of ferrite and austenite. The austenitic stainless steel used is a lower cost alternative to SS304 steel that also exhibits a lower corrosion resistance than SS304 steel (North American Stainless, 2019). This alloy can also be cold worked through drawing to achieve mechanical properties that withstand the service stress necessary to achieve optimal conditions for prestressed concrete structures. There is no information in the literature regarding the corrosion resistance of this alloy under severe exposure, so the Type 1080 carbon steel was used as a control material for comparison purposes.

Characterization of the Different Materials

A characterization was performed of the different materials. The different parameters determined included bulk chemical composition, hardness, microstructure composition, and crystal structure.

The chemical bulk composition (Table 2) highlighted the vast difference between the materials in terms of alloying elements that increase the corrosion resistance of alloys directly or indirectly: chromium (Cr), nickel (Ni), molybdenum (Mo), and nitrogen. SCW1080 steel contains negligible amounts of these elements (0.04% Ni, 0% N, 0.15% Cr, and 0.01% Mo) whereas CW201 steel contains 4.5% Ni, 0.25% N, and 17% Cr; SCW2205 steel presents the highest composition of these elements (5.28% Ni, 0.16% N, 21.74% Cr, and 3.16% Mo).

Table 2. Bulk Chemical Composition of the Different Steel Materials Evaluated[a]

Sample	Elements (wt. %)[b]										PREN	CPT
	Ni	Cu	N	Mn	Si	C	Cr	Mo	S	P		
SCW1080	0.04	0.13	---	0.75	0.26	0.858	0.15	0.01	0.005	0.008	0.18	-40.92
CW201	3.5-5.5	---	0.25	5.5-7.5	1.00	0.15	16-18	---	0.030	0.060	20-22	9.48
SCW2205	5.28	0.16	0.162	0.74	0.41	0.025	21.74	3.16	0.002	0.008	34.76	42.53

PREN = pitting resistance equivalent number, PREN = Cr + 3.3 Mo + 16 N (Lorenz and Medawar, 1969); CPT = critical pitting temperature, (°C), CPT = 2.5 Cr + 7.6 Mo + 31.9 N-41 (ASTM, 2011c); --- = not applicable.
[a]The analysis was performed using inductively coupled plasma optical emission spectrometry in accordance with ASTM E2594 (ASTM, 2014a).
[b]Iron provides the relative balance in weight percent.

Based on the bulk chemical composition, the PREN and the critical pitting temperature (CPT) were calculated (Table 2). For both parameters, a high number represents a better performance. The results showed the same ranking for both parameters: SCW1080 steel < CW201 steel < SCW2205 steel. The Vickers hardness was comparable for SCW1080 and SCW2205 steels, although the hardness was higher for CW201 steel (Table 3).

Figure 4 shows the microstructure for CW201 and SCW2205 steels, which is characterized by a lamellae microstructure. For both materials, the microstructure is elongated in the drawing direction. However, in the case of SCW2205 steel (Figure 4b), the direction of elongation is not uniform and it exhibits a more angular nature. A more detailed study was performed on the SCW2205 steel using transmission electron microscopy (Figure 4c and d) and SEM-EDS (Figure 5). This nanograph (Figure 4c) also evidences the lamellar structure of the SCW2205 steel material. Figure 4d shows a polycrystal diffraction pattern with texture. The (111) planes of austenite are perpendicular to the drawing direction. In addition, body-centered tetragonal (BCT) phases (a: 0.285 nm, c: 0.292 nm) were found on the nanograph and are indicated in blue, which demonstrate the presence of the martensite phase in SCW2205 steel. Figure 5a-c show a backscattered micrograph of SCW2205 steel and the EDS maps for nickel and chromium, respectively. The chemical distinctive phases present in this material are not discernable by overlapping these figures, as can be seen with the Z-contrast provided by the backscattered image (Figure 5a), but they can be clearly detected with the EDS maps for nickel and chromium (Figure 5b and c). Nickel is known to be an austenite stabilizer; therefore, the nickel map identifies the austenite (high in nickel) and the ferrite phases (low in nickel). In terms of the chromium content, EDS shows that the ferrite phase has more chromium when compared to austenite. A complete characterization of each phase is provided in Table 4.

The PRENs calculated for each phase from the EDS results are 27.18 and 36.55 for austenite and ferrite, respectively. However, it is important to notice that nitrogen cannot be detected using EDS since its characteristic energy is very small.

Table 3. Vickers Hardness of the Different Steel Materials Evaluated

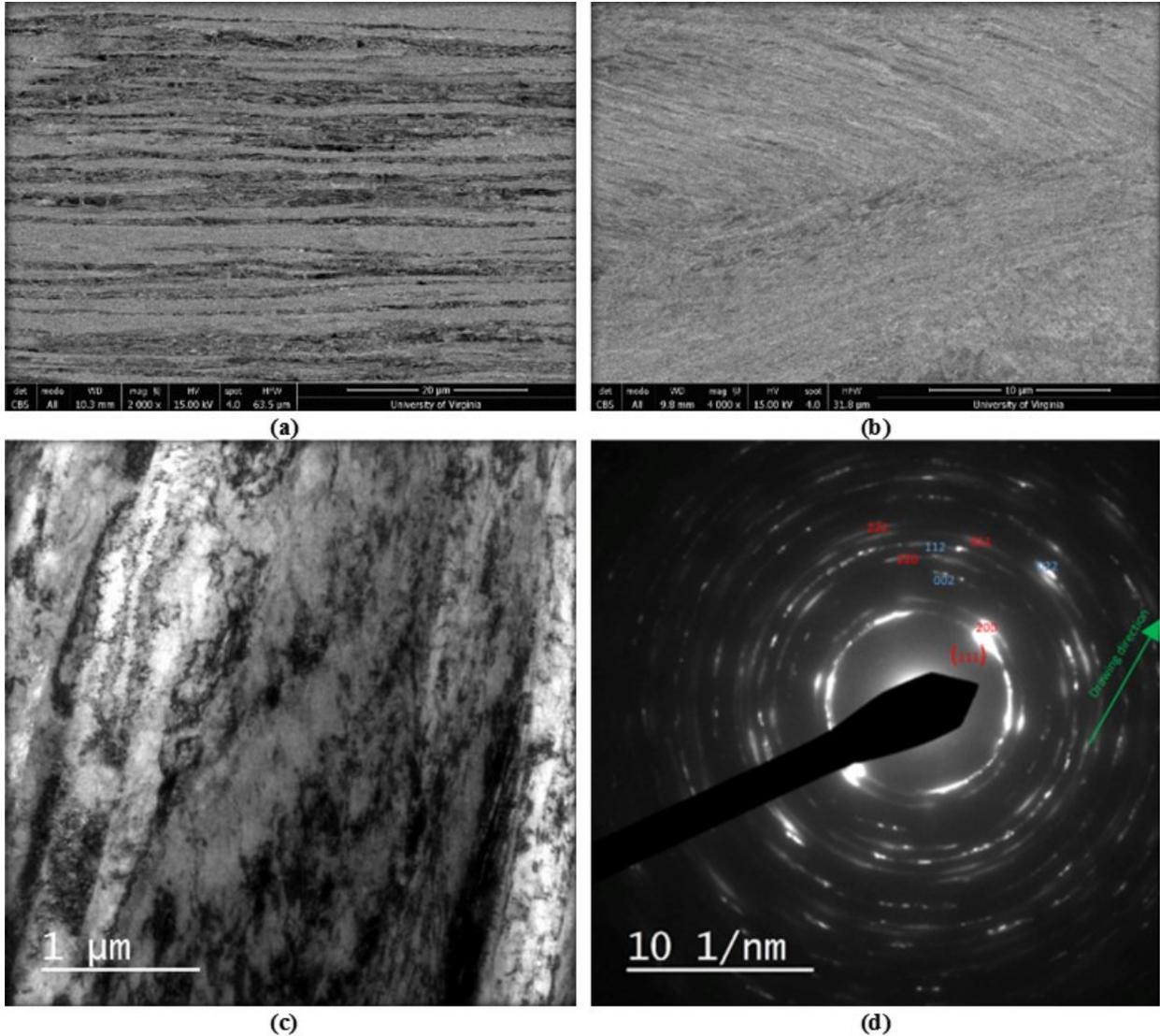| Material	Hardness
SCW2205	465.4
SCW1080	473.0
Non-CW201	232.8
CW201	526.2

Figure 4. Concentric Backscattered Images: (a) microstructure for cold worked 201 austenitic steel; (b) microstructure for stranded and cold worked 2205 duplex stainless steel and transmission electron microscopy; (c) lamellae microstructure on stranded and cold worked 2205 duplex stainless steel; (d) polycrystal diffraction patterns, showing BCT phase (indices marked in blue: a = 0.285 nm, c = 0.292 nm). BCT = body-centered tetragonal.
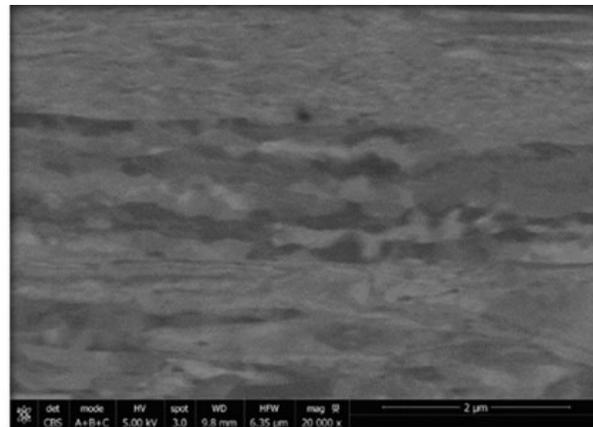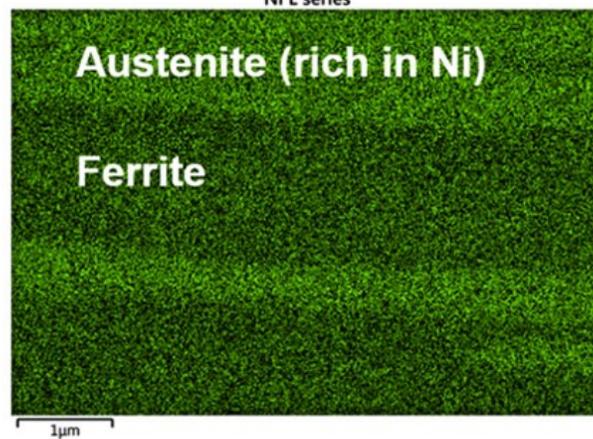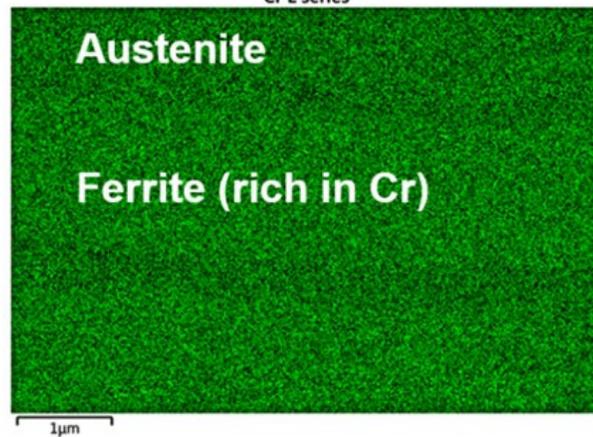
Figure 5. Chemical Characterization SCW2205 steel: (a) concentric backscattered image for stranded cold worked 2205 duplex stainless steel using energy dispersive spectroscopy; (b) Ni mapping; (c) Cr mapping

Table 4. Phase Composition Analysis of Stranded Cold Worked Type 2205 Steel Materials Using Energy Dispersive Spectroscopy (wt. %)

Element	Ferrite Phase Spectrum					Austenite Phase Spectrum				
	No. 5	No. 9	No. 12	No. 14	Average	No. 6	No. 10	No. 11	No. 13	Average
Fe	62.7	62.4	61.6	62.7	62.4	64.4	63.2	64.5	64.5	64.2
Cr	21.2	21.1	23.0	21.5	21.7	18.5	19.8	17.7	18.3	18.6
C	5.8	6.2	6.2	6.3	6.1	5.9	6.1	6.5	6.1	6.1
Mo	5.0	4.2	4.7	4.3	4.5	3.1	2.6	2.8	2.1	2.6
Ni	4.7	5.1	4.0	4.5	4.6	7.6	8.0	7.8	8.1	7.9
Si	0.6	0.6	0.5	0.7	0.6	0.5	0.4	0.8	0.5	0.6

The crystallographic microstructure was studied through XRD (Figure 6). The non-CW201 and CW201 steels revealed the creation of martensite through strain induction, as shown by the presence of body-centered cubic (BCC) peaks after the cold worked processing. It is important to recognize that martensite's crystallographic structure is characterized by a BCT crystal structure; however, XRD is not able to differentiate between the similar BCC and BCT crystal structures.
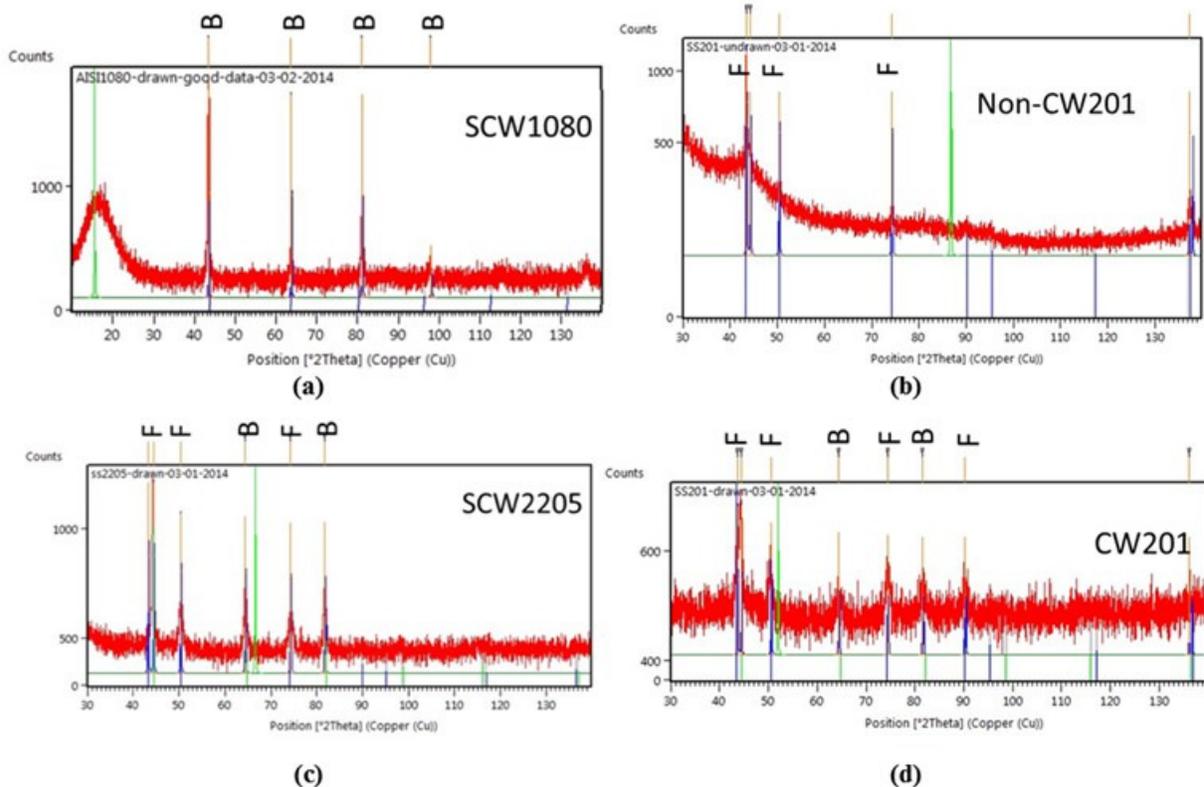
Figure 6. X-ray Diffraction Results: (a) stranded cold worked 1080 carbon steel; (b) non-cold worked 201 austenitic stainless steel; (c) SCW2205 duplex stainless steel; (d) cold-worked 201 austenitic stainless steel. B = body-centered cubic; F = face-centered cubic.

XRD results from the SCW2205 steel material showed both face-centered cubic and BCC diffraction results. This is expected since one of the characteristics of duplex stainless steels is the mixture of ferrite (BCC crystal structure) and austenite (face-centered cubic crystal structure). However, some of the BCC peaks are also related to the martensite phase, which, as previously mentioned, actually has a BCT crystal structure, as shown in the transmission electron microscopy characterization (Figure 4d).

Electrochemical Interrogation

Cyclic polarization curves were generated for the following four material samples:

1. non-CW201 steel
2. CW201 steel
3. SCW1080 steel
4. SCW2205 steel samples.

pH values of the test solutions used to generate the curves varied; it should be noted that the pH values used for evaluation are lower than what would be found at the surface of the strand in fresh concrete that is not contaminated chlorides. The difference in pH of each test solution is a function of the differences in the chloride concentration in each test solution. The chloride concentration in the solution is inversely related to the pH of the aqueous solution, so as the chloride concentration of the solution increases, the pH decreases. Higher chloride levels and lower pH levels create a more aggressive environment than the environment of steel embedded in fresh concrete that is not contaminated with chlorides. It is possible for steel to be subjected to high chloride levels and low pH solutions when concrete is cracked or damaged. Reinforcing steel is always exposed to a more corrosive environment when cracks or spalls reach to or beyond the level of the reinforcement. The cyclic polarization curves for each test sample and exposure environment combination are provided in Appendix B.

The specific chloride test solutions used for exposure evaluation along with the corresponding measured pH values for each test solution used were as follows:

- SOW, pH = 9.37
- 0.9 M NaCl, pH = 7.09
- 5.3 M NaCl, pH = 5.63
- 0.6 M $MgCl_2$, pH = 8.78
- 2.37 M $MgCl_2$, pH = 7.83
- 5.4 M $MgCl_2$, pH = 5.91.

When the four sample steel materials were evaluated to determine corrosion mechanisms, two types of electrochemical behaviors were found. The behaviors are dependent on the inherent corrosion resistance of each steel material.

SCW1080 steel has a negligible level of chromium, resulting in very little corrosion resistance; SCW1080 steel was found to corrode actively over much of the surface. SCW1080 steel is described as having general corrosion.

The two stainless steel alloys have much higher level of chromium; the stainless steel materials (non-CW201, CW201, and SCW2205 steels) were passivated at the open circuit potential in all the tested solutions; the open circuit potential is the potential difference measured between a reference electrode and a metal sample that is in a given solution. The implication of passivation, which is attributed to the high chromium content in the stainless steel materials, is that the passivated materials are likely to exhibit localized corrosion instead of more general corrosion.

Pitting (a form of localized corrosion) was observed to initiate in the Type 201 stainless materials when the cell potential was increased, with the amount of increase depending on the specific test solution. Therefore, these samples exhibited improved corrosion resistance compared to that of the SCW1080 steel, but pitting could be initiated during cyclic polarization testing.

The SCW2205 steel showed a passive region (the corrosion rate of the sample was considerably reduced as SCW2205 steel passivated) and then a transpassive region for all solutions except 5.4 M $MgCl_2$. This transpassive region is where the measured current increases (indicating passivity breakdown) as a result of the potential being increased toward more noble values than in the passive region and is commonly associated with the oxidation of the chromium present in the passivating film and/or oxygen evolution on very corrosion-resistant alloys containing chromium. In the case of samples exposed to 5.4 M $MgCl_2$, SCW2205 steel has a larger passive region (0.5 V vs. 0.25 V) and lower current density (7×10^{-8} A/cm^2 vs. 3×10^{-7} A/cm^2) when compared to CW201 steels. The lower current density indicates a lower corrosion current for the SCW2205 steel. The SCW1080 steel has no passive region; it actively corroded in 5.4 M $MgCl_2$. The active general corrosion of SCW1080 steel clearly demonstrates that the corrosion resistance of SCW1080 steel is inferior to that of the tested stainless steels. The best observed corrosion resistance was with the SCW2205 steel.

The pitting potential was extracted from the cyclic polarization curves. The pitting potential is the magnitude of the electronic potential, in volts, above which pitting can initiate. The pitting potential is displayed as solid squares in Figure 7. Figure 7 was used to assess the effect of chloride concentration and cold work on pitting.

The pitting potential of both non-CW201 and CW201 steels tends to decrease as the chloride concentration increases, as can be seen by the red and blue solid lines in Figure 7. The electronic pitting potential tended to be higher for the non-CW201 material (blue squares) when compared to the cold worked material (red squares). The higher electronic potential demonstrates that cold working has a negative effect on corrosion resistance. However, the difference in corrosion resistance gets smaller as the chloride concentration increases. The effect of cold working becomes negligible when the environment becomes more corrosive (high chloride concentration).
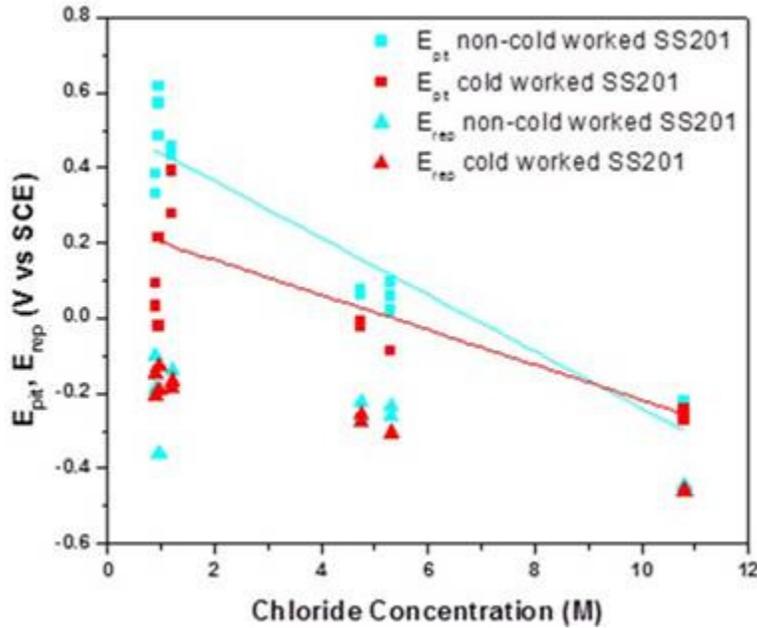
Figure 7. Effect of Chloride Concentration on Pitting (E_{pit}) and Repassivation Potential (E_{rep}) for Stranded Cold Worked AISI 1080, Non-Cold Worked 201 Austenitic Stainless, Cold Worked 201 Austenitic Stainless, and Stranded Cold Worked 2205 Duplex Stainless Steels

Another electrochemical parameter that was extracted from the cyclic polarization curves and evaluated was the repassivation potential. Repassivation is the potential, in volts, that indicates that the metal has returned to a low corrosion state as measured against the original passive current value. Repassivation occurs at more negative potential values. The electronic repassivation potential value is shown as solid triangles in Figure 7. Whether the CW201 material has been cold worked during fabrication or in the field does not seem to affect the repassivation potential. Overlapping red and blue triangles in Figure 7 indicate that cold working CW201 material only reduces corrosion resistance compared to non-cold worked material at lower chloride concentrations. As the chloride concentrations increase, the cold worked and non-cold worked materials have very close to the same corrosion resistance.

After the initial round of cyclic polarization testing was completed, additional testing was performed to mimic other possible exposure conditions. This additional testing incorporated the case of inland exposure, exposure resulting in strong oxidizing conditions, artificial seawater solution, and concrete saturated with salt (pore solution saturated with salt). In addition, the highest concentration of salt solutions used previously was also used in this test cycle for comparison.

For SCW1080 steel, except for the pore solutions where a pitting potential could be measured, this material showed active corrosion for all solutions. The CW201 steel showed better corrosion resistance than the SCW1080 steel. For CW201 steel, this material showed a pitting potential for all solutions except inland, indicating that it is prone to pitting whenever there are conditions that result in the open circuit potential being above the pitting potential. In this cycle of tests, the SCW2205 steel exhibited the best corrosion resistance. It was observed that SCW2205 steel is passivated when immersed in all solutions, showing a transpassive region for inland, artificial seawater, NaCl, and the oxidizing solutions (containing $FeCl_3$), whereas a

18

pitting potential is defined for the 5.4 M $MgCl_2$ solution and the pore solutions saturated with salt. However, the deflection in potentials for the pore solutions are very high and could correspond to chromium oxidation. This observation confirmed that the 5.4 M $MgCl_2$ solution was the most aggressive among the solutions tested for SCW2205 steel.

The cyclic polarization curves for these tests are provided in Appendix B. It was clear from this work that these finding supported the other findings that SCW2205 steel has a higher resistance to pitting than both CW201 and SCW1080 steels and that SCW1080 steel actively corrodes in most environments.

Pitting Resistance Evaluation in Controlled Environments Simulating Atmospheric Exposure

Another approach was used to test the pitting resistance of the different materials. In this specific case, pitting was allowed to take place under a droplet in a controlled environment (RH, droplet chemistry, temperature). The pH values of the solutions increase in the following order: 5.63 (5.3 M NaCl) < 7.09 (0.9 M NaCl) < 9.37 (SOW, contains 420 mM NaCl) and 5.91 (5.4 M $MgCl_2$) < 7.83 (2.37 M $MgCl_2$) < 8.78 (0.6 M $MgCl_2$) < 9.40 (SOW) (Rinson Troconis et al., 2016). For reference, it should be noted that a harsh industry test by Sandvik Corp at 0.300 V vs. saturated calomel electrode (V_{SCE}) found that the CPT of Sandvik SAF 2205 is above 70 °C at 2 wt % Cl^-. Extrapolation revealed that 5% Cl^- might produce a decrease in CPT to below 70 °C but still remaining above 60 °C. Thus, pitting was not expected in the current set of tests on SCW2205 steel at room temperature. However, pitting was observed on CW201 and non-CW201 steels in 38% RH in the presence of 5.4 M $MgCl_2$ (Table 5).

It is also important to recognize how the % RH affects corrosion. If a surface is dried, there is no corrosion. As the % RH increases from very low RH, water monolayers start building up on the surface and therefore some corrosion starts and then increases as the solution resistivity decreases. If there are water monolayers on the surface already (NaCl or $MgCl_2$, or SOW droplet) and the % RH is adjusted (current experimental case), as RH goes up, the Cl concentration goes down and vice versa.

Table 5. Pitting Resistance Results for SCW1080, CW201, and SCW2205 Steels After 32 Days of Exposure at Room Temperature

Steel Material	RH (%)	Salts		
		MgCl₂	NaCl	SOW
Non-CW201	38	3/3	0/3	0/3
CW201	38	3/3	0/3	0/3
	80	0/3	0/3	0/3
	97	0/3	0/3	0/3
SCW2205	38	0/3	0/3	0/3
	80	0/3	0/3	0/3
	97	0/3	0/3	0/3

Pitting resistance = number of droplets with pits larger than 5 µm in diameter / total number of droplets; RH = relative humidity; SOW = simplified ocean water

A direct correlation of the effect of each exposure condition on the corrosion morphology of SCW2205 steel is shown for each temperature in Appendix C. These figures show the corrosion morphology of each sample by presenting the change in surface topography, initially starting as a smooth surface, after each sample was exposed to a given environment and set temperature.

In the case of NaCl, artificial seawater, inland, and pore solution + NaCl, pitting was not seen below 95 °C. In pore solution + $MgCl_2$, or $MgCl_2$, pitting was observed at 75 °C. In the case of $FeCl_3$ + NaCl, pitting was seen from 25 to 35 °C, indicative of the very aggressive nature of these environments. In $FeCl_3$ + $MgCl_2$, which has the controlled exposure with the most severe oxidizer and Cl^- level, pitting was seen at 25 °C. These results suggest that SCW2205 steel should resist pitting in almost all conditions unless a strong oxidizer is present, which is unfeasible if the SCW2205 steel strand is embedded in concrete as part of a pile.

The pit growth rate over time was not monitored, and determination of rates was not possible. However, the depth of attack after exposure revealed that the depth was generally 10 to 50 µm deep with a trend toward deeper pits and greater density of pits and higher volume loss as temperature increases. Unless the temperature was documented to be around 75 to 95 °C, which is unlikely for a strand embedded in a concrete pile, the pit depth was quite shallow, showing a depth of about 10 to 20 µm.

Only in the case of environments with the presence of a strong oxidizer ($FeCl_3$) were the pits found to be deep. The effect of temperature was also very noticeable in some environments—specifically in those without oxidizer, such as artificial seawater (this solution is different from the previously mentioned SOW solution), saturated NaCl, and saturated $MgCl_2$ (equivalent to semi-spherical pits ranging between 0 and 50 µm in diameter). A milder effect of temperature on corrosion was observed for the pore solutions saturated with salt, showing a volume loss equivalent to the volume of a 1 to 10 µm semi-spherical pit.

These results indicate that pitting would be unlikely in Virginia in an environment such as intact concrete with NaCl or even cracked concrete. As the data show, the highest temperature recorded in Virginia was 110 °F (43 °C), and inside the concrete, the strand would be insulated from the heat (National Oceanic and Atmospheric Administration, 2019). However, if the SCW2205 steel is exposed in severe wetting and drying environments containing a severe oxidizer, pitting could occur, but this combination of conditions is unlikely in this type of application. Appendix C shows the results from exposure to each environment.

FPBT in Controlled Environments

The electrochemical test results showed that the 5.4 M $MgCl_2$ solution was the most aggressive among the solutions tested. Therefore, the following results discuss only this solution at different temperatures.

In Appendix D, Figure D1 shows optical microscope images of the same droplet (initially 5.4 M $MgCl_2$) at 38 % RH and room temperature taken at 0, 24, 48, 96, 144, 192, 312, and 341 hours during FPBT experiments with the CW201 steel sample under an approximate stress of

970 MPa. It is important to note that pitting readily takes place after less than 24 hours for CW201 steel, whereas for SCW2205 steel, no pitting takes place even after 341 hours (see Appendix D, Figure D2). For stainless steel, the pitting location depends on the heterogeneities of the engineering alloy and how the chemistry related to the exposure makes some microstructural features more prone to corrosion than others because of microgalvanic coupling.

An SEM was used to characterize the corrosion morphology of the CW201 steel samples, as shown in Figure 8a. The pits were localized and a cross section was prepared by cutting the sample and then carefully polishing the specimen until the pit was reached to look for cracks that had emanated from the pits. Figures 8b and c show examples of these cross sections, which show the presence of cracks.

As part of this work, for 32 days, experiments were performed at low RH and 72 °C (Figure 9) on CW201 and SCW2205 steels, which resulted in stress corrosion cracking inside the pits that had formed in both materials. The crack was readily seen inside the pit for CW201 steel. However, a higher magnification was needed in the case of SCW2205 steel to be able to observe the crack (20,000x vs. 4,000x). After this test, crevice formers as shown in Figure 2d were used to accelerate the SCC process. Figure 10 shows the results of an FPBT of SCW2205 steel in low RH at 95 °C. Cracking took place inside the pit in multiple places. A magnification of one of the cracks in shown in Figure 10b. This crack propagates through the wire in a perpendicular orientation with respect to the oriented microstructure. This is because of the sample orientation when stressed having the highest resolved shear stress perpendicular to the tensile stress applied on the specimen. Figure 10c shows another crack that was captured at a different location.

Chemical characterization using EDS (Figure 11) of the tested sample showed that the ferrite was the phase that was more prone to corrode when compared to the austenite (rich in nickel). This observation, that pitting was controlled by dissolution of the ferrite phase, agrees with previous research observations on pitting initiation (do Nascimento et al., 2008; Garfias-Mesias et al., 1996; Garfias-Mesias and Sykes, 1998) and Volta potential studies (Femenia et al., 2003).

A summary plot showing the results of the FPBT of creviced samples exposed is shown in Figure 12. This plot also contains SCC data from Prosek et al. This plot indicates that there is a threshold temperature needed for the onset of SCC and that SCW2205 steel (PREN 34.76) has higher SCC resistance than CW201 steel (PREN 21). It is important to note that for a highway structure, the highest temperature to which the strand would be subjected would be during steam curing. Steam curing is used to accelerate the curing process during fabrication, and it is done prior to the concrete element being placed in a salt laden environment. During this process, the concrete and strand could be exposed to temperatures that would approach 160 F° (80 °C) and possibly higher with the careful addition of supplementary cementitious materials. However, if these strands are subjected to corrosive conditions, the temperatures at those times would influence the corrosive reaction rather than the earlier temperatures that were generated during the steam curing stage. In addition, temperatures this high do not normally occur in the field, as routinely the precast elements would be subjected only to temperatures below 100 °F (38 °C),

with the highest temperature on record in Virginia being 110 °F(43 °C) (National Oceanic and Atmospheric Administration, 2019).
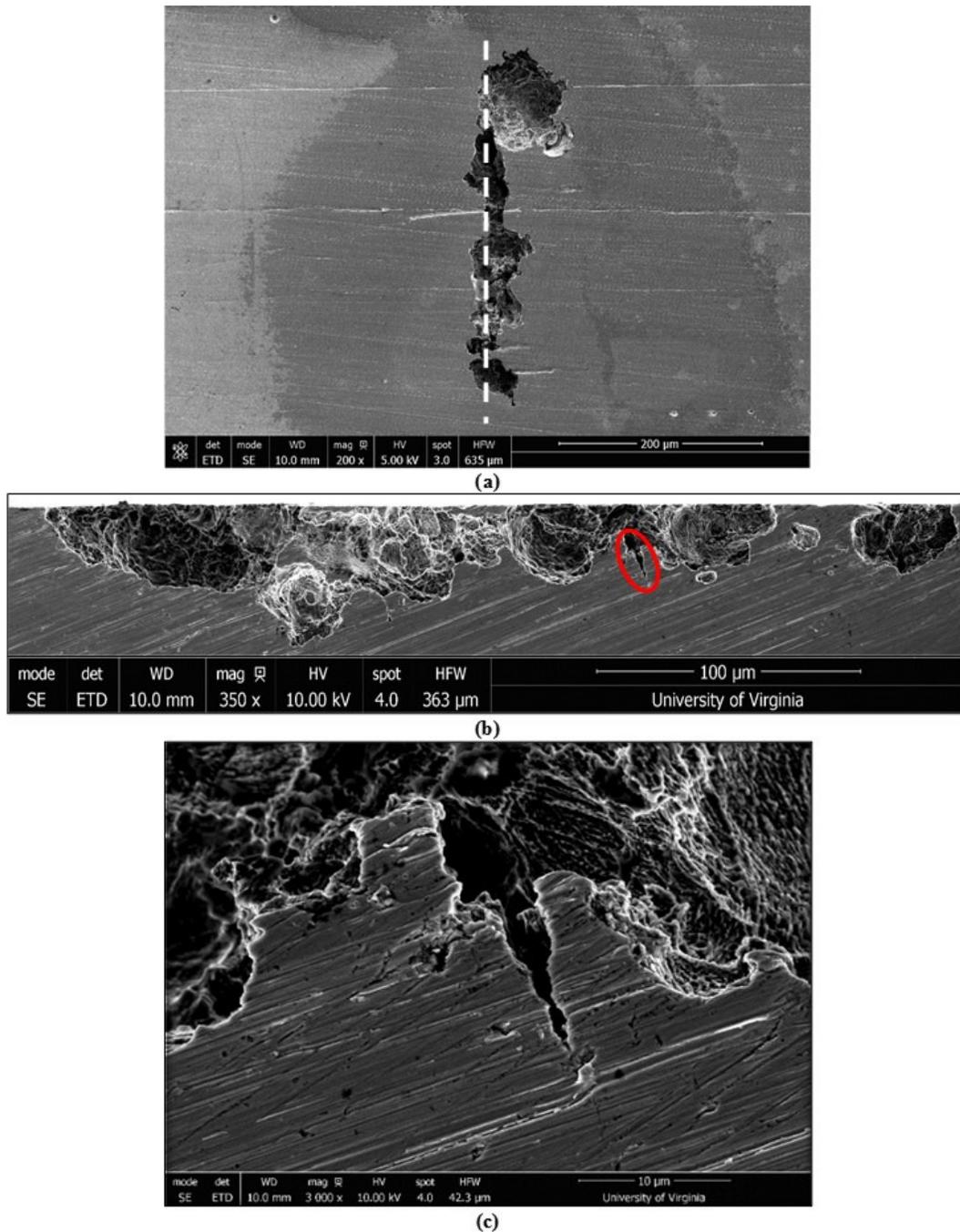

Figure 8. SEM Image of Pits in CW201 Steel Samples: (a) secondary image of pit inside sample after exposure to a 0.1 μL 5.4 M MgCl₂ droplet on a CW201 steel specimen subjected to a four-point bend test stressed at 970 MPa in a controlled environment chamber (38% RH, 25 °C) for 32 days. Image also shows the cross-sectional cut location (white dashed line) to obtain figure showing (b) secondary image of cross-sectional surface showing pit morphology, including (c) secondary image at 3,000x of a crack (red circle in middle image). SEM = scanning electron microscope; RH = relative humidity.
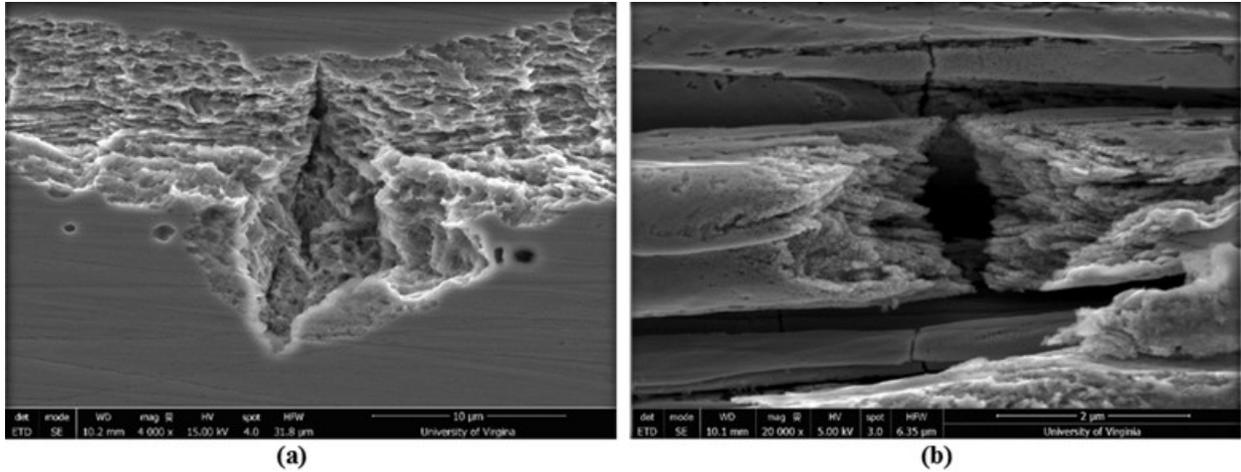
Figure 9. Secondary Images of Pitting-Induced Stress Corrosion Cracking on Specimens Under Four-Point Bend Testing Stressed at 970 MPa in Controlled Environments (X % RH, X °C) Exposed During X Time: (a) CW201 steel sample (30% RH, 72 °C, 32 days); (b) SCW2205 steel sample (27 % RH, 72 °C, 32 days). RH = relative humidity.
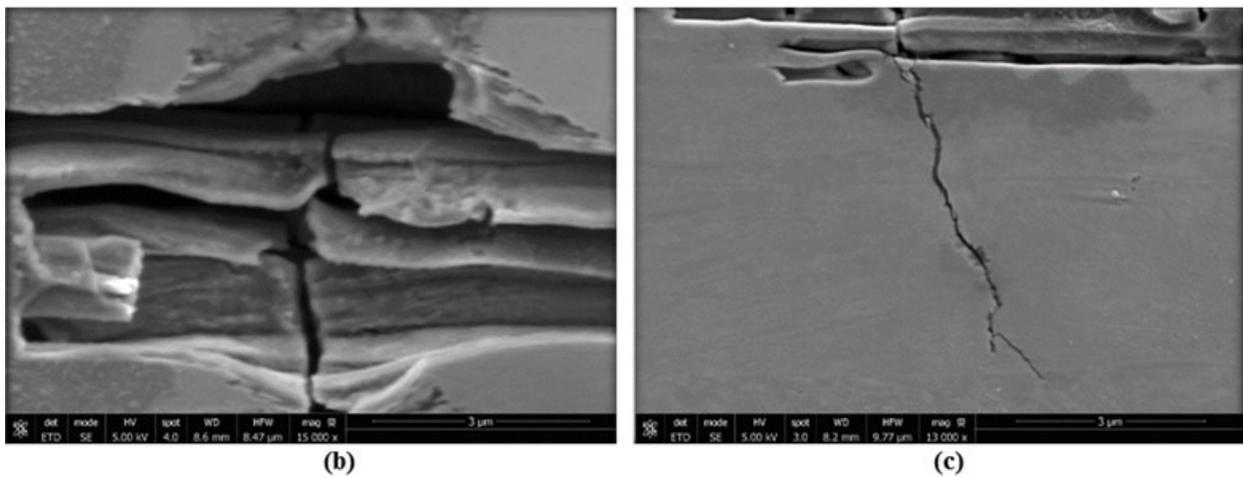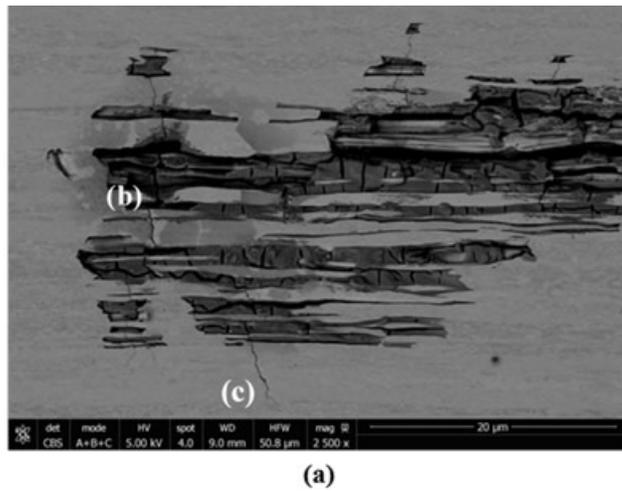
Figure 10. SCW2205 Steel Sample After Four-Point Bend Test: (a) top view of pitting-induced stress corrosion on specimens under creviced four-point bend test stressed at 970 MPa in controlled environments (27 % RH, 95 °C) exposed during 1 day; (b) magnification of selected region highlighted in Figure 10a as "(b)" showing cracks inside of pit; (c) magnification of selected region highlighted in Figure 10a as "(c)" showing crack propagating outside pitted area. RH = relative humidity.

23
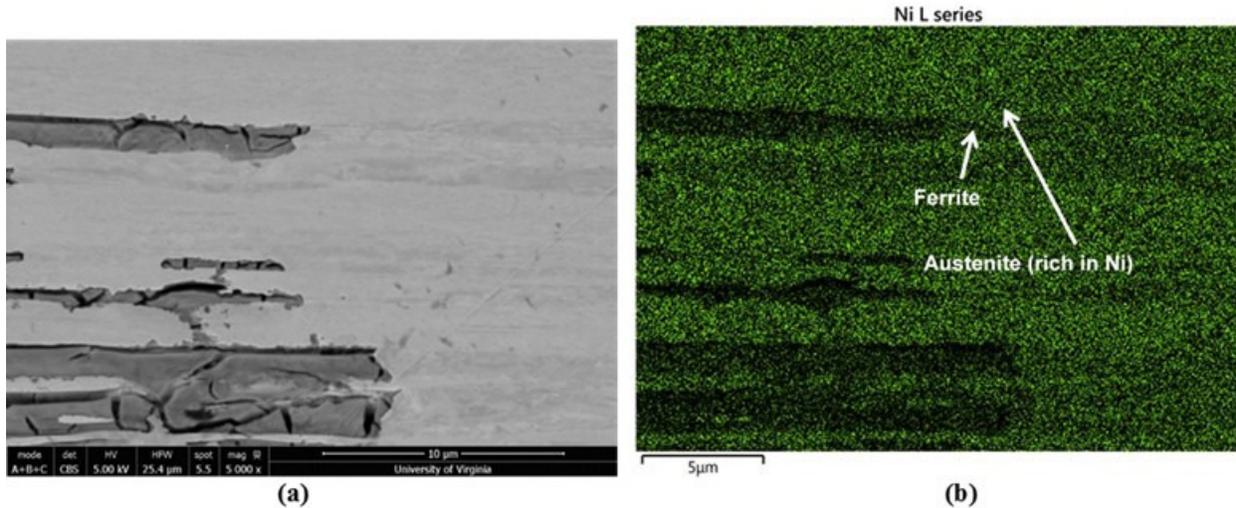
Figure 11. Chemical Characterization of SCW2205 Steel Sample Using EDS: (a) secondary image of pitting site on specimens under creviced four-point bend test stressed at 970 MPa in controlled environments (27 % RH, 95 °C) exposed during 1 day; (b) energy dispersive spectroscopy map of nickel in same location as (a), showing selective dissolution of ferrite phase. EDS = energy dispersive spectroscopy; RH = relative humidity.
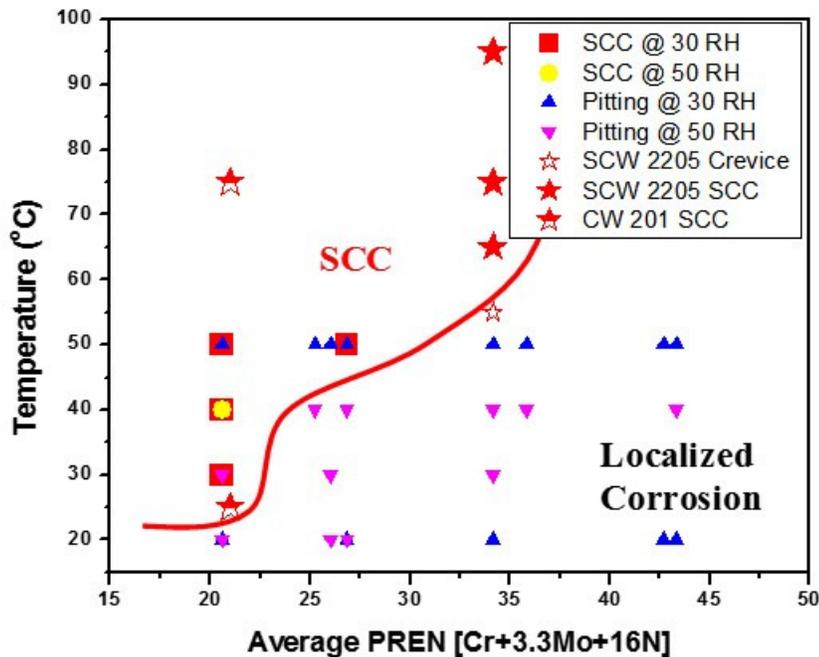
Figure 12. Stress Corrosion Cracking Susceptibility Map in Terms of Temperature and Pitting Resistance Equivalent Number. Includes data for cold worked 201 austenitic stainless steel, data for stranded cold-worked 2205 duplex stainless steel, and data from Prosek et al. (2009).

As discussed earlier, the test samples were sectioned along the z-axis to look for evidence of SCC. This cross section is paramount in determining the material's response to the electrolyte, concentrated in a high-stress area, under high-temperature conditions. Upon examination of the SCW1080, CW201, and SCW2205 steel samples, cracks were observed in the SCW1080 and CW201 steel samples but not in the SCW2205 steel sample. This observation strongly reinforces the findings from the electrochemical results.

FPBT in Field Exposure

It was observed that the FPBT SCW1080 steel field test samples had a noteworthy amount of rust on the surface, whereas the two stainless steel samples did not have any apparent rust spots. On the CW201 steel sample, there was some evidence of pitting and repassivation as discussed earlier. The results from these tests were that SCW2205 steel showed no signs of stress corrosion cracking, very little pitting, and no signs of rust in any of the chosen environments. An example of what was typically observed is shown in Figure 13, which is from the Covington exposure site.
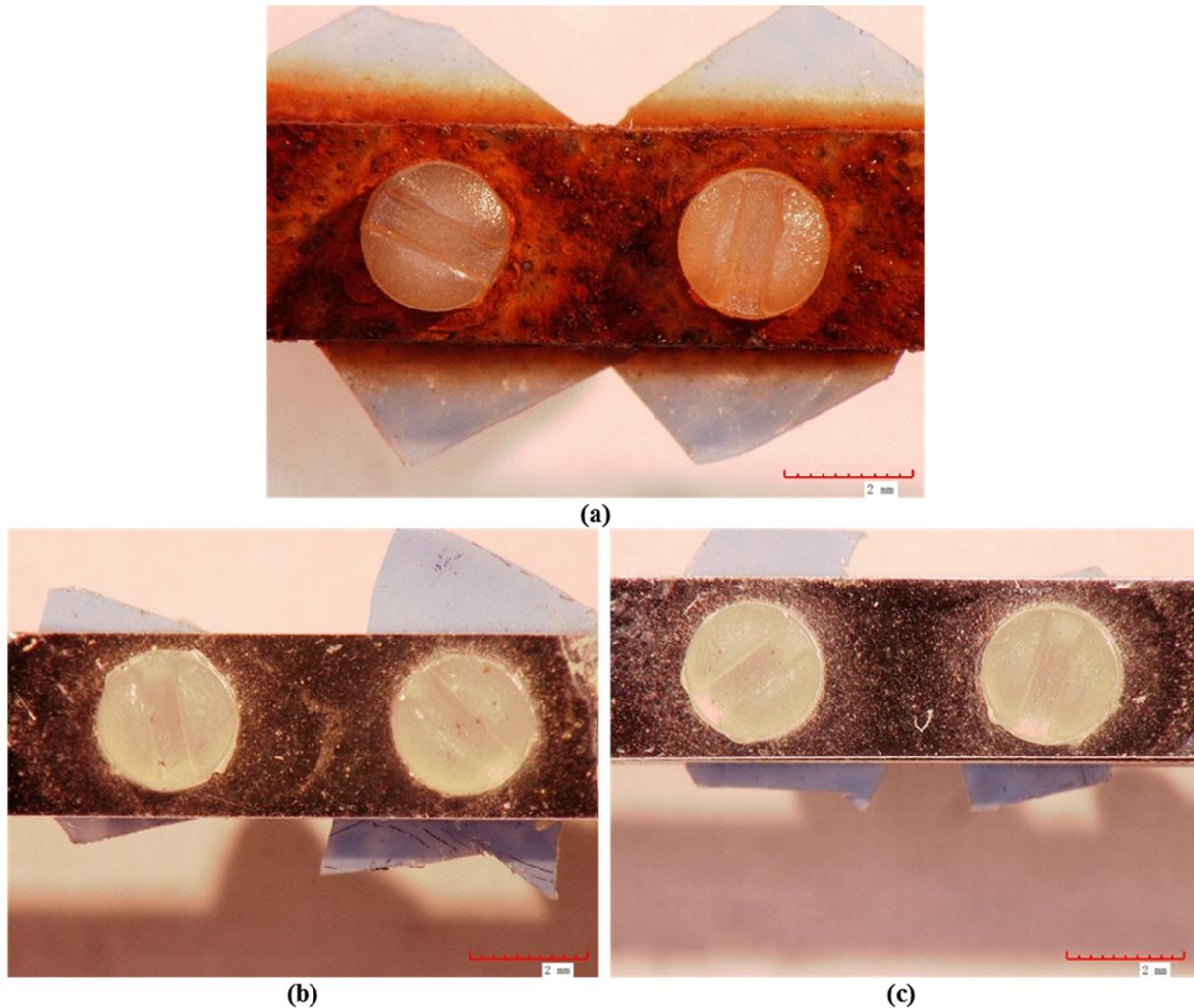
Figure 13. Close-up Image of Typical Four-Point Bend Test Exposure Sample After 295 Days: (a) SCW1080 steel; (b) CW201 steel; (c) SCW2205 steel

A corrosion volume loss analysis was performed after topographical information was obtained from the exposed samples by using an optical profiler. Figure 14 shows that the corrosion resistance of SCW1080 steel is inferior to that of CW201 and SCW2205 steels in more aggressive environments, presenting higher corrosion volume loss. In terms of the best performance, according to this parameter, SCW2205 steel performed the best in the Hampton Roads location, and CW201 steel performed the best in the Covington location. These two materials had similar behavior in the Harrisonburg location.

After consideration of the results from characterizing the three field sites, which are given in Appendix A, it was determined that the highest values of corrosion volume loss were at Hampton Roads, which was attributed to the highest chloride deposition rate in this site. Further, this was verified through all experiments performed in the laboratory, which showed that the higher corrosion volume loss and the susceptibility to SCC were found in conditions leading to high chloride concentrations (low RH and $MgCl_2$). For each 1 M of $MgCl_2$, there is 2 M of Cl^-, whereas for each 1 M of NaCl, there is 1 M Cl^-, and thus the reason having conditions leading to the saturated $MgCl_2$ solutions led to the highest corrosion attack.
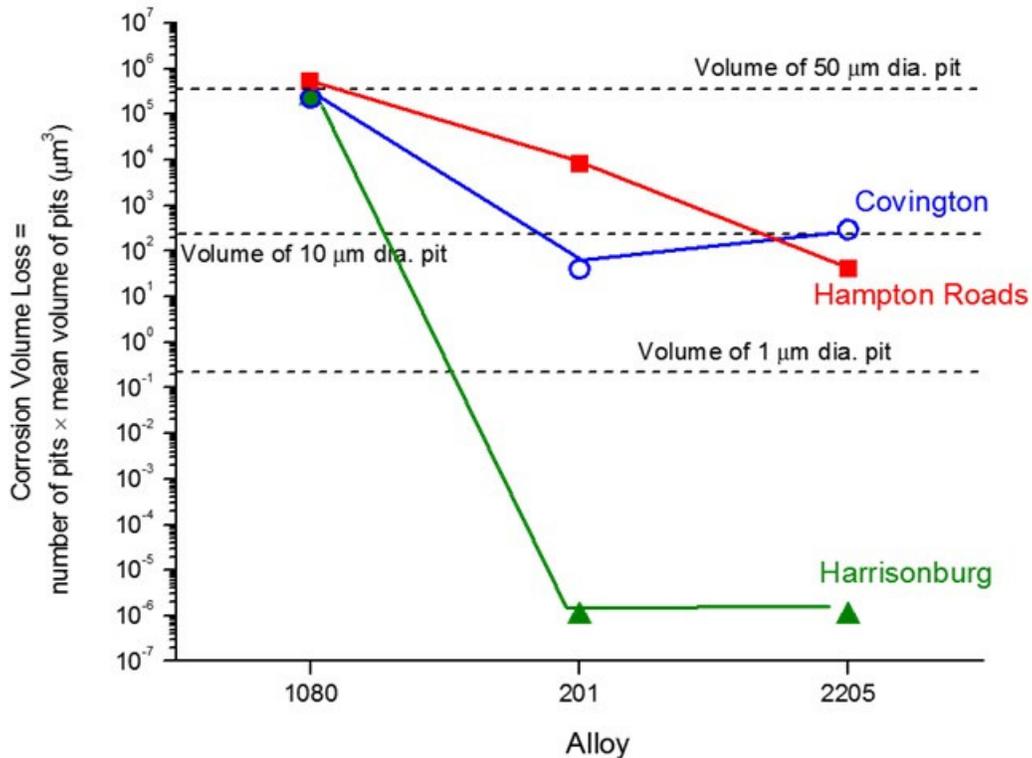
Figure 14. Corrosion Volume Loss Analysis of the Different Materials Exposed to Different Field Locations

Stress Corrosion Cracking Testing Using U-Bends in Field Exposure

The final test performed was a U-bend environmental test exposed in the field at Hampton Roads, Harrisonburg, and Covington. It was shown through a dye penetration test that no SCC was seen in the samples, and only some surface rust was observed. To verify that no SCC occurred, samples were also observed under the SEM. Figures 15 and 16 show that there is no SCC damage to the SCW2205 steel, as indicated in Table 6.

26

Electron Image 200x
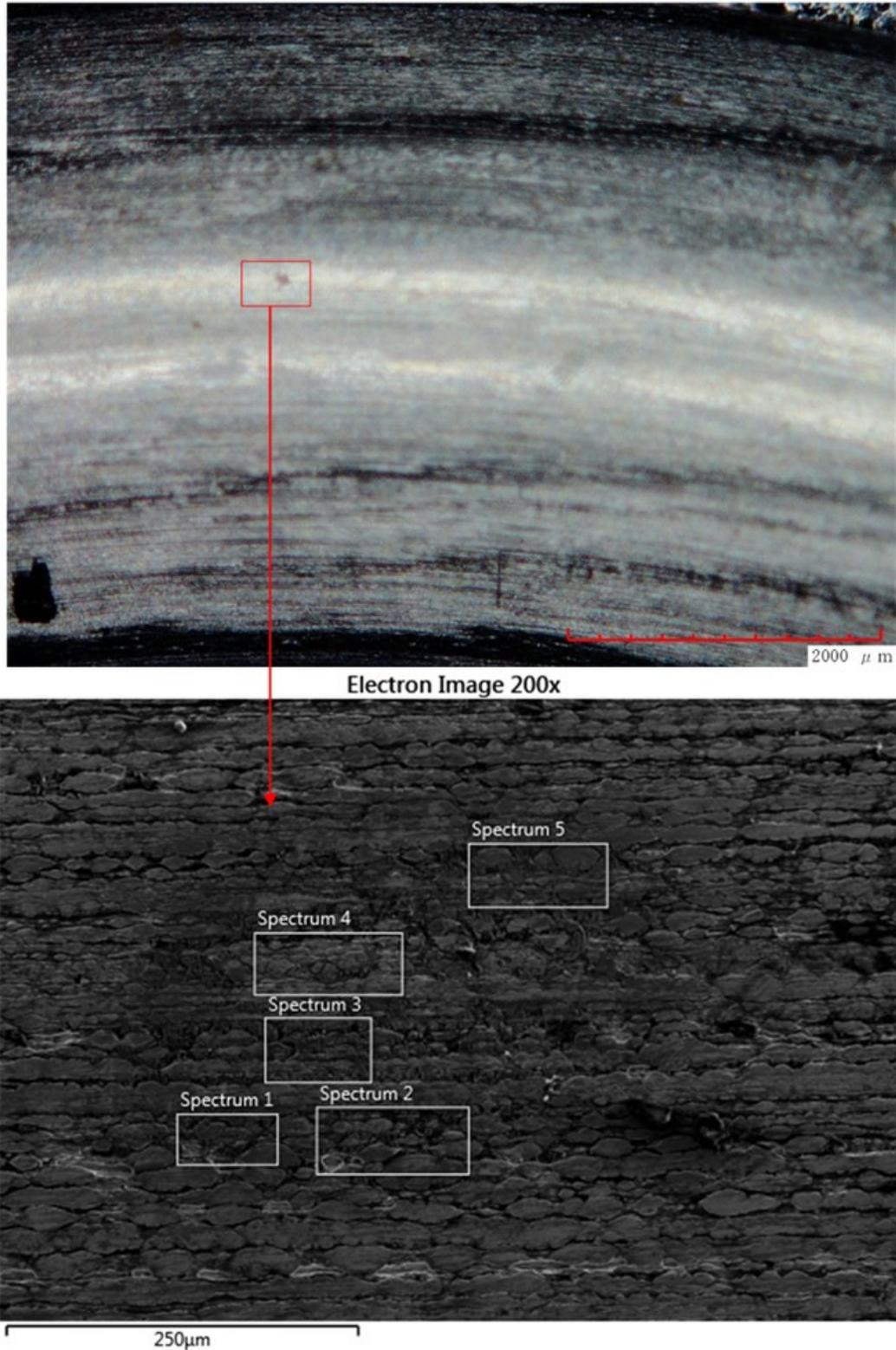
Figure 15. No SCC Damage Found on SCW2205 Steel Samples: top, optical image at a magnification of 50x of a SCW2205 steel U-bend sample with a spot on it; bottom, electron image of the same area at a magnification of 200x. SCC = stress corrosion cracking.
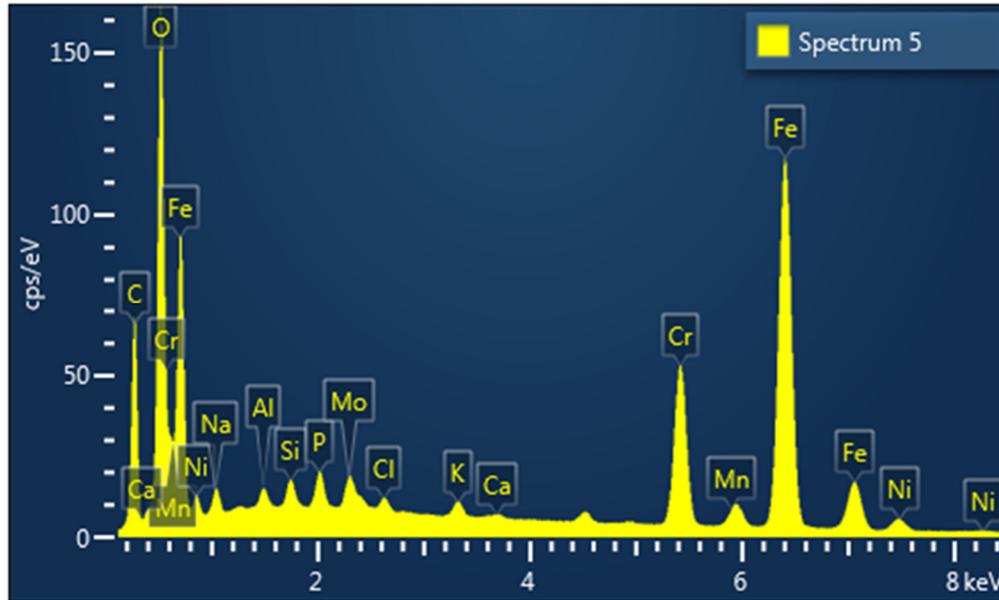
Figure 16. Typical EDS Spectrum From Locations Shown in Figure 15. EDS = energy dispersive spectroscopy.

Table 6. Overview of Damage Condition for SCW2205 Steel U-bend Test Samples After 295 Days of Exposure: July 2016-May 2017

Item	Location	Damage Under Optical Microscopy (1X to 150X) (Rust Staining / Pitting / Cracking)	Cracks Under Dye Penetration
U-Bend 2205 T	Hampton Roads	No	No
U-Bend 2205 V	Hampton Roads	No	No
U-Bend 201 V	Hampton Roads	Rust stains	No
U-Bend 2205 T	Harrisonburg	No	No
U-Bend 2205 V	Harrisonburg	No	No
U-Bend 201 V	Harrisonburg	No	No
U-Bend 2205 T	Covington	No	No
U-Bend 2205 V	Covington	No	No
U-Bend 201 V	Covington	No	No

The only observation was a very shallow corrosion indication in the form of a dark stain. An example of the typical results of chemical characterization in several locations inside the stain is provided in Figure 16, which showed that stain corresponds to an oxide layer. For ease of comparison, the other EDS results for the other four locations are provided in Appendix E.

In the current work, the focus was on localized corrosion, which can lead to hydrogen generation. This pathway is through pitting corrosion or localized corrosion, which depends on materials and environment. The environments were pore water solution with carbonation and chloride, artificial seawater, or highly concentrated chloride solutions formed by wetting and drying or by salt deposition and deliquescence. During this type of attack, acid-induced pitting may occur. The highly acidified environments formed in pits or at local corrosion sites could enable hydrogen embrittlement, especially if pitting and martensite both occurred. The probability of this is unknown, but the susceptibility can be gauged first through the dependency of local corrosion on material temperature and environment and second through the experiments conducted herein. CW201 steel has a PREN of 20 to 22 depending on nitrogen content and a

CPT of 48 °C. Type 2205 steel has a much higher PREN and an experimental CPT above 65 °C, whereas the calculated CPT is 42.5 °C. In this study, pitting and general corrosion occurred easily on CW201 steel and SCW1080 steel, respectively, in a variety of environments. CW201 steel could be used only in pore solutions substantially free of Cl^-. In the case of SCW2205 steel, pitting was produced only in $FeCl_3 + MgCl_2$, which might be more severe than any expected exposure condition. The corrosion potential in this test was above transpassive potentials, which is unlikely even in severe conditions for this application. Pitting was also observed in 5.4 $MgCl_2$ above 0.0 $V_{SCE,}$ which is not an impossible condition to attain but could be achieved only in concentrated droplets of $MgCl_2$. The next question would be whether small pits could supply enough hydrogen to induce hydrogen embrittlement. While this situation seems unlikely, it is not impossible during an expected service life of 100 years.

Based on the corrosion test results in this work, it is expected that SCW2205 steel strand will provide a much more corrosion-resistant option in prestressed concrete product. In pore solution (strands embedded in quality concrete with no chloride); concrete exposed to artificial seawater (strands embedded in concrete with the chloride concentration slowly increasing in pore solution); and direct contact with artificial seawater (concrete damaged and strand exposed to artificial seawater), the SCW2205 steel outperformed the other steels tested. It was observed that SCW2205 steel (Type 2205 stainless steel) exhibited much better corrosion resistance compared to CW201 steel, and the CW201 steel outperforming conventional steel strand.

Field Demonstration

Pile Fabrication and Driving for the Nimmo Parkway Bridge

The Nimmo Parkway Bridge had concrete piles prestressed with one of three different materials, (1) ASTM A416 conventional steel prestressing strand, (2) CFRP prestressing strand, or (3) Type 2205 stainless steel prestressing strand and Type 304 stainless steel spiral.

Since the Type 2205 stainless strand prestressed piles incorporate steel products, compliance with the "Buy America" requirements is required for federally funded highway projects. The Type 2205 strand material was made from stainless steel that originated in Scandinavia; therefore, only a limited amount of Type 2205 prestressing material could be used and still conform to the Buy America requirements. It was determined that to stay within the cost confinements of these requirements, five piles with SCW2205 steel strand reinforcement could be constructed for this project.

The SCW2205 steel strand selected for this project was 0.5-in-diameter low relaxation strand. Although there are similarities between the two types of steel strand, some properties are different when compared to those of conventional ASTM A416 steel strand, such as the ultimate strength of the strand. Another difference, which is also the case for CFRP strand, is that the total elongation does not meet the requirements of ASTM A416, which has a minimum requirement of 3.5%. Therefore, it is important to consider these differences during the design stage. The mill report for the SCW2205 steel strand is provided in Appendix F.

Initially, sufficient strand was purchased for the construction of five 24-in-square piles. However, during fabrication of the first set of piles several of the strands unexpectedly fractured at the wedge tip (Figure 17) after tensioning but before concrete placement in the bed. It was evident that several factors could have contributed to the failures. First, upon examination of the fractured wires, the wedge teeth showed the greatest penetration at the front of the wedge. Second, the load cell data indicated that loading was not evenly applied, as some values exceeded the design load of 27.5 kips, with the largest value of the four strands being measured failing first (Figure 18). Third, an adjacent connected form was cast and being cured using steam as the source of heat (Figure 19). The load cell data during this period indicated that the two inner load cell readings slowly exhibited the largest increases in load with time whereas the two load cells that were the farthest from the adjacent form being heated showed the lowest rate of change, although all had positive slope. It is expected that this combination of factors discussed in this report caused the resulting sequence of strand failures.

Figure 17. Fracture at Wedge Tip Location With Strand Breaking Before Completing Fabrication of First Set of Stainless Reinforced Concrete Piles
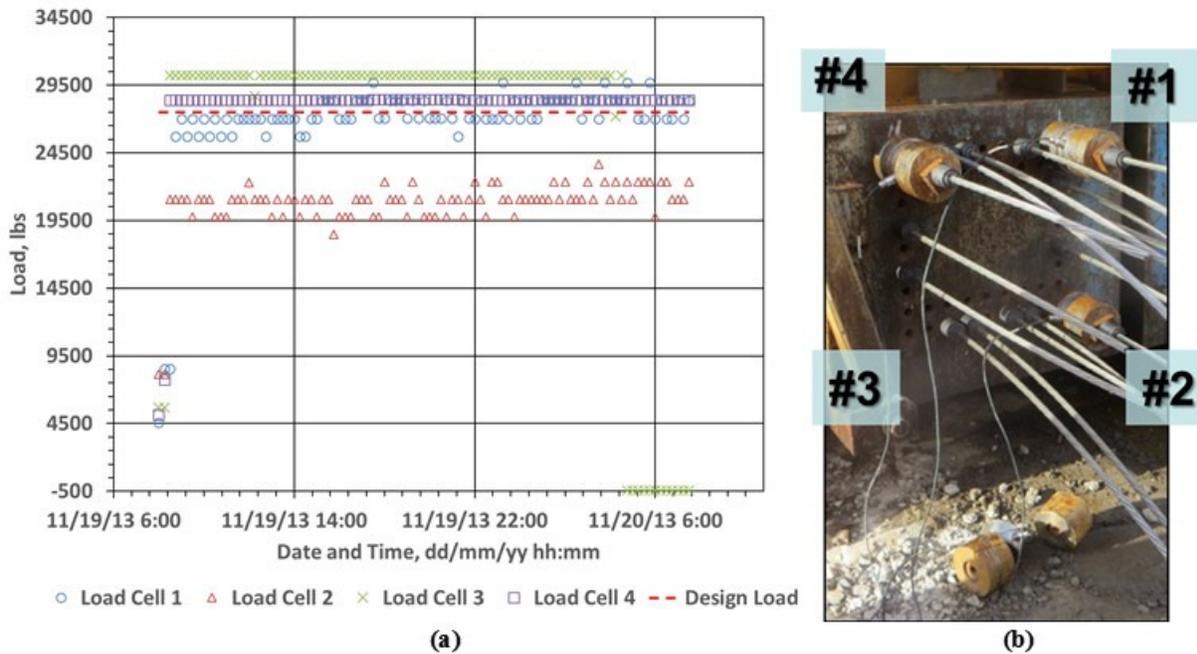
Figure 18. Load Data Captured During Failure of Several Stainless Steel Strands: (a) load cell data; (b) photograph showing the corresponding load cell with each channel number indicated

Figure 19. Preparing to Make 24-in-Square Prestressed Concrete Piles. Conventional steel strand shown on the left and 2205 stainless strand shown on the right in a 400-ft-long bed. Not shown are the steam curing pipes that lay adjacent to the bed near the ground.

Adjustments were made to the pile design that addressed this issue. This was done by increasing the number of ½-in strands in each pile from 20 to 22. This allowed for the initial tension per strand to be reduced from 27.5 to 22.5 kips, with the assumed minimum effective prestress decreasing from 800 to 750 psi. With this change, four SCW2205 stainless steel reinforced concrete piles were successfully fabricated. These piles included a Type 304 stainless steel square spiral and conventional lift approach. Plastic ducts were also embedded at the top of the piles to help with connecting to the cap. This is shown in Figure 20.

After the pile fabrication was completed, the piles were transported to the project site. At the site, these piles were handled in a manner similar to that for piles reinforced with conventional strand. The same equipment used for driving the conventional piles was used for the SCW2205 steel strand piles.

The driving of the pile is a physical process, as the repetitive hammer blows to the pile head drive the pile into the ground. The ram weight during this operation weighed 10,141 lb with the open-end diesel hammer stroke having a range between 5.7 and 9.2 ft. For this bridge, four SCW2205 steel piles were successfully driven in December 2013.
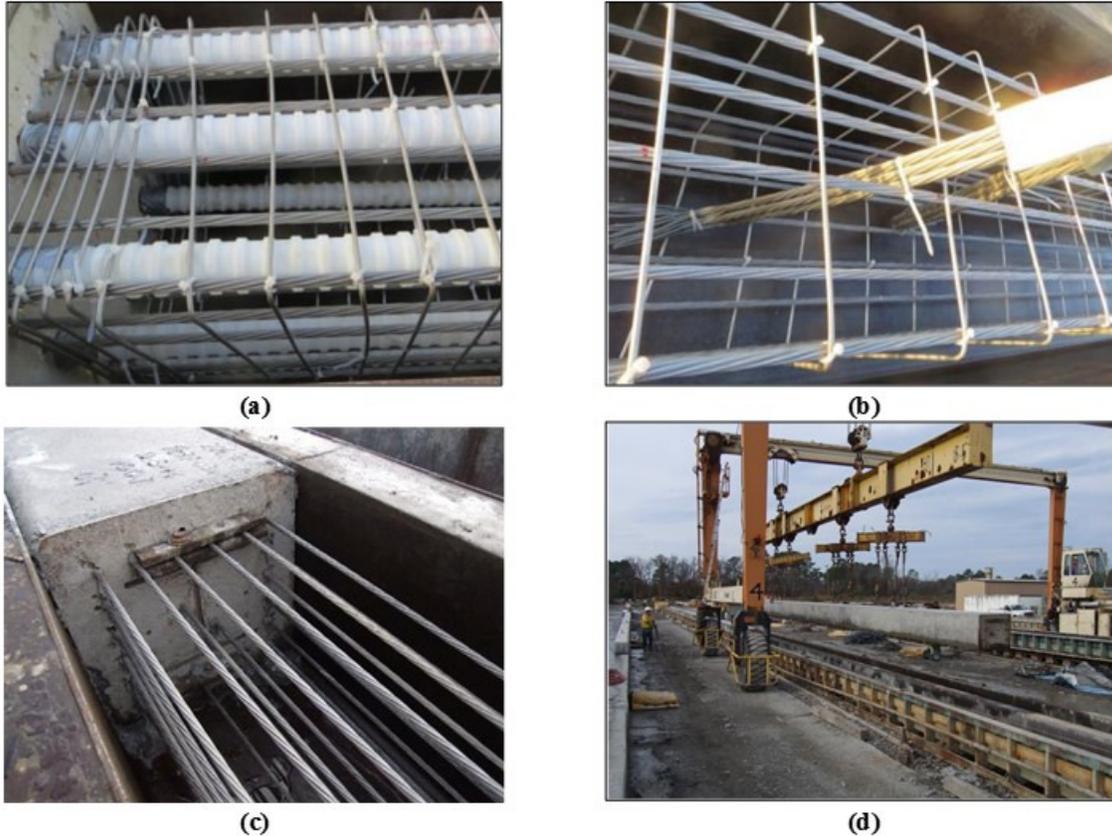
Figure 20. Successful Fabrication of Stainless Steel Reinforced Concrete Piles: (a) plastic tie and ducts; (b) square spiral and conventional lift approach; (c) pile in forms after concrete has cured; (d) pile lifted from form

Construction for Route 621 and Route 680 Bridges Using SCW2205 Steel Piles

This project was located on two bridges: (1) the Route 621 Bridge over Passenger Swamp, and (2) the Route 680 Bridge over Stallings Creek, both in Isle of Wight County.

For both bridges, 16-in-square piles reinforced with stainless steel were required. All strands were a low relaxation stainless steel with an ultimate strength of 250 ksi. To fabricate each pile, twelve ½-in strands were used with a No. 5 gage Type 304 stainless steel wire formed into a square spiral. All of the materials met the Buy America requirements, and it is expected that the earlier issue leading to strand failure has been solved. The concrete specified was a Class A5 concrete, with a 28-day minimum compressive strength of 5,000 psi. The release strength was 3,500 psi.

Twenty-two corrosion-resistant piles were fabricated using Type 2205 stainless steel strand and Type 304 stainless steel spiral reinforcement for use in two bridges in VDOT's Hampton Roads District. The two Isle of Wight bridge projects were combined and awarded as a single contract.

The Route 680 Bridge over Stallings Creek was constructed using 12 of the 22 corrosion-resistant piles as part of the replacement of a structure that had been built in 1952. The Route

621 Bridge over Passenger Swamp was built using the remaining 10 corrosion-resistant piles as part of the replacement of a structure that had been built in 1945. Construction of both bridges started on May 2, 2016, and had been completed on time by December 30, 2016.

SCW2205 Steel Pile Fabrication for the High Rise Bridge

After the successful completion of several projects and the demonstration that SCW2205 reinforced concrete piles could be successfully fabricated and driven, procedures were established by VDOT for routine use of the material as reinforcement in piles (VDOT, 2018). The geographical area to the right of the red line on the map in Figure 21 shows the region where VDOT now requires the use of either CFRP or SCW2205 steel strands in piles exposed to tidal waters. The corrosion-resistant piles can also be used at other locations with corrosive characteristics throughout the state. This region includes the High Rise Bridge, which is currently under construction and is one component of a more sizable construction project. This portion of the project includes construction of a new High Rise Bridge that will be higher and wider than the old bridge when finished. The piles used in the High Rise Bridge will include prestressed CFRP strand reinforcement in some piles and SCW2205 steel strand reinforcement in other piles.

Figure 21. Region Requiring Use of CFRP or SCW2205 Steel Strands in Piles. Region to the east (right) of the red line requires CFRP or SCW2205 steel reinforcement (VDOT, 2018). CFRP = carbon fiber reinforced polymer

Figure 22 shows a SCW2205 steel pile for this bridge at different stages of pile fabrication and construction. These piles are 66-in cylinder piles, which will be the largest diameter pile reinforced with SCW2205 stainless strand in the VDOT inventory. In addition, 36-in piles will be fabricated with SCW2205 steel as part of this project.
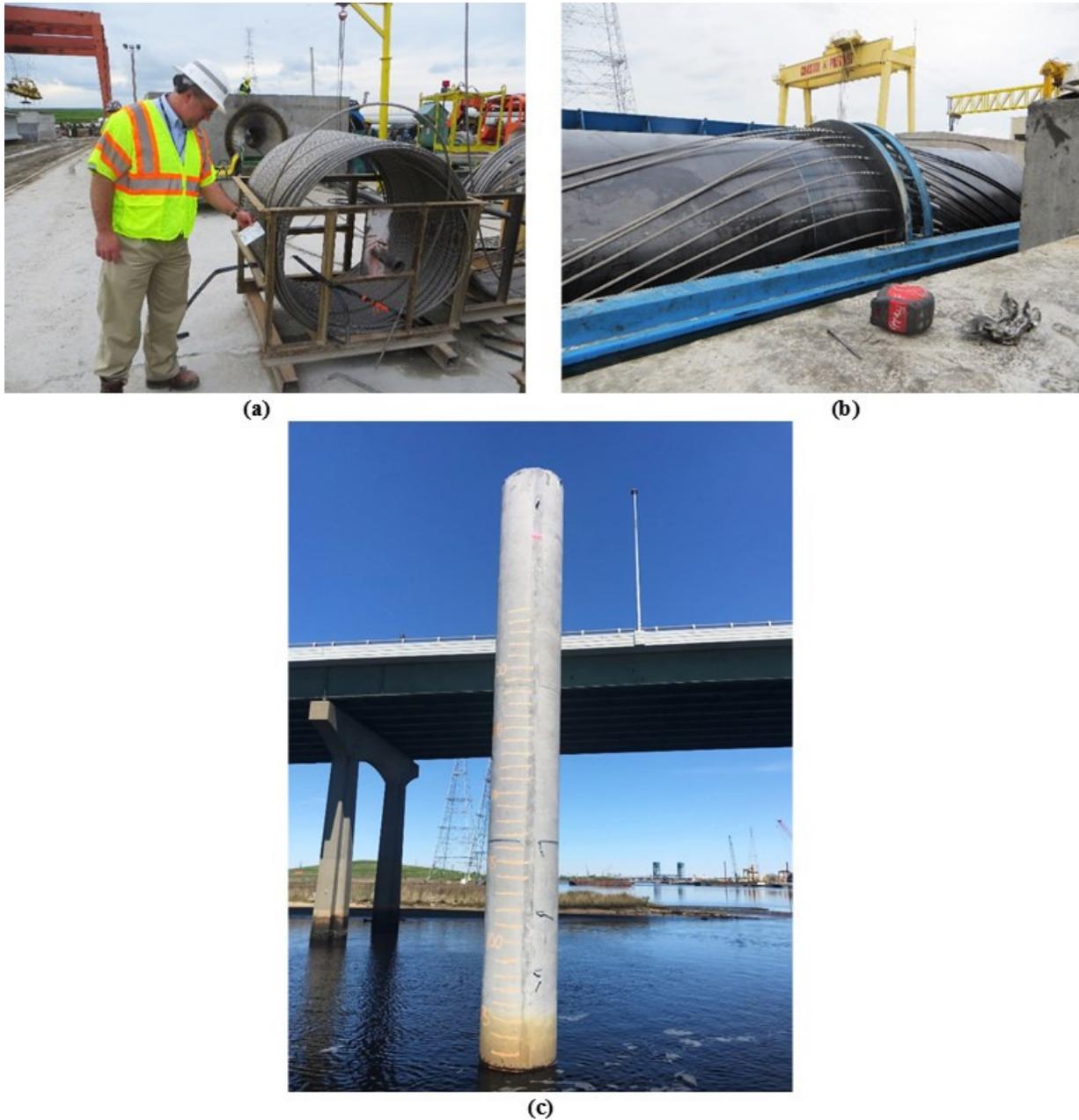
Figure 22. Fabrication and Placement of SCW2205 Steel-Reinforced 66-in Cylinder Piles: (a) SCW2205 steel strand; (b) strand in pile form as pile is being fabricated; (c) completed SCW2205 steel reinforced concrete 66-in circular pile after driving

Comparison of the Properties and Initial Costs of Conventional and Corrosion-Resistant Strands

Table 7 provides an overview of selected strand properties and the cost per lineal foot for conventional steel, SCW2205 steel, and CFRP strands, with the cost estimates being gathered during March 2019. With different material characteristics and levels of corrosion resistance, it is best to look at each application and then determine which material is the most cost appropriate. It is important to recognize that during LCCA, associated reinforcing materials such as stirrups or spirals should be included in the analysis. These associated reinforcing materials can be more expensive because of the additional fabrication requirements, e.g., the precise bending of stirrups.

When costs are considered, it is also important to recognize the influence of competition on costs. Based on the favorable corrosion results in this study, VDOT has the ability to implement the use of a corrosion-free (i.e., CFRP) and corrosion-resistant (i.e., SCW2205 steel) strand in prestressed concrete bridge elements where corrosion is a concern, such as concrete elements exposed to brackish water, saltwater, or deicing salts. It is expected that having two strand products available for competition will also benefit VDOT. Competing corrosion-resistant materials will constrain costs and provide similar benefits of long service life with low maintenance costs.

Table 7. Selected Properties and Estimated Costs of Strand Materials for Piles as of March 2019

Strand Properties, Characteristics, and Cost	Conventional Steel (ASTM A416)	CFRP	Type 2205 Stainless Steel
Tensile strength (min), ksi	270	338	250
Elastic modulus, ksi	28,600	22,500	24,500
Elongation at break, %	3.5 (minimum)	1.7	1.5
Corrosion resistant or corrosion free	---	Corrosion free	Corrosion resistant
Estimated cost/ft, $	• 0.5-in 270 ksi at $0.305/ft • 0.6-in 270 ksi at $0.435/ft	• 0.6-in 338 ksi at 3.45$/ft • 0.7-in 338 ksi at $4.51/ft	• 0.5-in 250 ksi at $2.30/ft • 0.6-in 250 ksi at $3.25/ft

CFRP = carbon fiber reinforced polymer; --- = not applicable.

CONCLUSIONS

- *The analysis conducted in this study suggests that SCW2205 steel is the optimal choice as a stainless steel (corrosion-resistant material) prestressing strand with limited pathways for corrosion that threaten strand integrity.*

- *The following ranking of conventional and stainless steel strand materials is offered, where "<" equals greater than, and "<<" equals much greater than:*

  —*In pore solution (strand embedded in quality concrete with no chloride), the relative corrosion resistance of the steels tested are (worst corrosion resistance to best): conventional steel strand < CW201 steel << SCW2205 steel.*

—*In concrete exposed to artificial seawater (strand embedded in concrete with the chloride concentration slowly increasing in pore solution), the relative corrosion resistance of the steels tested are (worst corrosion resistance to best): conventional steel strand < CW201 steel << SCW2205 steel.*

—*In direct contact with artificial seawater (concrete damaged and strand exposed to artificial seawater), the relative corrosion resistance of the steels tested are (worst corrosion resistance to best): conventional steel strand < CW201 steel << SCW2205 steel.*

• *Each project should allow precasters the freedom to consider the different properties and costs of these materials so it can be determined which material is the most cost appropriate.*

RECOMMENDATIONS

1. *VDOT's Structure and Bridge Division should continue using stainless steel to reinforce piles, based on corrosion performance, and enabling competition between CFRP and stainless steel in piles exposed to severe environments.* This will allow piles of equal load capacity to be treated interchangeably over the defined service life of the structure being designed.

IMPLEMENTATION AND BENEFITS

Implementation

Implementation of Recommendation 1 allows VDOT the ability to use stainless steel strand where it is needed for corrosion resistance at a lower cost than with CFRP. For Recommendation 1, this might also include replacement structures that have deteriorated at an accelerated rate because of corrosion, thus exhibiting a much shorter service life than expected. This might occur where aggressive soil contact with conventionally reinforced concrete elements have exhibited spalling and corrosion damage to strands. Recommendation 1 has been implemented by VDOT's Structure and Bridge Division.

Benefits

Implementing Recommendation 1 will provide VDOT a corrosion-resistant strand for use in structural applications where corrosion is a concern, such as concrete elements exposed to brackish water, saltwater, or deicing salts. This study identified a second strand product that can compete with CFRP strand, which will benefit VDOT by reducing costs and driving innovation in this area.

ACKNOWLEDGMENTS

REFERENCES

ASTM International. *ASTM G1-03: Standard Practice for Preparing, Cleaning, and Evaluating Corrosion Test Specimens.* West Conshohocken, PA, 2011a.

ASTM International. *ASTM G39-99: Standard Practice for Preparation and Use of Bent-Beam Stress-Corrosion Test Specimens.* West Conshohocken, PA, 2011b.

ASTM International. *ASTM G48-11: Standard Test Methods for Pitting and Crevice Corrosion Resistance of Stainless Steels and Related Alloys by Use of Ferric Chloride Solution.* West Conshohocken, PA, 2011c.

ASTM International. *ASTM E384-11: Standard Test Method for Knoop and Vickers Hardness of Materials.* West Conshohocken, PA, 2011d.

ASTM International. *ASTM E104-02: Standard Practice for Maintaining Constant Relative Humidity by Means of Aqueous Solutions.* West Conshohocken, PA, 2012.

ASTM International. *ASTM D1141-98(2013): Standard Practice for the Preparation of Substitute Ocean Water.* West Conshohocken, PA, 2013.

ASTM International. *ASTM E2594-09: Standard Test Method for Analysis of Nickel Alloys by Inductively Coupled Plasma Atomic Emission Spectrometry (Performance-Based Method).* West Conshohocken, PA, 2014a.

ASTM International. *ASTM G5-14: Standard Test Method for Making Potentiodynamic Anodic Polarization Measurements.* West Conshohocken, PA, 2014b.

Baker, E.A. Long-Term Corrosion Behavior of Materials in the Marine Atmosphere. In *Degradation of Metals in the Atmosphere.* Dean, S.W., and Lee, T.S. (eds.). ASTM International, West Conshohocken, PA, 1987, pp. 125-144.

do Nascimento, A.M., Ierardi, M.C.F., Kina, A.Y., and Tavares, S.S.M. Pitting Corrosion Resistance of Cast Duplex Stainless Steels in 3.5% NaCl Solution. *Materials Characterization,* Vol. 59, 2008, pp. 1736-1740.

Femenia, M., Canalias, C., Pan, J., and Leygraf, C. Scanning Kelvin Probe Force Microscopy and Magnetic Force Microscopy for Characterization of Duplex Stainless Steels. Journal of the Electrochemical Society, Vol. 150, Is. 6, 2003, pp. B274-B281.

Garfias-Mesias, L.F., Sykes, J.M., and Tuck, C.D.S. The Effect of Phase Compositions on the Pitting Corrosion of 25 Cr Duplex Stainless Steel in Chloride Solutions. *Corrosion Science,* Vol. 38, 1996, pp. 1319-1330.

Garfias-Mesias, L.F., and Sykes, J.M. Effect of Copper on Active Dissolution and Pitting Corrosion Of 25% Cr Duplex Stainless Steels. *Corrosion,* Vol. 54, 1998, pp. 40-47.

Griffiths, A.J., and Turnbull, A. Hydrogen Uptake and Cracking In 22% Cr Duplex Stainless Steel under Galvanic Coupling Conditions. *Corrosion,* Vol. 53, 1997, pp. 700-704.

Hinds, G., and Turnbull, A. Threshold Temperature for Stress Corrosion Cracking Of Duplex Stainless Steel under Evaporative Seawater Conditions. *Corrosion,* Vol. 64, 2008, pp. 101-106.

Lorenz, K., and Medawar, G. Über das Korrosionsverhalten austenitischer Chrom-Nickel-(Molybdän-) Stähle mit und ohne Stickstoffzusatz unter besonderer Berücksichtigung ihrer Beanspruchbarkeit in chloridhaltigen Lösungen. *Thyssenforschung,* Vol. 1, Issue 3, 1969, pp. 97-108.

Masuda, H. SKFM Observation of SCC on SUS304 Stainless Steel. *Corrosion Science,* Vol. 49, Issue 1, 2007, pp. 120-129.

Moser, R.D., Singh, P.M., Kahn, L.F., and Kurtis, K.E. Chloride-Induced Corrosion Resistance of High-Strength Stainless Steels in Simulated Alkaline and Carbonated Concrete Pore Solutions. *Corrosion Science,* Vol. 57, 2012, pp. 241-253.

North American Stainless. Flat Products Stainless Steel Grade Sheet, 2019. https://www.northamericanstainless.com/wp-content/uploads/2010/10/Grade-201-201LN.pdf. Accessed May 16, 2019.

National Oceanic and Atmospheric Administration. State Climate Extremes Committee (SCEC): Records, 2019. https://www.ncdc.noaa.gov/extremes/scec/records. Accessed May 16, 2019.

Prosek, T., Iversen, A., Taxen, C., and Thierry, D. Low-Temperature Stress Corrosion Cracking of Stainless Steels in the Atmosphere in the Presence of Chloride Deposits. *Corrosion,* Vol. 65, 2009, pp. 105-117.

Rincon Troconis, B., Scully, J., and Sharp, S. Susceptibility of High Strength SCW2205 and SS201 to Pitting-Induced Stress Corrosion Cracking. In *Corrosion 2016 Conference & Expo,* NACE International, Vancouver, BC, Canada, 2016.

Sanchez, J., Fullea, J., Andrade, C., and Alonso, C. Stress Corrosion Cracking Behavior of Duplex Stainless Steel by Slow Strain Rate Tests. *Corrosion,* Vol. 65, 2009, pp. 154-159.

Sandvik. Alloys Data Sheet: Sandvik SAF 2205. Sandviken, Sweden, 2013.

Sharp, S.R., Ozyildirim, H.C., and Moruza, A.K. *Corrosion-Free Carbon Fiber Reinforced Polymer for Prestressed Piles.* VTRC 19-R13. Virginia Transportation Research Council, Charlottesville, 2019.

Shiwa, M., Masuda, H., Yamawaki, H., Ito, K., and Enoki, M. In-Situ Observation and Acoustic Emission Analysis for SCC of $MgCl_2$ Droplet in SUS304 Stainless Steel. *Journal of the Japan Institute of Metals and Materials,* Vol. 76, 2012a, pp. 535-540.

Shiwa, M., Masuda, H., Yamawaki, H., Ito, K., and Enoki, M. In-Situ Observation and Acoustic Emission Analysis for Corrosion Pitting of $MgCl_2$ Droplet in SUS304 Stainless Steel. *Materials Transactions,* Vol. 53, 2012b, pp. 1069-1074.

Shiwa, M., Masuda, H., Yamawaki, H., Ito, K., and Enoki, M. In-Situ Observation and Acoustic Emission Analysis for Corrosion Pitting of $MgCl_2$ Droplet in SUS304 Stainless Steel. *Journal of the Japan Institute of Metals,* Vol. 76, 2012c, pp. 122-128.

Shoji, S., and Ohnaka, N. Effects of Relative Humidity and Kinds of Chlorides on Atmospheric Stress Corrosion Cracking of Stainless Steels at Room Temperature. *Boshuku Gijutsu,* Vol. 38, 1989.

Turnbull, A., Zhou, S., Nicholson, P., and Hinds, G. Chemistry of Concentrated Salts Formed By Evaporation of Seawater on Duplex Stainless Steel. *Corrosion,* Vol. 64, 2008, pp. 325-333.

Virginia Department of Transportation. *Prestressed and Post-Tensioned Concrete.* October 31, 2018. http://www.virginiadot.org/business/resources/bridge/Manuals/Part2/Chapter12.pdf. Accessed April 29, 2019.

APPENDIX A

CHARACTERIZATION OF VDOT OUTDOOR EXPOSURE TEST SITES

Methodology for Atmospheric Contaminants Analysis

The Virginia Transportation Research Council and VDOT identified three locations for installing and monitoring test samples mounted to outdoor exposure test racks. These were selected to provide some contrast in the exposure conditions and included the North Island of the Hampton Roads Bridge Tunnel system; a more remote location in Harrisonburg, Virginia; and a more industrial area in Covington, Virginia. It is important to note that the Harrisonburg and Covington sites have deicing salt storage facilities on-site whereas the Hampton Roads site does not. The Center for Electrochemical Science and Engineering at the University of Virginia performed dust and chloride quantification to characterize each site better.

Dust Quantification (ASTM D1739)

The insoluble and soluble contaminants were determined using different procedures. For the insoluble contaminants, a watch glass with a clean folded Whatman filter paper was dried in the oven at 105 °C for at least 1 hour and cooled in a desiccator for at least 30 minutes. The weight of the watch glass and filter paper was then measured and used as the tare weight. A 250 ml solution (water with captured dust) from each site was thoroughly mixed and then filtered using a funnel with filter paper in it to separate the soluble and insoluble contaminants. The watch glass and filter paper (with trapped insoluble contaminants) were dried in the oven at 105 °C for at least 90 minutes and cooled afterward in the desiccator for at least 1 hour. Then, the dried filter paper with insoluble contaminant matter was weighed, and the gain in mass indicated the mass of insoluble contaminants.

For determining the soluble contaminants, a watch glass was dried in the oven at 105 °C for at least 1 hour and cooled in the desiccator for at least 30 minutes. The weight of the watch glass and filter paper was then measured and used as the tare weight. The filtrate (typically a volume of 250 ml) from the separation of insoluble and soluble contaminants was slowly boiled away to a final volume of 50 ml, which was transferred to the tared watch glass and slowly evaporated to dryness. The watch glass with the dried soluble contaminants was then dried in the oven at 105 °C for at least 2 hours and cooled afterward in the desiccator for at least 1 hour. The dried watch glass with the precipitated soluble contaminant matter was weighed, and the weight of the contaminants was determined by the gain in mass.

The area was determined by measuring the inner diameter of the collecting cylinder. The deposition rate (D) results were reported for the two masses obtained.

Chloride Quantification Through the Wet Candle Technique (Modified ISO 9225)

The chloride determination was performed using the mercurimetric titration. Different solutions were prepared such as 0.25 M NaOH solution (indicator adjustment), 0.05 MHNO$_3$ solution (indicator adjustment), 0.025 M NaCl solution (standard reference), 0.0125 M mercury

(II) (titrant). For the titration, a diphenylcarbazone + bromophenol blue solution was used as indicator solution. The exact concentration of the prepared titrant was determined by titration of the 0.025 M NaCl and found to be 0.012 M. A blank titration was performed on 50 ml of deionized water; then 10 ml of the 200 ml of solution from each site was sampled and titrated using the mercury (II) nitrate titrant. The results were expressed in terms of a deposition rate calculated from the titration results as follows:

$$R_{Cl} = \frac{2 \times (V_3 - V_4) \times C_2 \times 35.5 \, V_T}{V_A \times A \times t}$$

where

V$_3$ = volume in ml of titrant used for titration of the sample
V$_4$ = volume in ml of the deionized (DI) water blank
V$_A$ = volume of the sample titrated (10 ml)
V$_T$ = total volume of the sample (200 ml)
C$_2$ = exact concentration of titrant determined using the standard reference
A = area of the collecting gauze in m^2
t = exposure time in days (30).

Results and Discussion of Atmospheric Contaminants Analysis

Insoluble and Soluble Contaminants Quantification

The values obtained in the field exposure sites range from 1.2×10^{-3} to 5.6×10^{-3} g and from 0.6×10^{-3} to 64.3×10^{-3} g for the insoluble and soluble contaminants, respectively (Table A1). The site with the highest weight of insoluble contaminants was the Covington test site, which represents an industrial environment and therefore explains the high value on this parameter, whereas the other two testing sites presented a similar value equal to almost one third of that of the Covington site. In terms of the soluble contaminants, the Harrisonburg site presented the highest value. This site is located near a city that is not on the coast or next to an industrial site. The reason behind this elevated observation, relative to the other two sites, is not understood. Furthermore, the same observation with respect to the different field exposure sites is obtained for the contamination rates since this parameter is calculated based on the weight of the contaminants and the area exposed.

Table A1. Weight and Deposition Rate of Soluble and Insoluble Contaminants in Atmosphere of the Covington, Harrisonburg, and Hampton Roads Field Exposure Sites

Site	Weight of Insoluble Contaminants (g)	Weight of Soluble Contaminants (g)	Area (m^2)	Insoluble Contaminants Deposition Rate (g/m^2 x 30 day)	Soluble Contaminants Deposition Rate (g/m^2 x 30 day)
Covington	5.6×10^{-3}	3.0×10^{-3}	0.0172	0.3256	0.1744
Harrisonburg	1.9×10^{-3}	64.3×10^{-3}	0.0172	0.110	3.738
Hampton Roads	1.2×10^{-3}	0.6×10^{-3}	0.0177	0.06779	0.03389

Determined in accordance with ASTM D1739.

Chloride Deposition Quantification

The results from this site characterization are given in Table A2. The deposition rate of chloride had the following trend: Hampton Roads > Harrisonburg > Covington. The highest chloride deposition rate was found in Hampton Roads as a result of the close proximity of a chloride source. The Hampton Roads exposure site is located on an artificial island in the Chesapeake Bay between Hampton and Norfolk, which can be seen in Figure A1. This island is less than 20 miles from the mouth of the bay that leads into the Atlantic Ocean. Therefore, the chloride desorption rate at this site was definitely influenced by the proximity of a chloride source, the Chesapeake Bay, which connects to the ocean. The two other sites, Harrisonburg and Covington, have salt storage sites nearby, which are stored inside the dome buildings shown in Figure A1. The Harrisonburg site has a direct line of site from the exposure area to the salt storage. The Covington site has several buildings separating the exposure and salt storage areas. This difference, a barrier (building) as opposed to none, at the last two sites is most likely the reason for the difference in the chloride deposition rate, shown in Table A2.

Table A2. Deposition Rate of Chloride in Atmosphere of the Covington, Harrisonburg, and Hampton Roads Field Exposure Sites

Site	Area (m^2)	Deposition Rate (g/m^2 x 30 day) (mg/m^2 x day)
Covington	0.0544	2.088
Harrisonburg	0.0544	4.176
Hampton Roads	0.0544	9.396

Determined in accordance with ISO 9225.
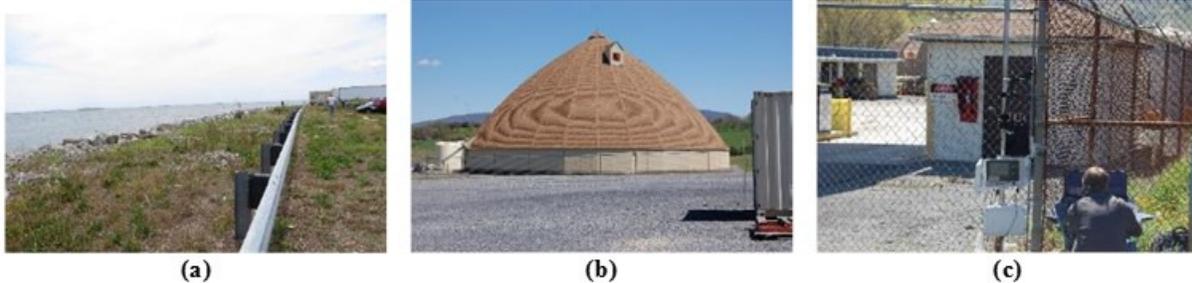
Figure A1. View of Salt Source From Exposure Area: (a) Hampton Roads; (b) Harrisonburg; (c) Covington

APPENDIX B

CYCLIC POLARIZATION RESULTS COMPARING TEST STRANDS IN DIFFERENT ENVIRONMENTS

Chloride-Only Conditions

The results from the cyclic polarizations on the different materials in 0.9 M NaCl, 0.6 M $MgCl_2$, SOW, 5.3 M NaCl, 2.37 M $MgCl_2$, and 5.4 M $MgCl_2$ are displayed. The pH values increased in the following order: 5.63 (5.3 M NaCl) < 7.09 (0.9 M NaCl) < 9.37 (SOW, contains 420 mM NaCl) and 5.91 (5.4 M $MgCl_2$) < 7.83 (2.37 M $MgCl_2$) < 8.78 (0.6 M $MgCl_2$) < (SOW, contains 55 mM $MgCl_2$).

Findings Supported by Data

- The SCW1080 steel was found to actively corrode.
- The stainless steel materials (non-CW201 steel, CW201 steel, and SCW2205 steel) were passivated at open circuit potentials in all the tested solutions as a result of the chromium content in these materials.
- Pitting was initiated in the CW201 steel materials when the potential was increased to specific values depending on the solution, whereas the SCW2205 steel showed a transpassive region for all solutions except 5.4 M $MgCl_2$.
- In the case of samples exposed to 5.4 M $MgCl_2$, SCW2205 steel has a larger passive region (0.5 V vs. 0.25 V) and lower current density (7 x 10^{-8} A/cm^2 vs. 3 x 10^{-7} A/cm^2) than CW201 steel.
- SCW1080 steel has no passive region and is actively corroding in 5.4 M $MgCl_2$.

Chloride Conditions With Additions and Conditions Simulating an Inland Environment

After the initial round of cyclic polarization testing was completed, additional testing was performed to mimic other possible exposure conditions. This additional testing would incorporate the case of inland exposure, exposure resulting in strong oxidizing conditions, artificial seawater solution, and concrete saturated with salt (pore solution saturated with salt). In addition, the highest concentration of salt solutions used previously was used in this test cycle for comparison.

Findings Supported by Data

- SCW2205 steel has a higher resistance to pitting than both CW201 and SCW1080 steels.
- SCW1080 steel actively corrodes in most environments.
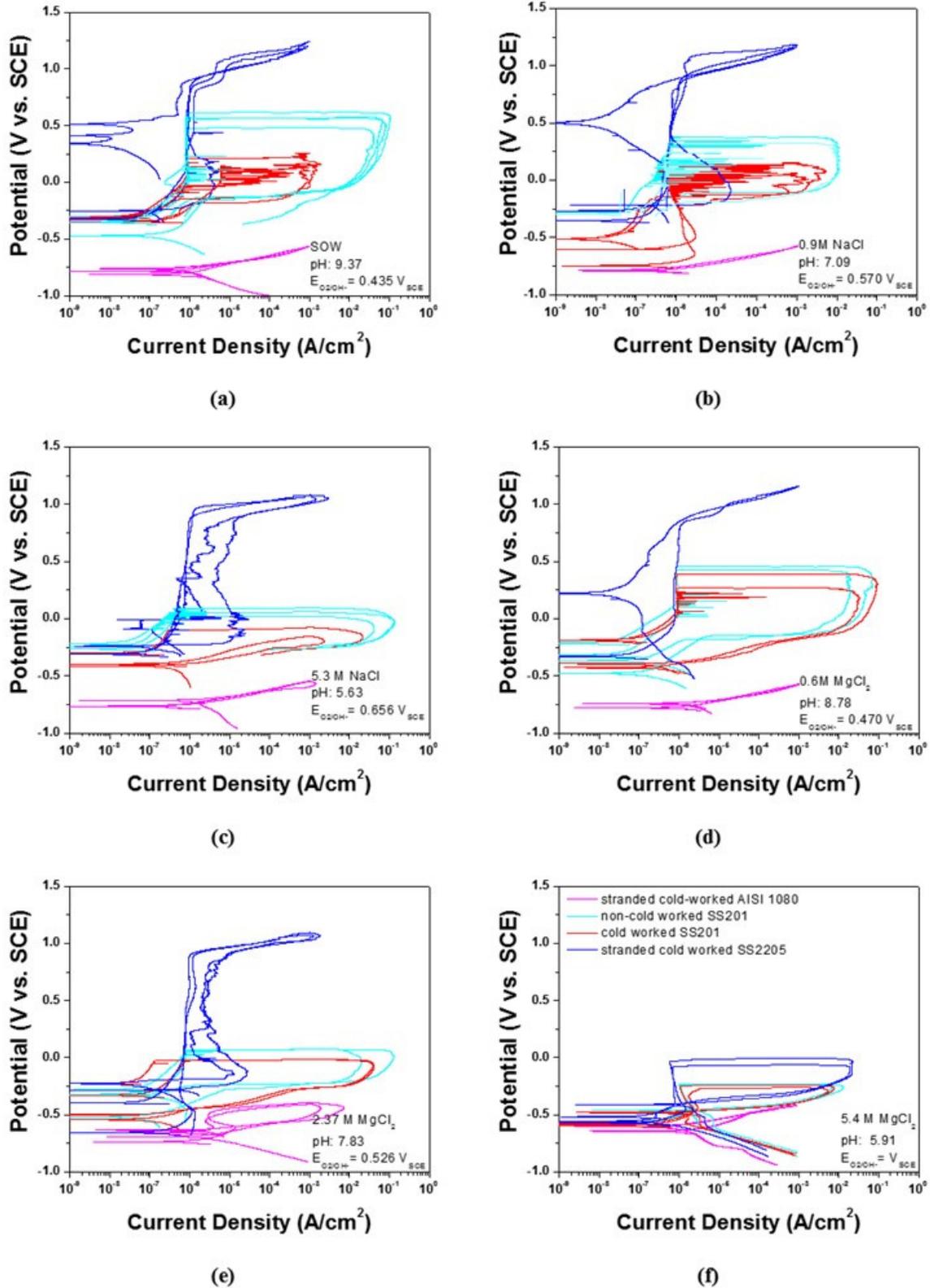
Figure B1. Cyclic Polarization Curves: Stranded Cold Worked AISI 1080, Non-Cold Worked 201 Austenitic Stainless, Cold Worked 201 Austenitic Stainless, and Stranded Cold Worked 2205 Duplex Stainless Steels in Simplified Ocean Water: (a) 55 mM MgCl₂ + 420 mM NaCl; (b) 0.9 M NaCl; (c) 5.3 M NaCl; (d) 0.6 M MgCl₂; (e) 2.37 M MgCl₂; (f) 5.4 M MgCl₂
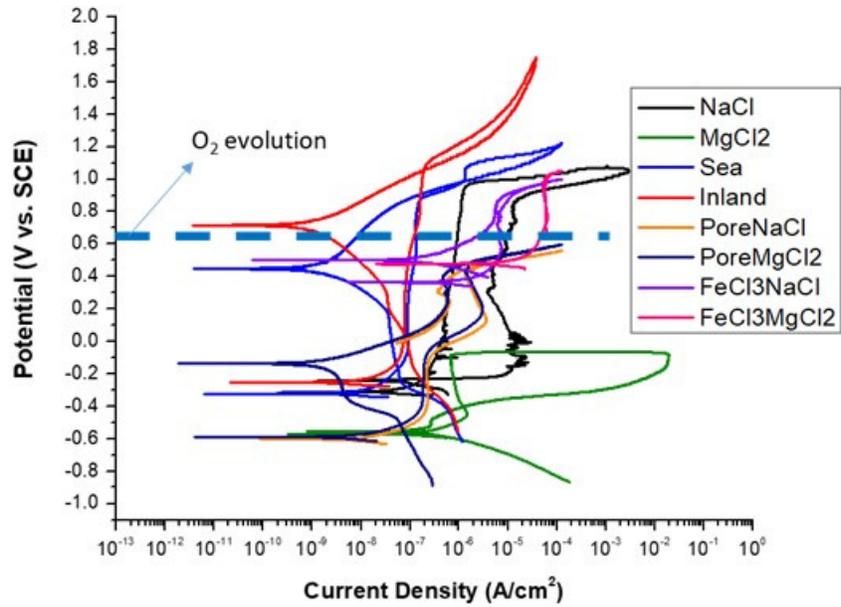
Figure B2. Cyclic Polarization at 25 °C Showing Effect of Various Electrolytes on Electrochemical Behavior of SCW2205 Steel
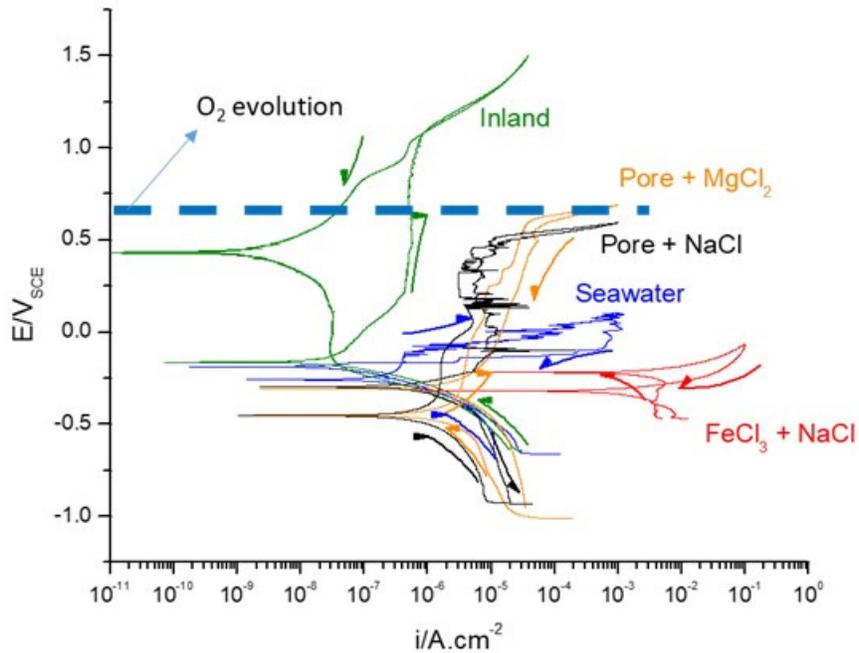
Figure B3. Cyclic Polarization at 25 °C for CW201 Steel Material
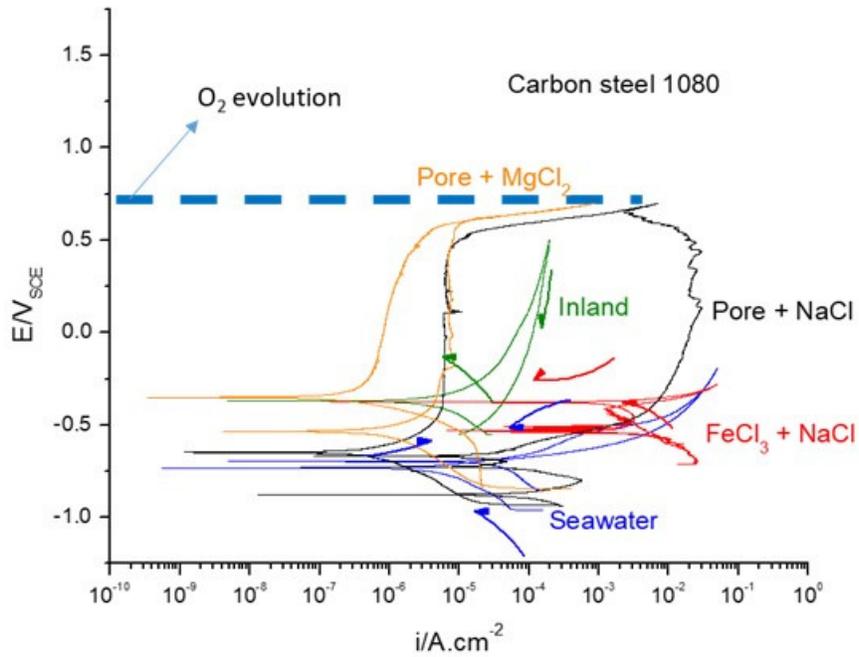
Figure B4. Cyclic Polarization at 25 °C for SCW1080 Steel
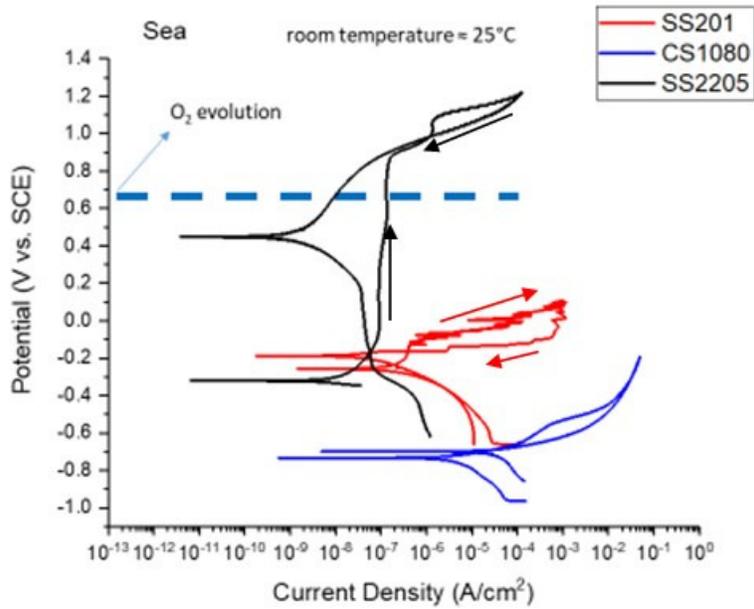
Figure B5. Cyclic Polarization at 25 °C for All Materials in Artificial Seawater
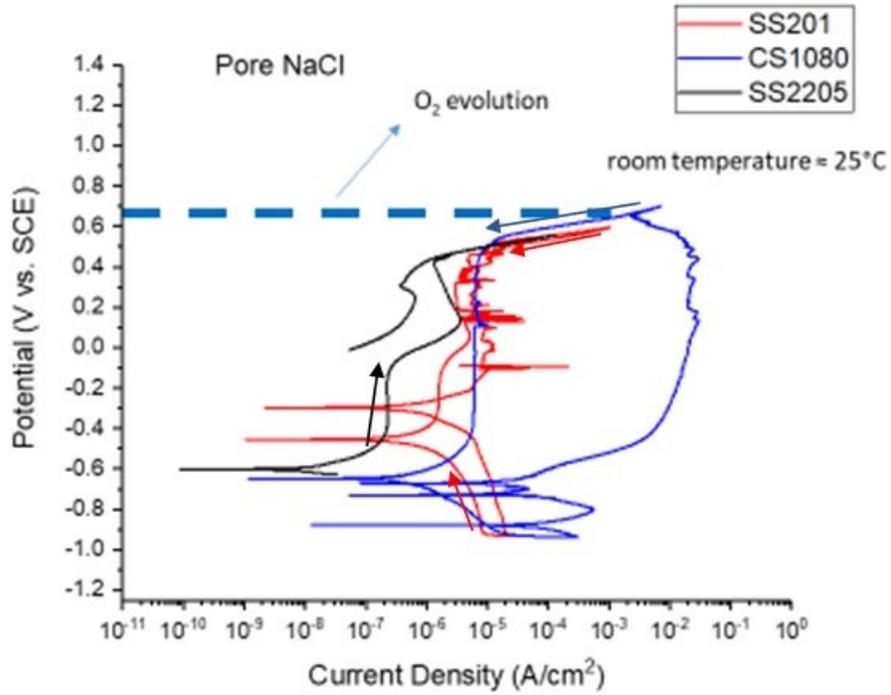
Figure B6. Cyclic Polarization at 25 °C for All Materials in Pore Solution Saturated With NaCl
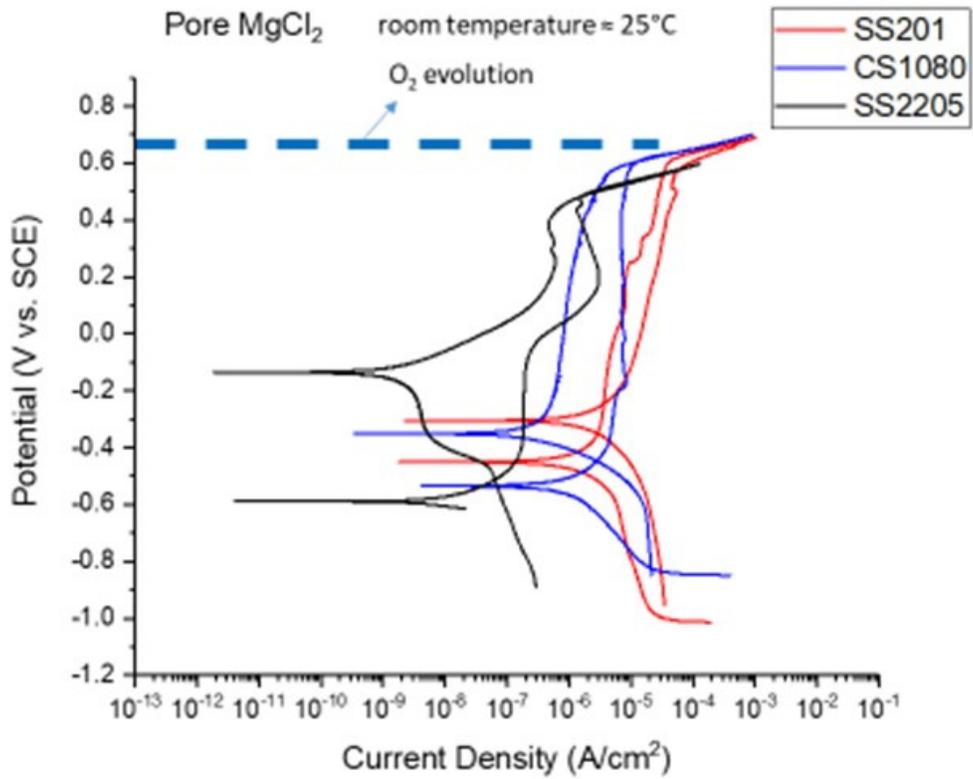
Figure B7. Cyclic Polarization at 25 °C for All Materials in Pore Solution Saturated With MgCl₂
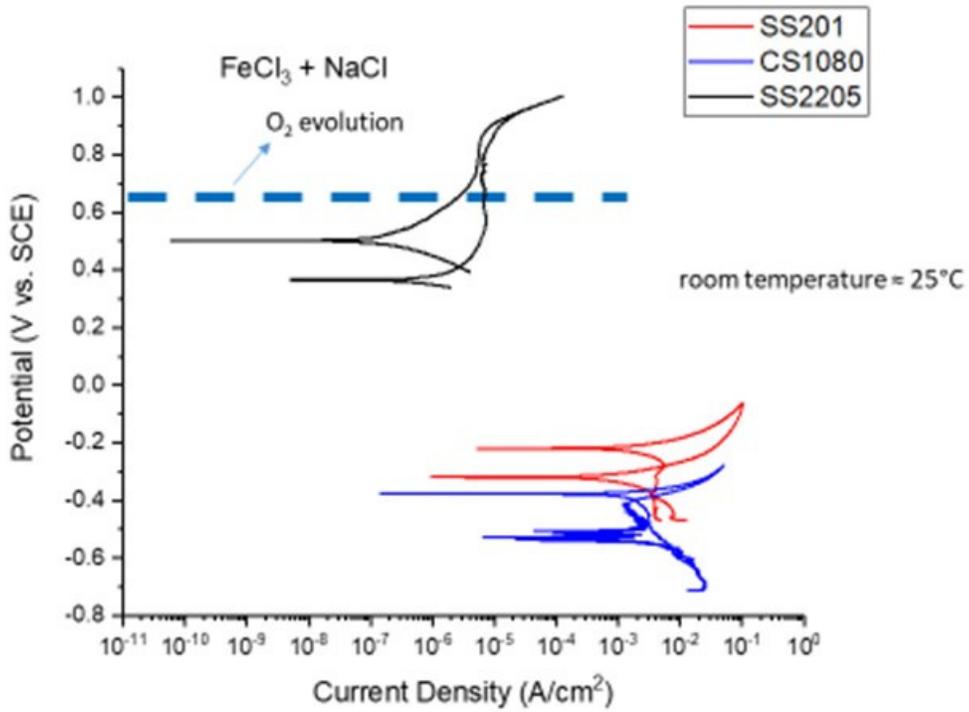
Figure B8. Cyclic Polarization at 25 °C for All Materials in FeCl₃ + NaCl Solution
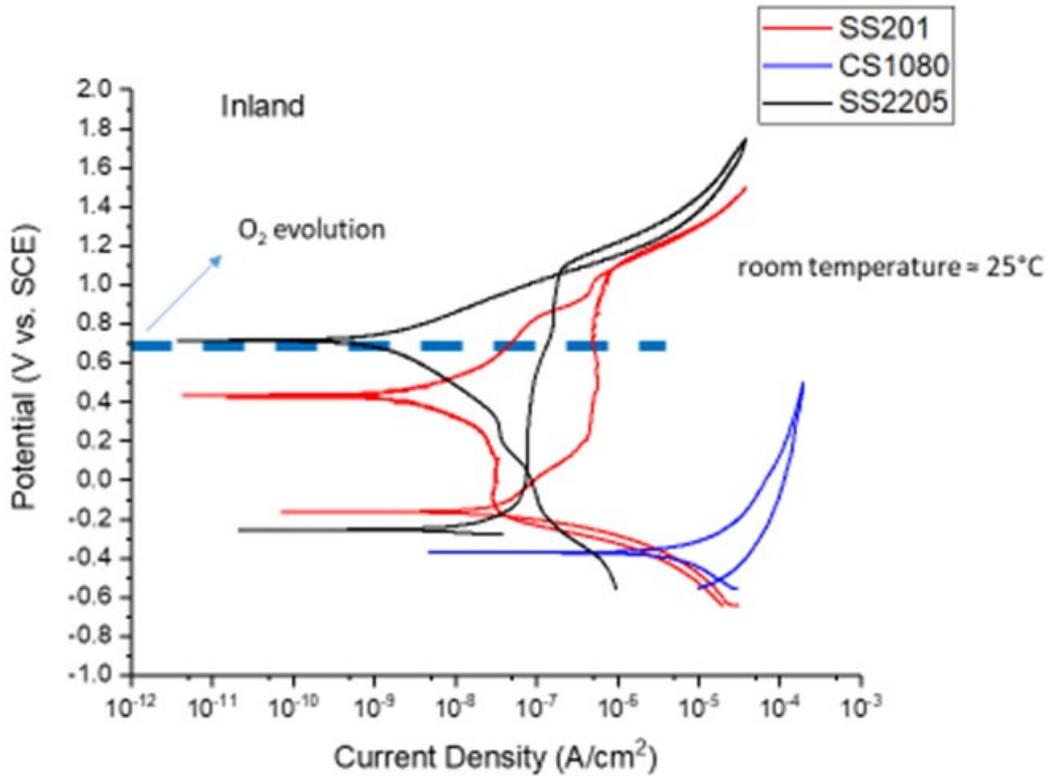
Figure B9. Cyclic Polarization at 25 °C for All Materials in Solution Simulating Inland Exposure
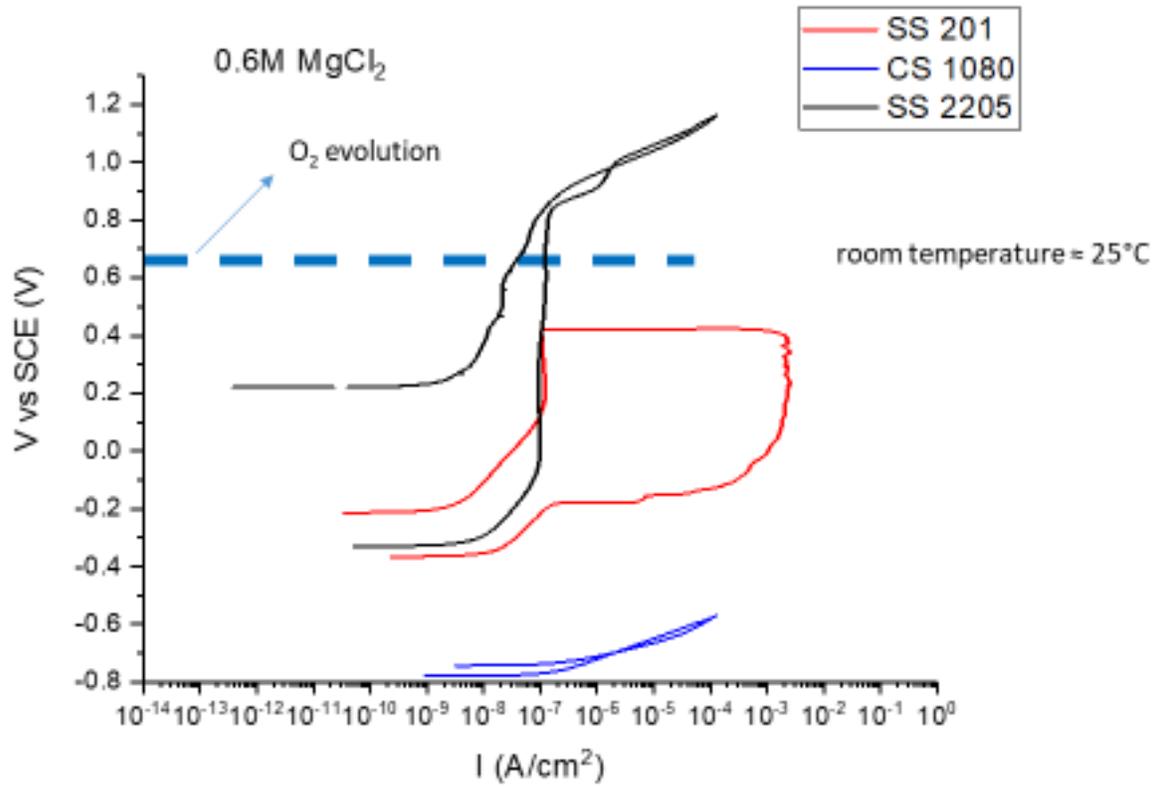
Figure B10. Cyclic Polarization at 25 °C for All Materials in 0.6 M MgCl₂ Solution
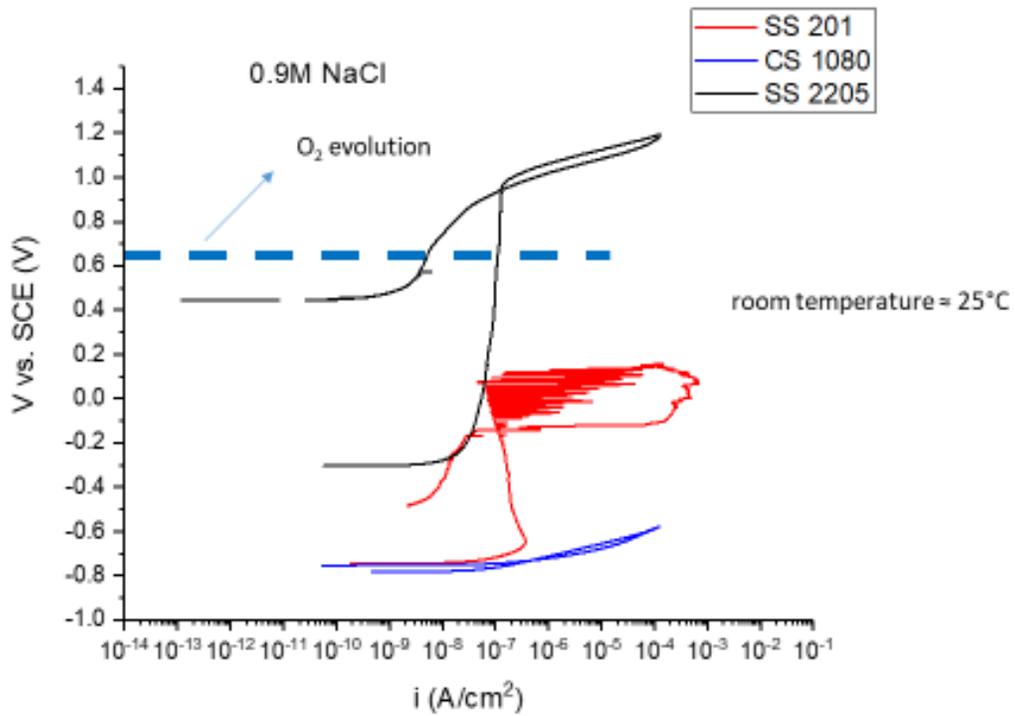
Figure B11. Cyclic Polarization at 25 °C for All Materials in 0.9 M NaCl Solution
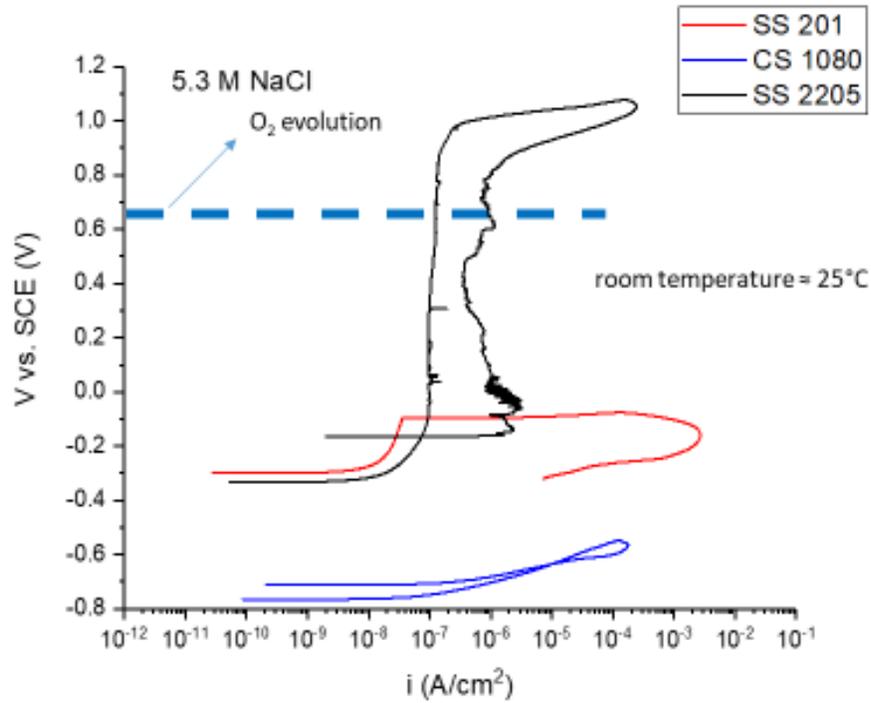
Figure B12. Cyclic Polarization at 25 °C for All Materials in 5.3 M NaCl Solution
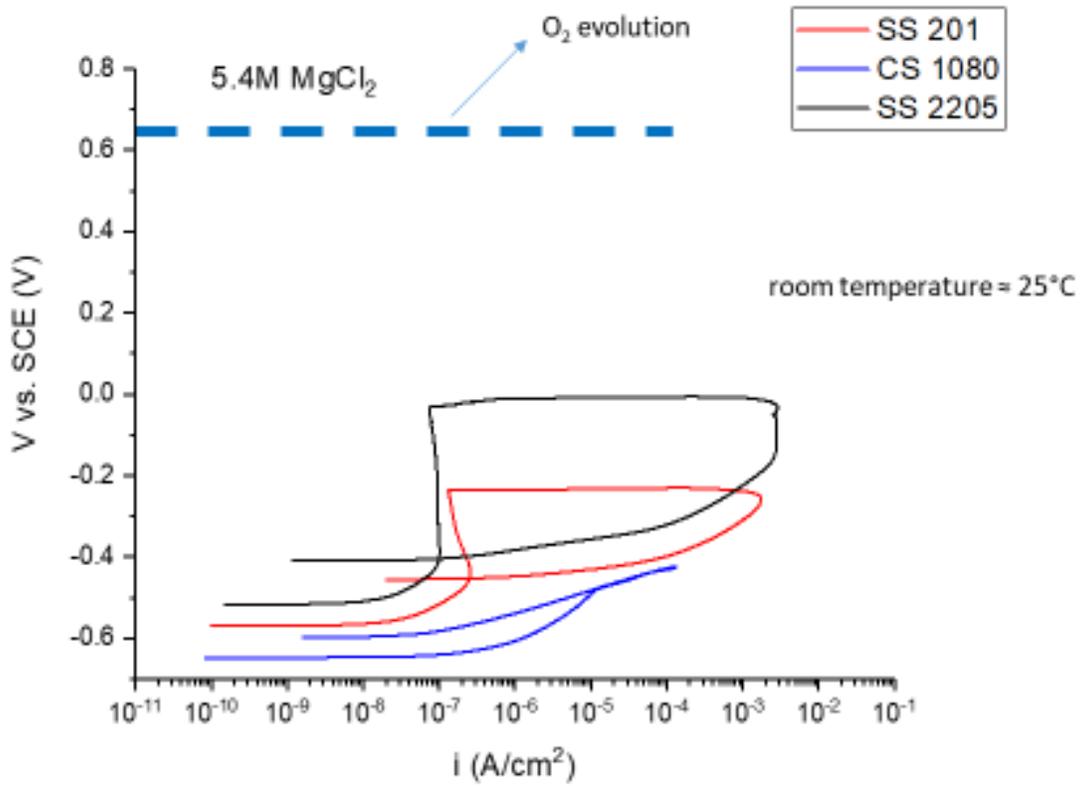
Figure B13. Cyclic Polarization at 25 °C for All Materials in 5.4 M MgCl₂ Solution
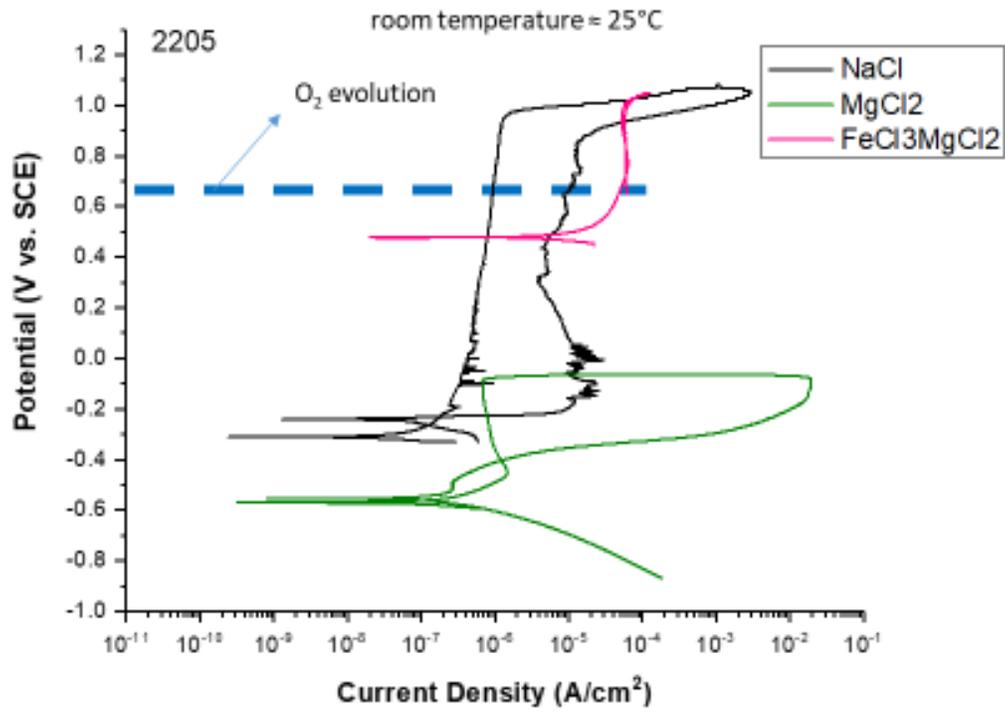
Figure B14. Cyclic Polarization at 25 °C for SCW2205 in 5.3 M NaCl, 5.4 M MgCl₂, and FeCl₃ + MgCl₂ Solutions

APPENDIX C

CORROSION MORPHOLOGY OF PIT GROWTH INTO A POLISHED SCW2205 STEEL SURFACE

Each image is for a sample that has been exposed to a droplet with a predetermined temperature and composition. The first number listed in the upper left of each figure is the constant exposure temperature and the abbreviation following the underscore is the composition of the droplet that was used to create the exposure environment.

Finding From These Data

- Pitting would be unlikely in an environment such as intact concrete with NaCl or in cracked concrete but might occur in a bare SCW2205 steel in severe wetting and drying environments containing a severe oxidizer.
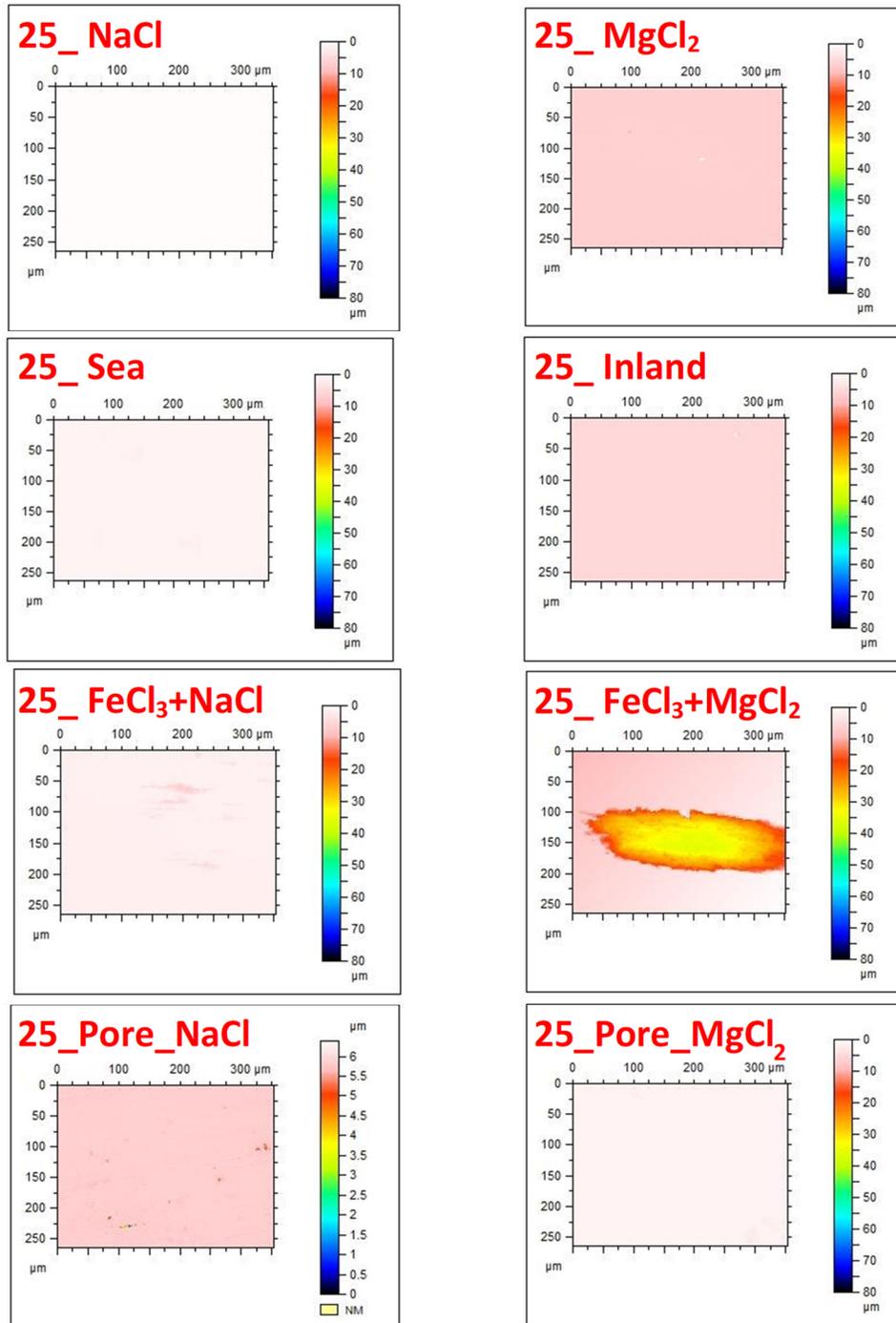
Figure C1. Corrosion Morphology of Pits Grown on SCW2205 Steel at 25 °C Under Droplets of Various Environments. Each image first identifies in red in the upper left corner the temperature in Celsius, followed by an underscore, and then the exposure environment that was used for corrosion testing.
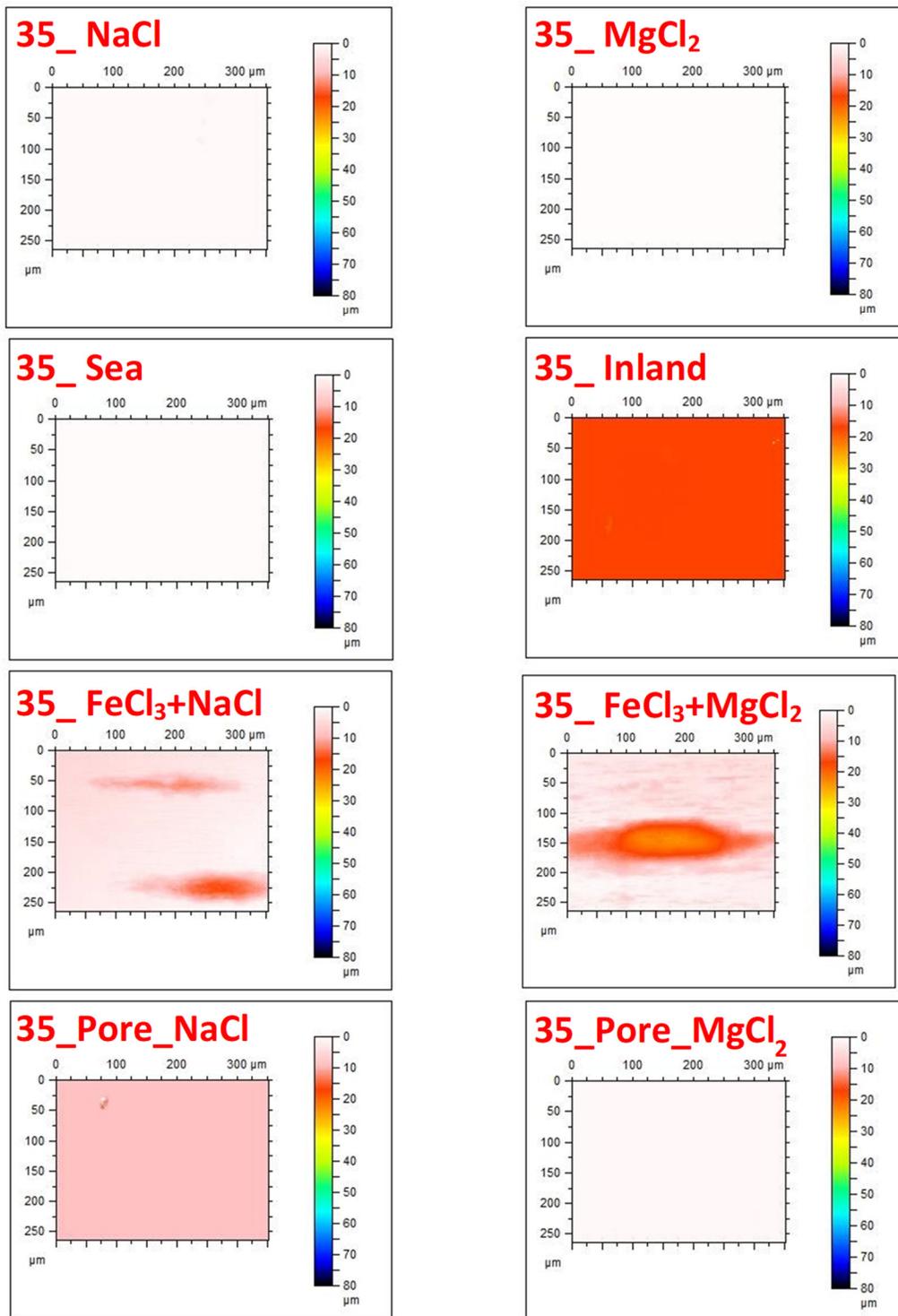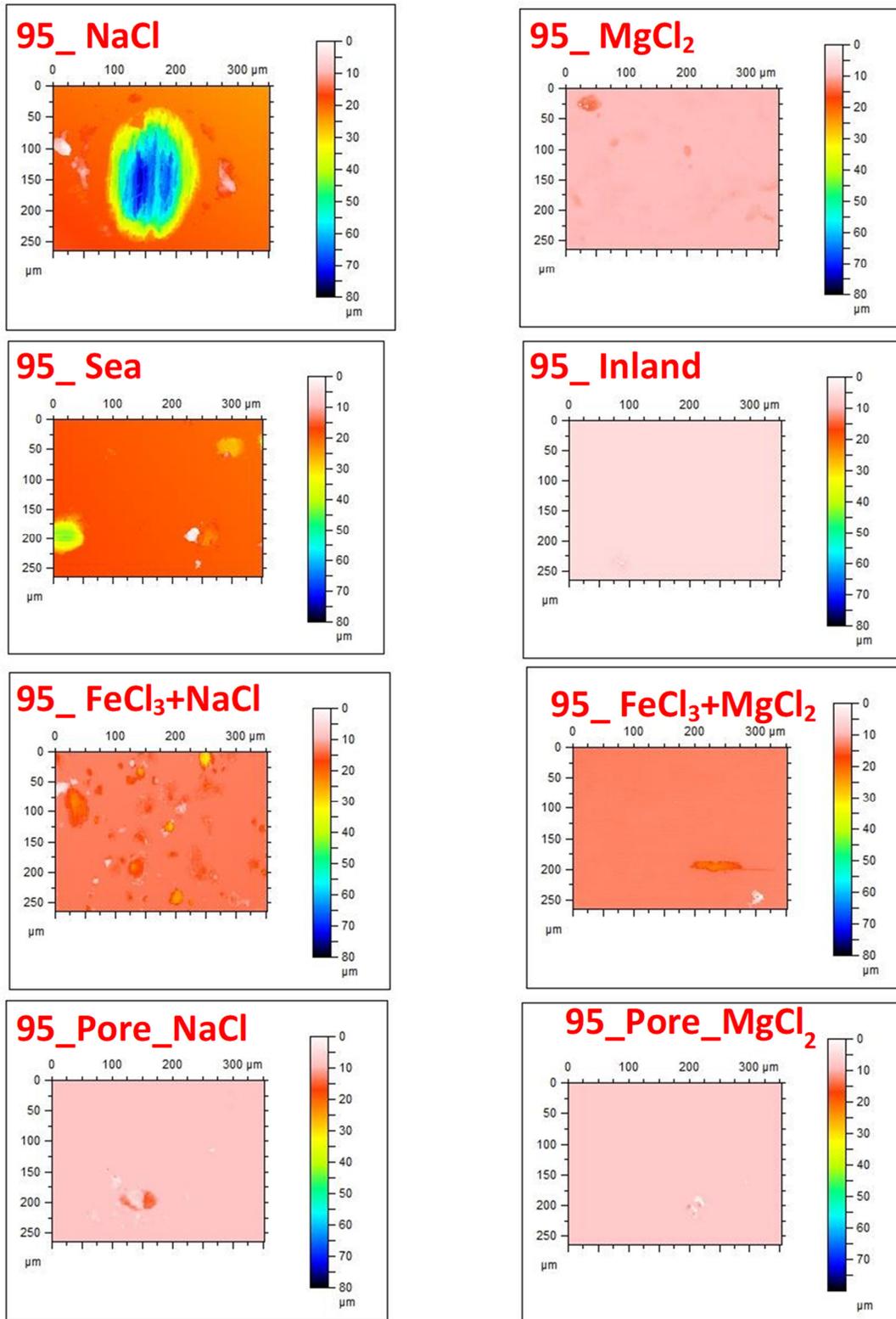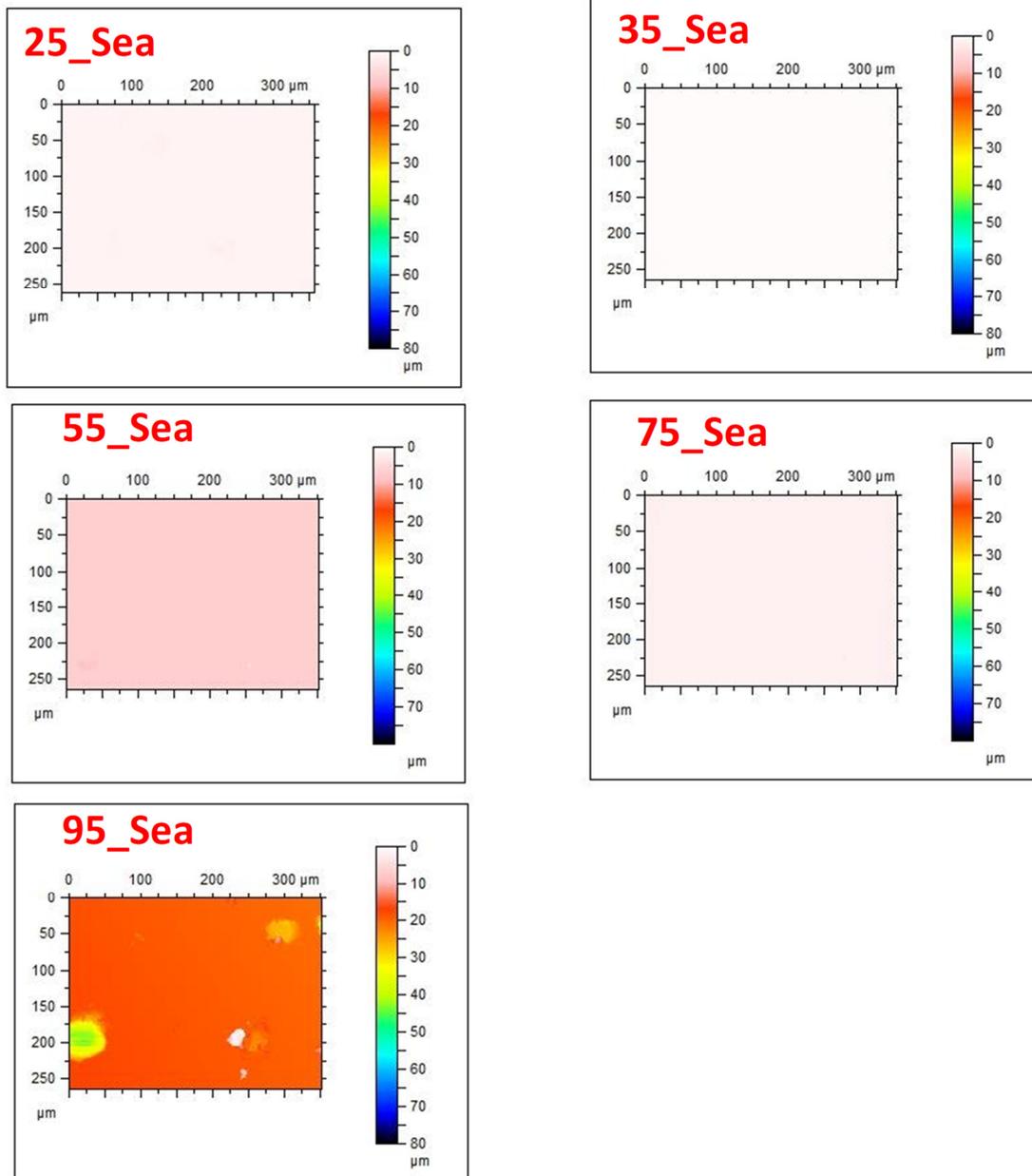
Figure C2. Corrosion Morphology of Pits Grown on SCW2205 Steel at 35 °C Under Droplets of Various Environments. Each image first identifies in red in the upper left corner the temperature in Celsius, followed by an underscore, and then the exposure environment that was used for corrosion testing.
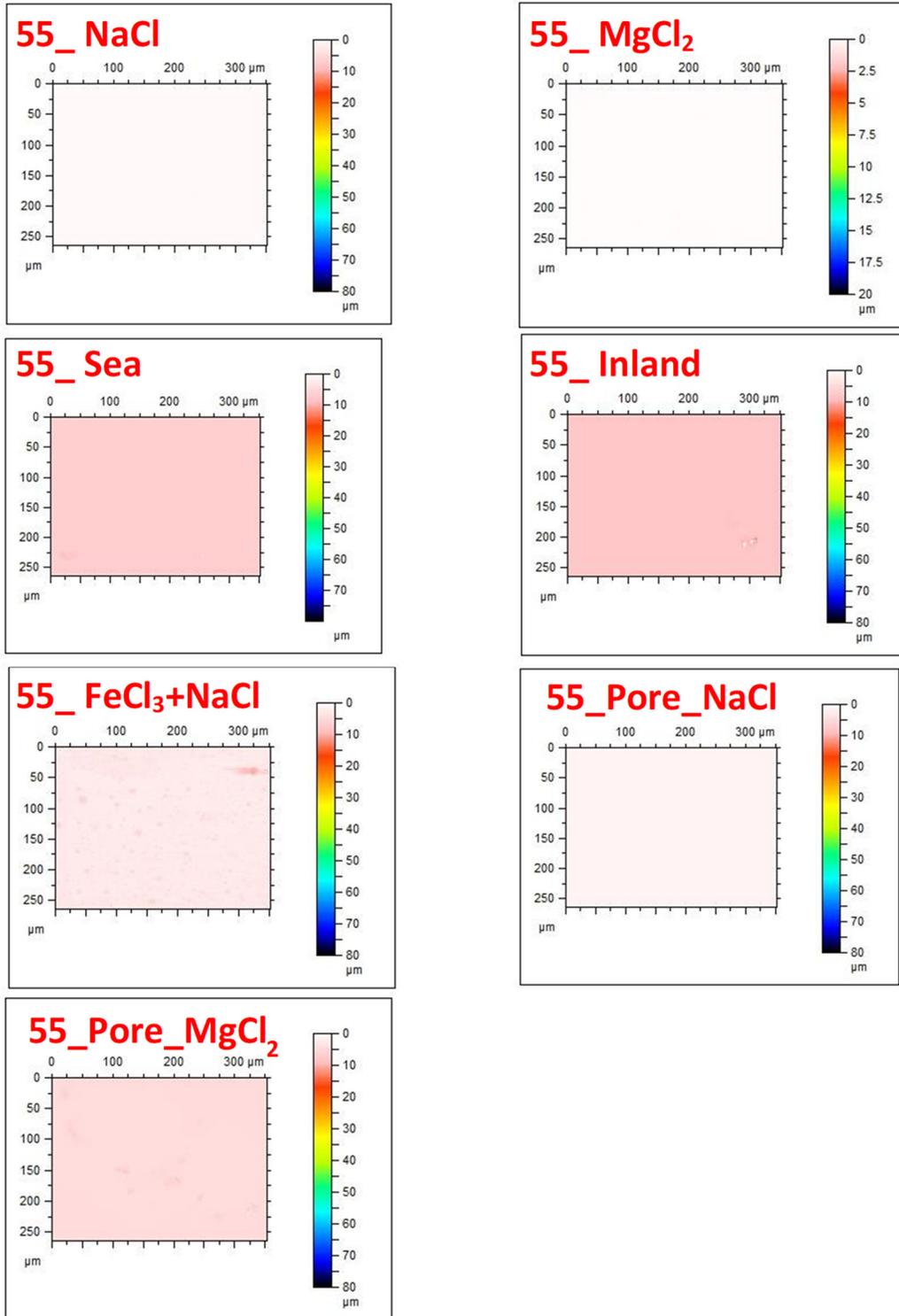
Figure C3. Corrosion Morphology of Pits Grown on SCW2205 Steel at 55 °C Under Droplets of Various Environments. Each image first identifies in red in the upper left corner the temperature in Celsius, followed by an underscore, and then the exposure environment that was used for corrosion testing.
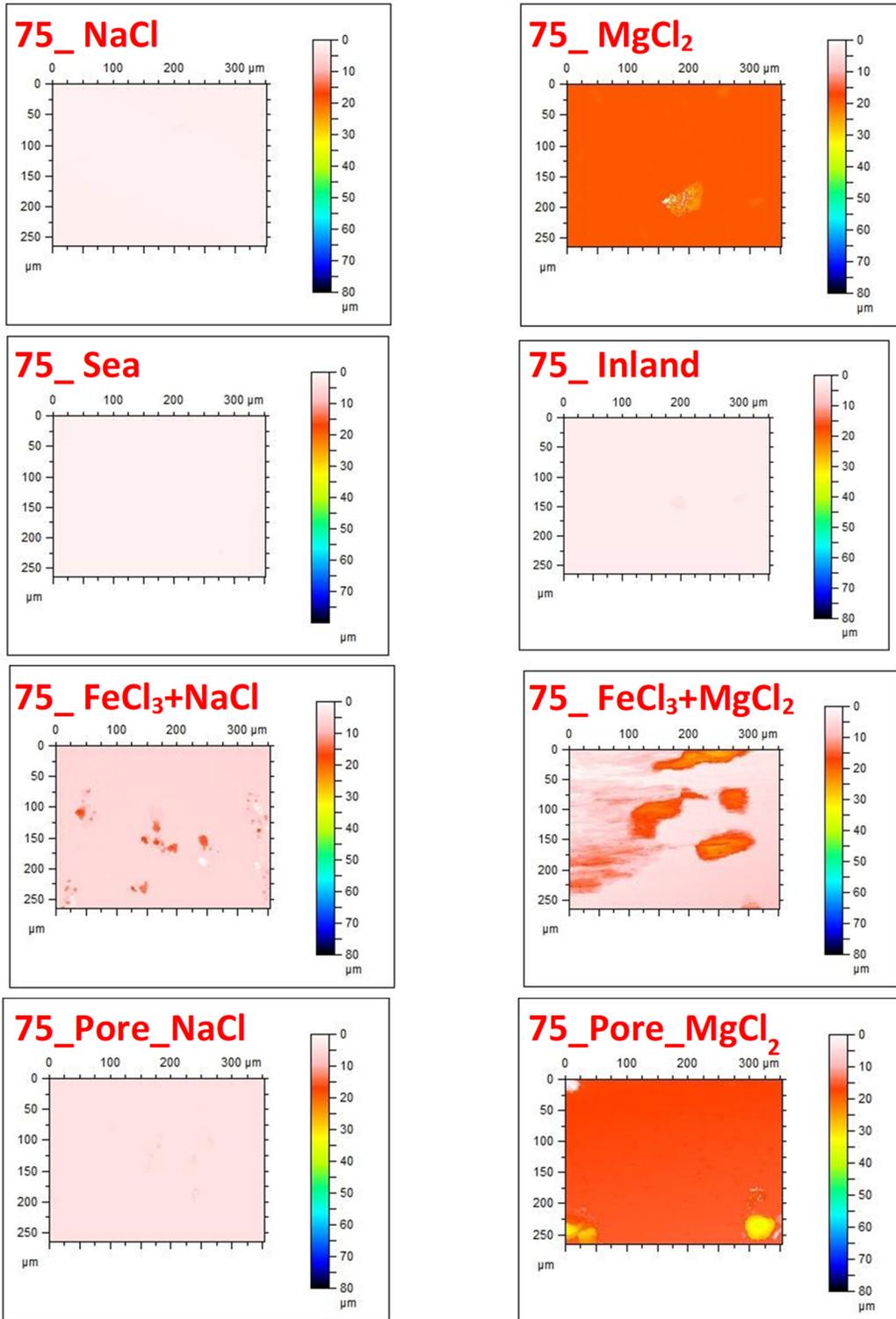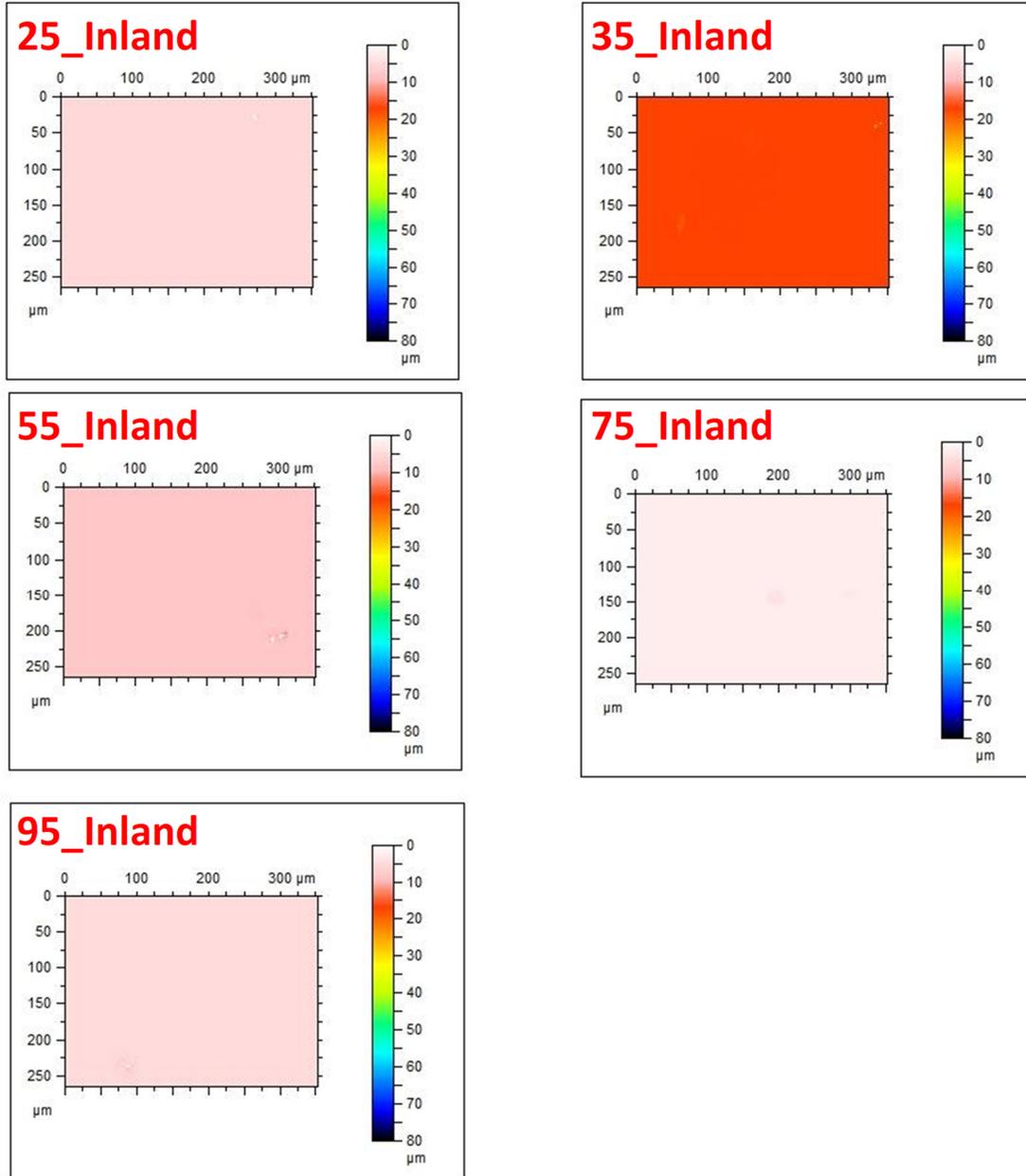
Figure C4. Corrosion Morphology of Pits Grown on SCW2205 Steel at 75 °C Under Droplets of Various Environments. Each image first identifies in red in the upper left corner the temperature in Celsius, followed by an underscore, and then the exposure environment that was used for corrosion testing.
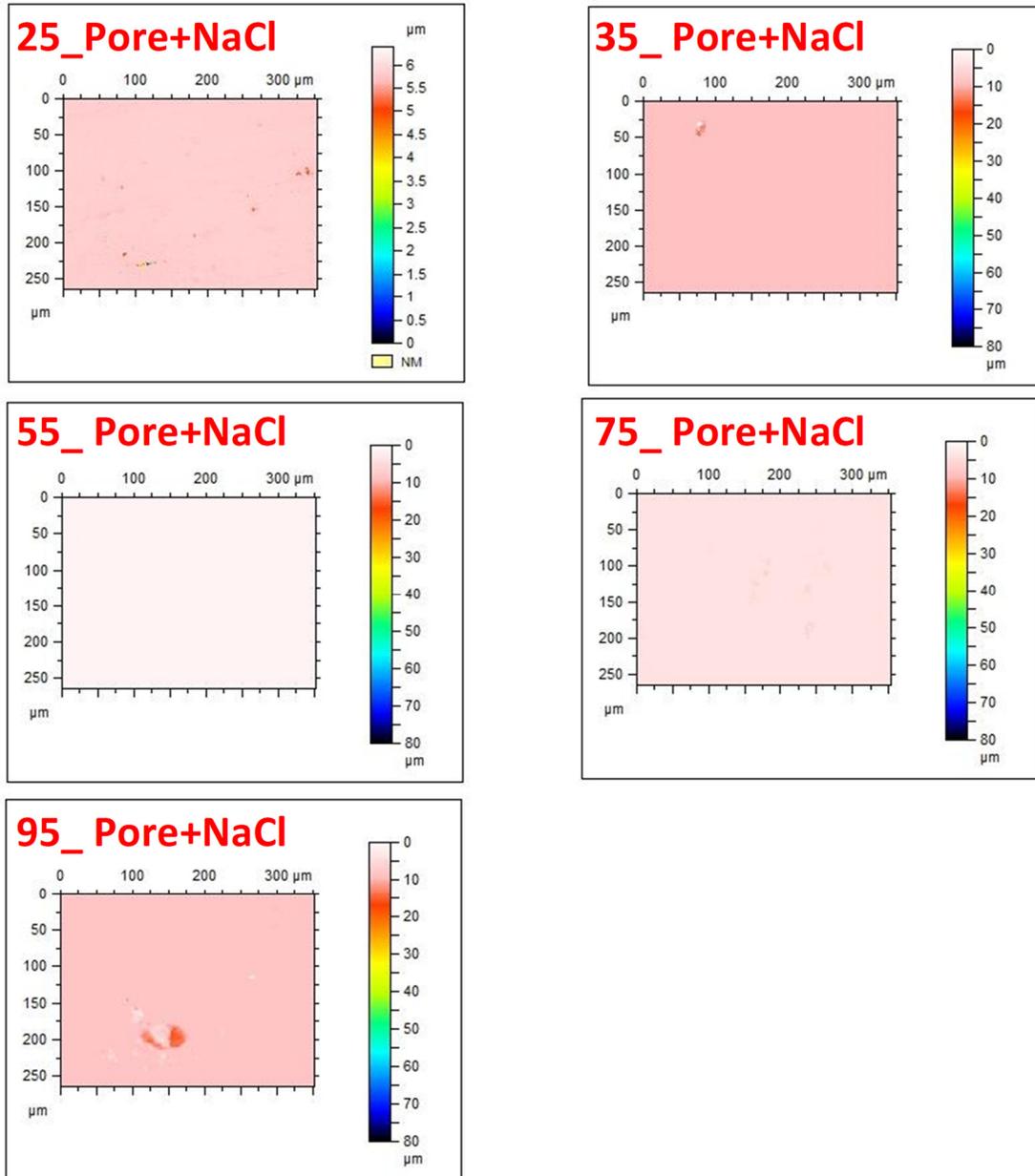
Figure C5. Corrosion Morphology of Pits Grown on SCW2205 Steel at 95 °C Under Droplets of Various Environments. Each image first identifies in red in the upper left corner the temperature in Celsius, followed by an underscore, and then the exposure environment that was used for corrosion testing.

Figure C6. Corrosion Morphology of Pits Grown on SCW2205 Steel Under Droplets of Artificial Seawater at Different Temperatures. Each image first identifies in red in the upper left corner the temperature in Celsius, followed by an underscore, and then the exposure environment that was used for corrosion testing.
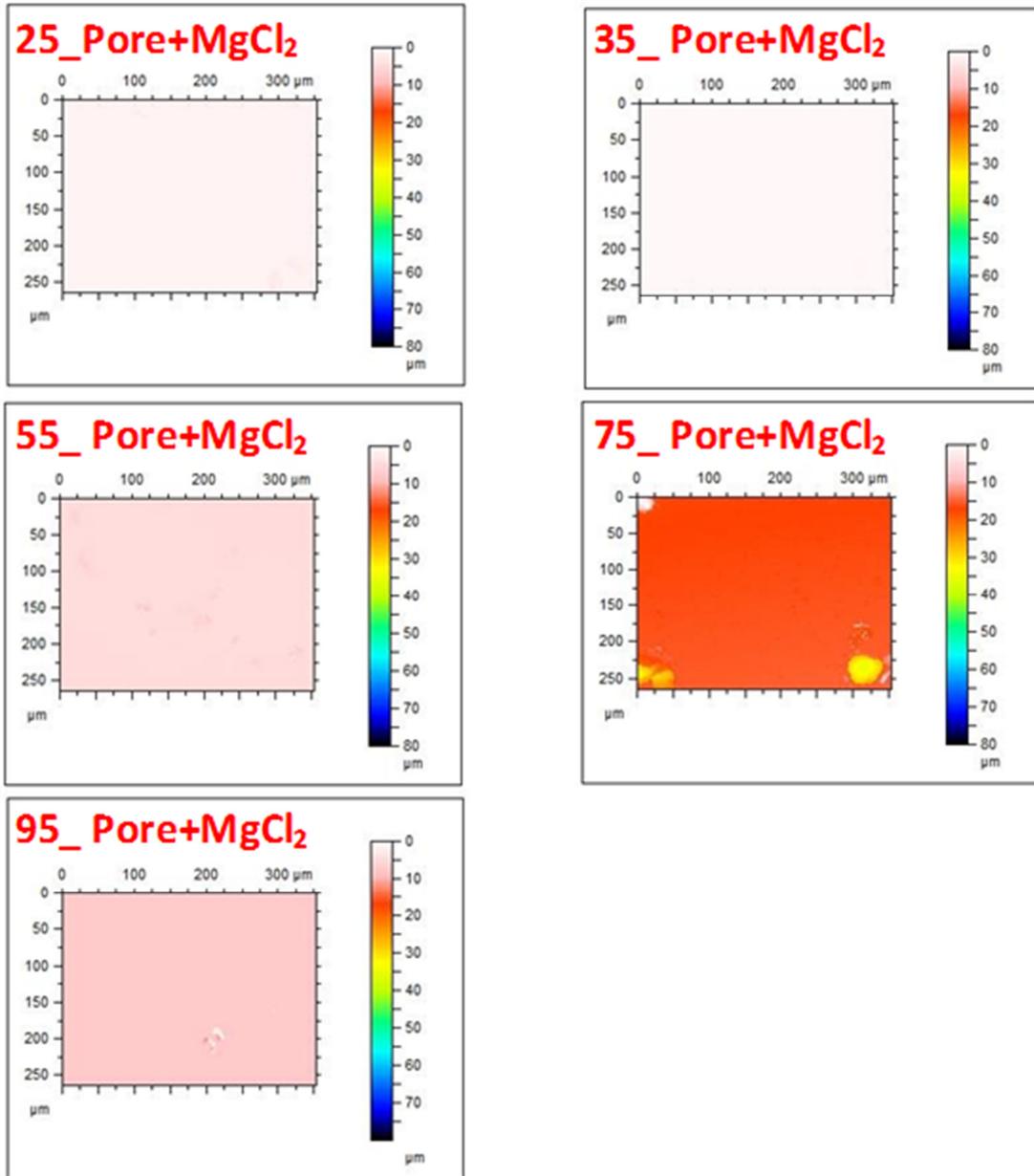
Figure C7. Corrosion Morphology of Pits Grown on SCW2205 Steel Under Droplets of Inland Environment ((NH$_4$)$_2$SO$_4$ + NaCl) Solution at Different Temperatures. Each image first identifies in red in the upper left corner the temperature in Celsius, followed by an underscore, and then the exposure environment that was used for corrosion testing.
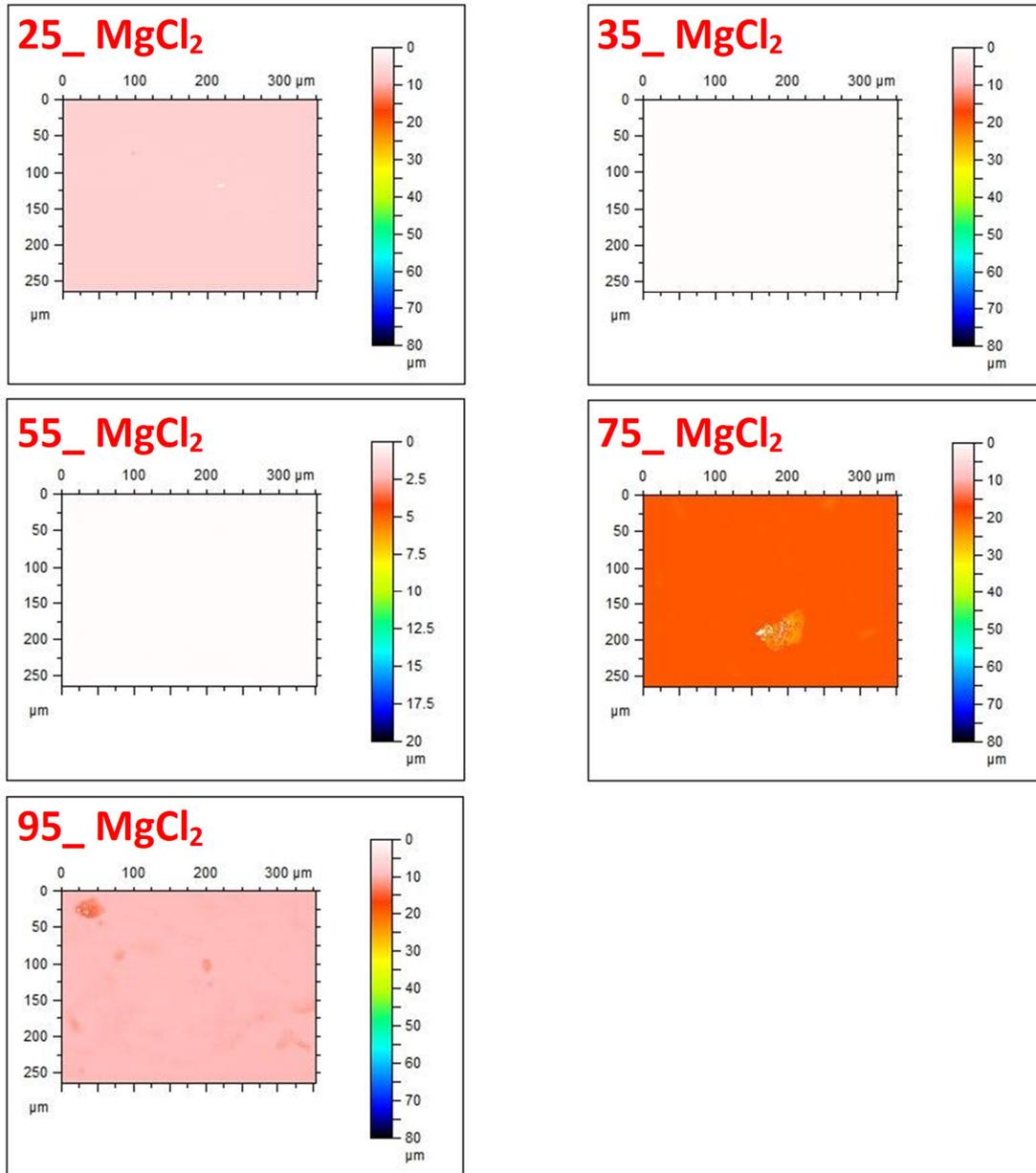
Figure C8. Corrosion Morphology of Pits Grown on SCW2205 Steel Under Droplets of Concrete Pore Environment With Added Saturated NaCl at Different Temperatures. Each image first identifies in red in the upper left corner the temperature in Celsius, followed by an underscore, and then the exposure environment that was used for corrosion testing.
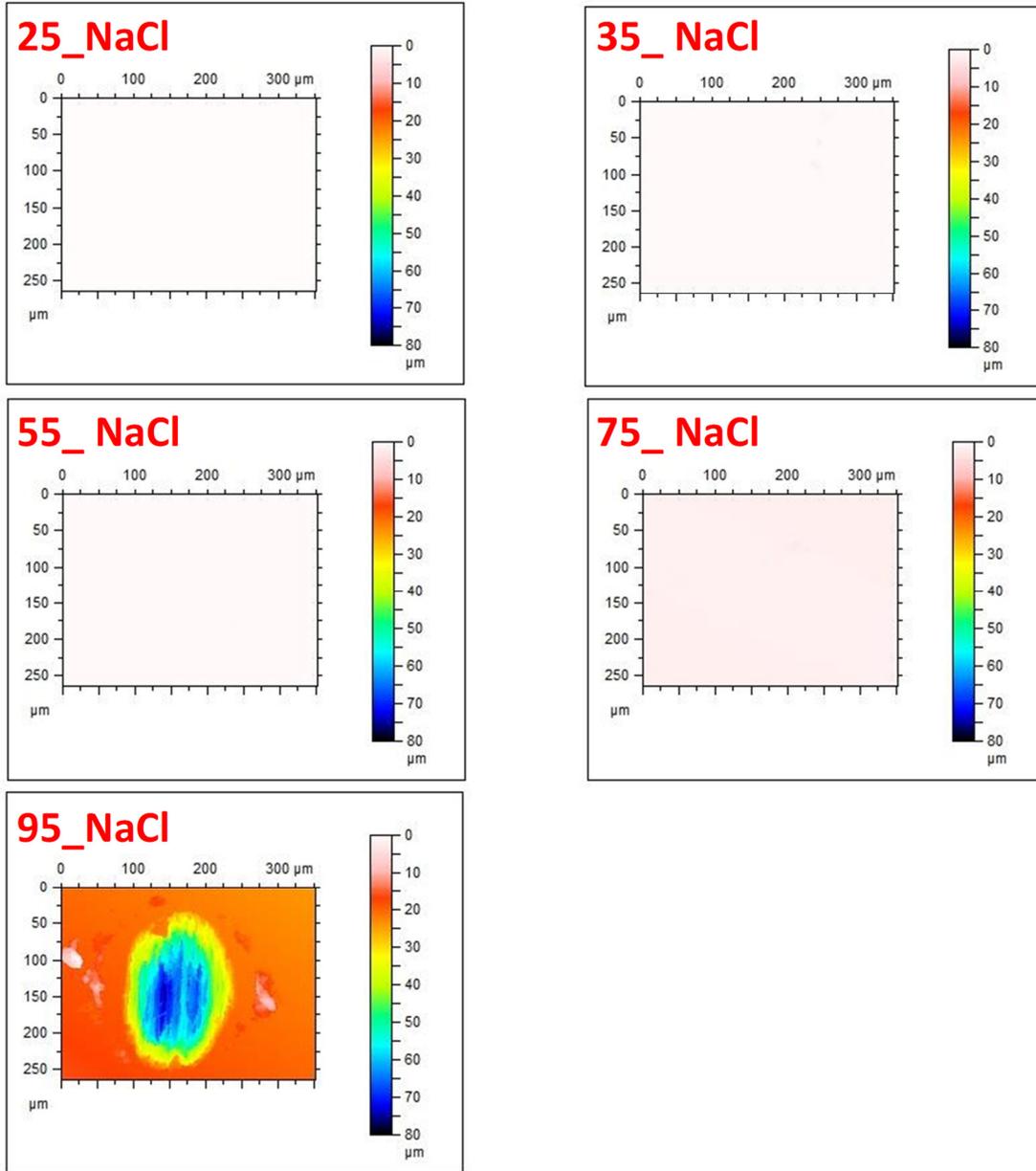
Figure C9. Corrosion Morphology of Pits Grown on SCW2205 Steel Under Droplets of Concrete Pore Environment With Added Saturated MgCl₂ at Different Temperatures. Each image first identifies in red in the upper left corner the temperature in Celsius, followed by an underscore, and then the exposure environment that was used for corrosion testing.

Figure C10. Corrosion Morphology of Pits Grown on SCW2205 Steel Under Droplets of Saturated MgCl₂ at Different Temperatures. Each image first identifies in red in the upper left corner the temperature in Celsius, followed by an underscore, and then the exposure environment that was used for corrosion testing.
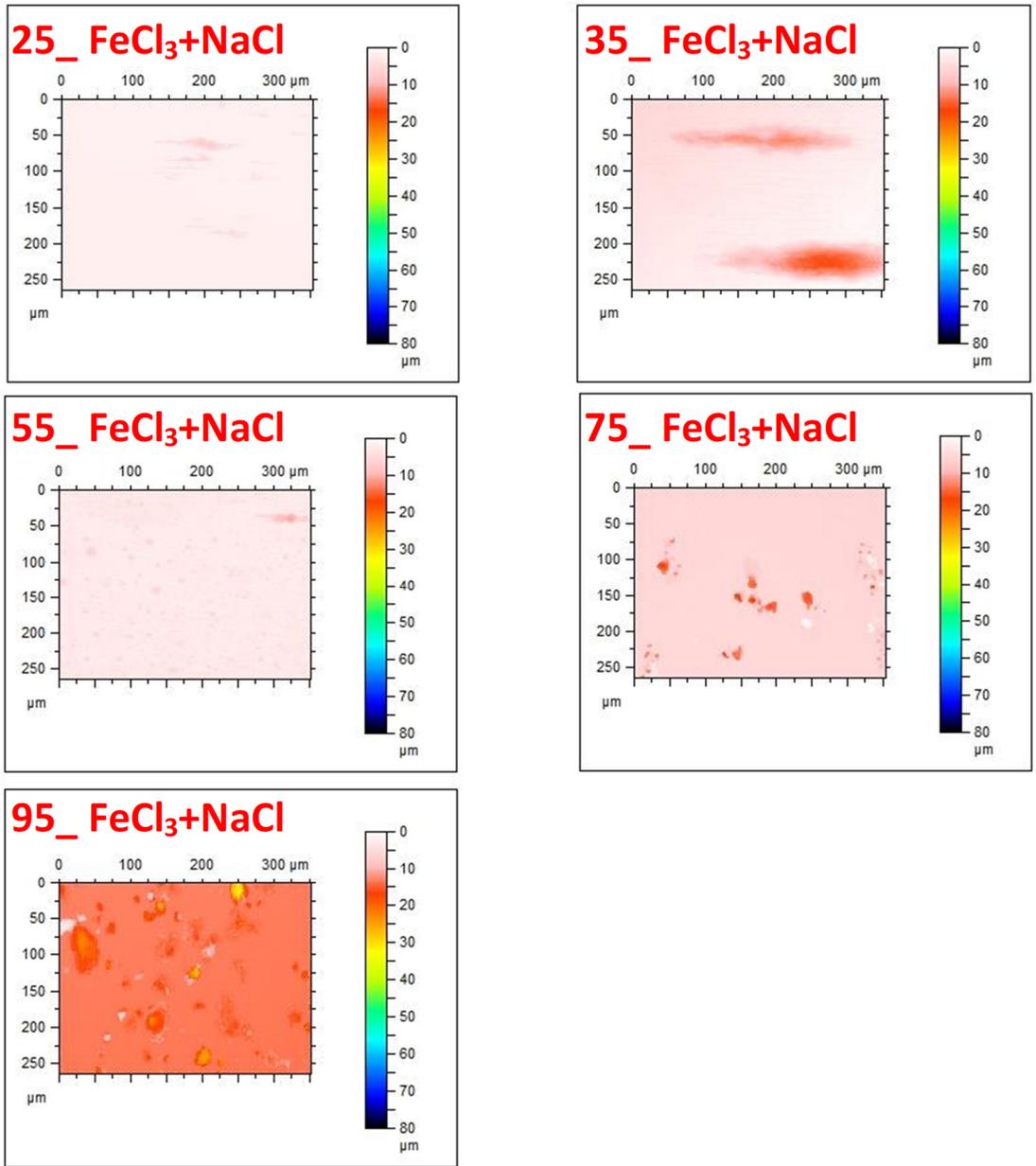
Figure C11. Corrosion Morphology of Pits Grown on SCW2205 Steel Under Droplets of Saturated NaCl at Different Temperatures. Each image first identifies in red in the upper left corner the temperature in Celsius, followed by an underscore, and then the exposure environment that was used for corrosion testing.
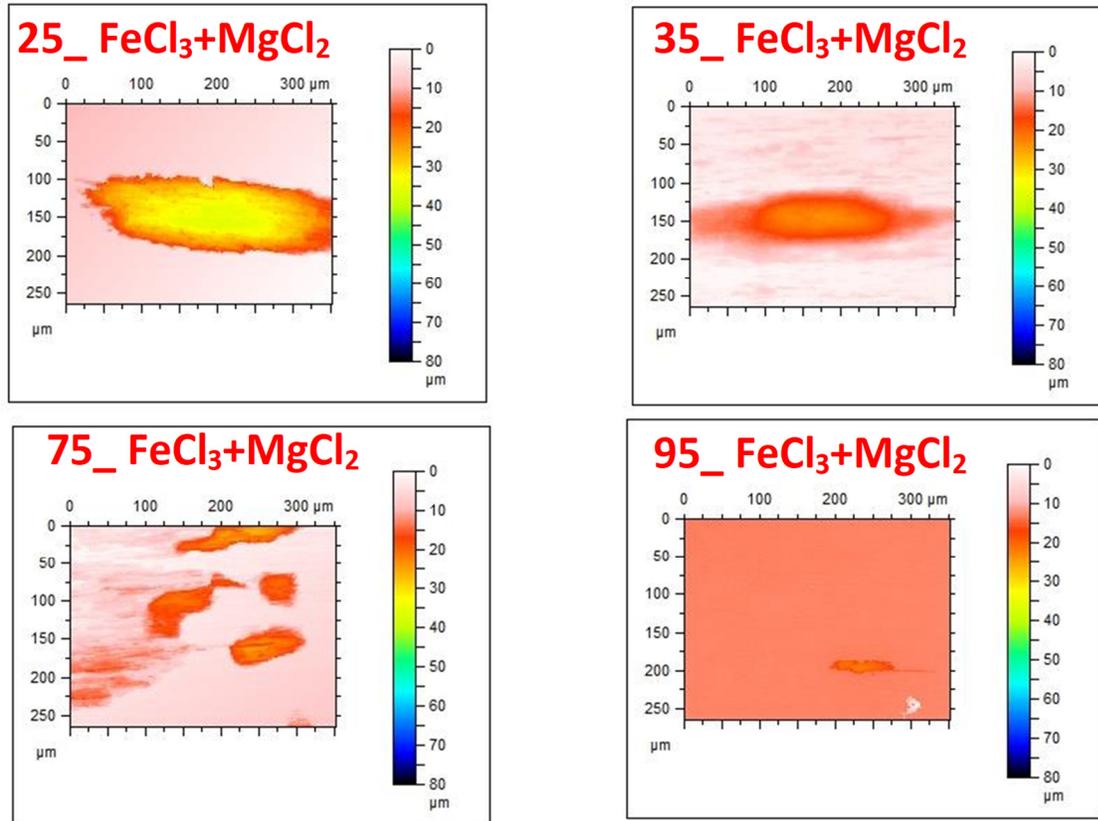
Figure C12. Corrosion Morphology of Pits Grown on SCW2205 Steel Under Droplets of FeCl₃ + NaCl at Different Temperatures. Each image first identifies in red in the upper left corner the temperature in Celsius, followed by an underscore, and then the exposure environment that was used for corrosion testing.

Figure C13. Corrosion Morphology of Pits Grown on SCW2205 Steel Under Droplets of FeCl$_3$ + MgCl$_2$ at Different Temperatures. Each image first identifies in red in the upper left corner the temperature in Celsius, followed by an underscore, and then the exposure environment that was used for corrosion testing.

OPTICAL IMAGES OF FOUR-POINT BEND TEST SAMPLES DURING TESTING IN CONTROLLED ENVIRONMENTS

t: 0 h (2.02 mg/cm^2)

t: 24 h

t: 48 h

t: 96 h

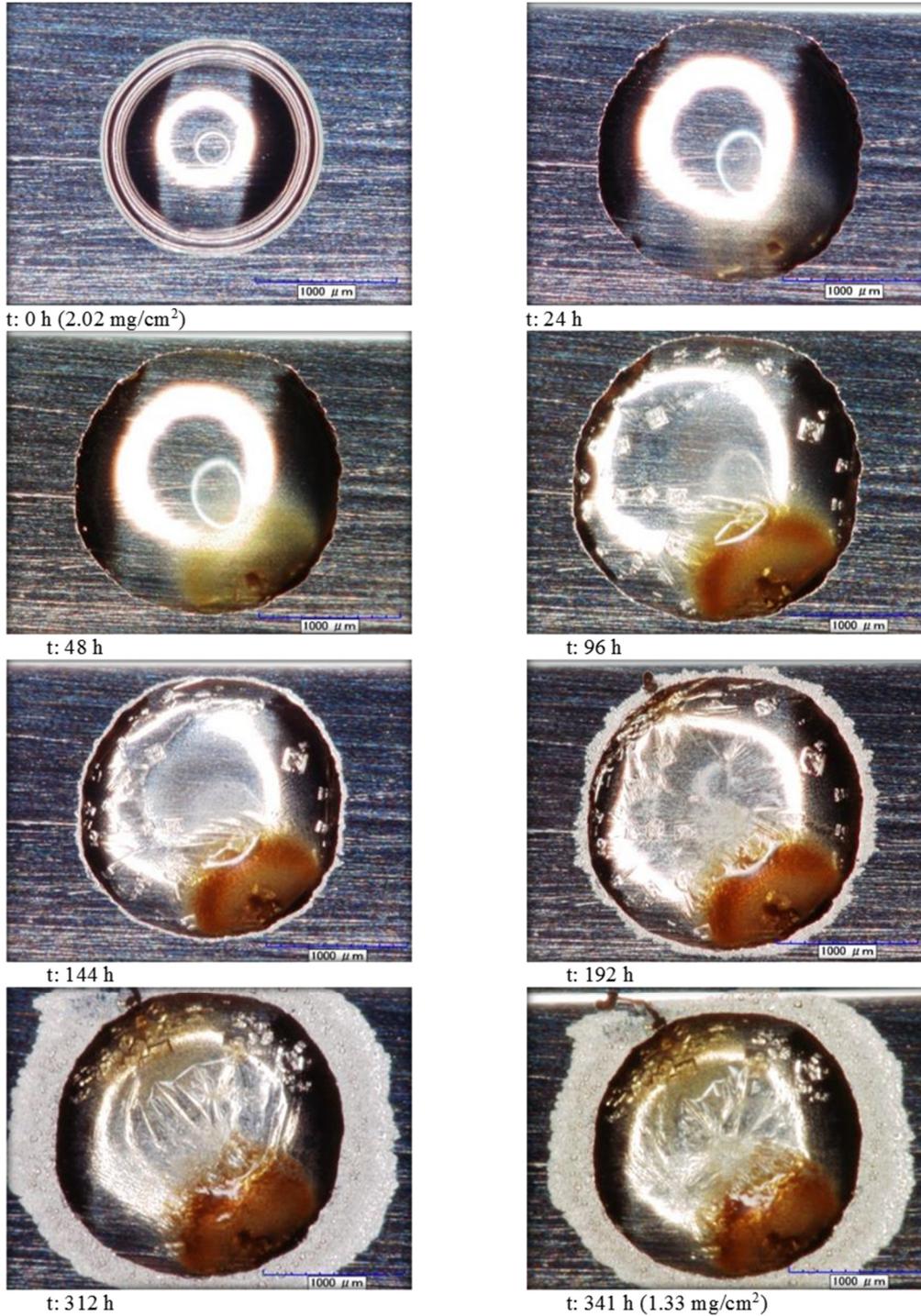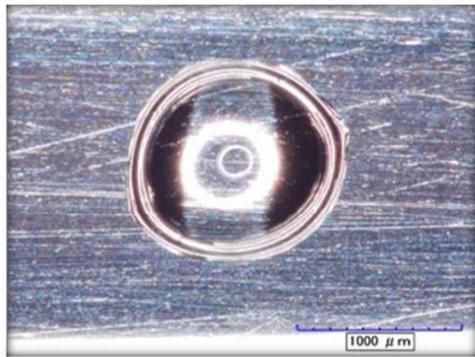t: 144 h

t: 192 h

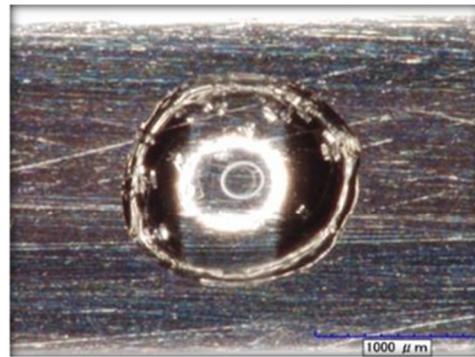t: 312 h

t: 341 h (1.33 mg/cm^2)

Figure D1. Optical Microscope Images of Same Droplet (initially 5.4 M MgCl$_2$) at 38 % RH and RT. Taken at 0, 24, 48, 96, 144, 192, 312, and 341 hr during four-point bend test experiments with the CW201 steel sample under an approximate stress of 970 MPa. RH = relative humidity; RT = room temperature.

t: 0 h

t: 341 h

Figure D2. Optical Microscope Images of Same Droplet (initially 5.4 M MgCl$_2$) at 38 % RH and RT. Taken at 0 and 341 hr during four-point bend test experiments with the SCW2205 steel sample under an approximate stress of 970 MPa. RH = relative humidity; RT = room temperature.

EDS RESULTS FROM CHARACTERIZING OBSERVED RUST STAIN AT SEVERAL LOCATIONS ON U-BEND SCW2205 STEEL FIELD EXPOSURE SAMPLE
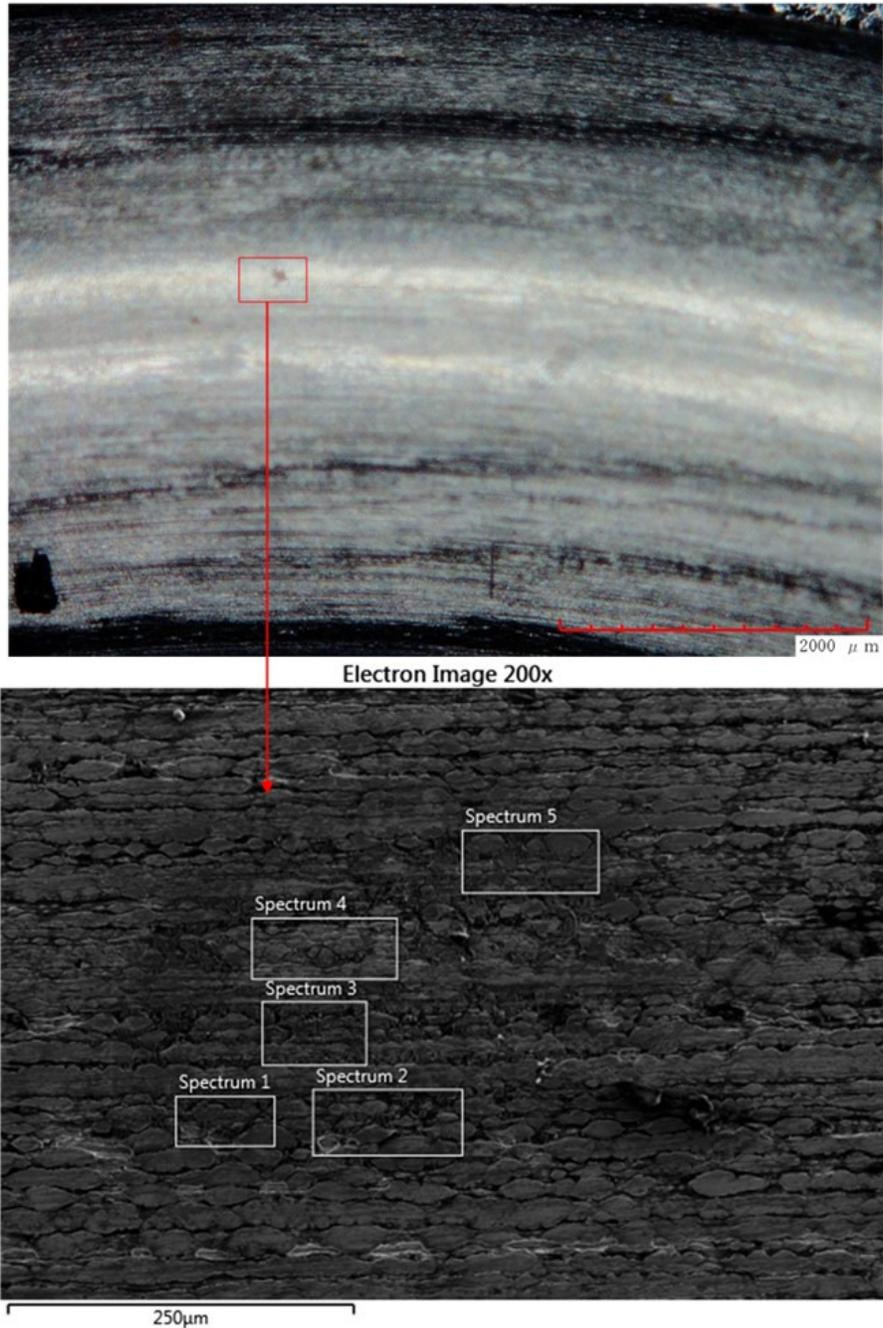

Figure E1. SCW2205 Steel Samples That Were Shown in Figure 16: top, optical image at a magnification of 50x of a SCW2205 steel U-bend sample with a spot on it; bottom, electron image of same area at a magnification of 200x provides four EDS sample locations shown in Figure E2. EDS = energy dispersive spectroscopy.
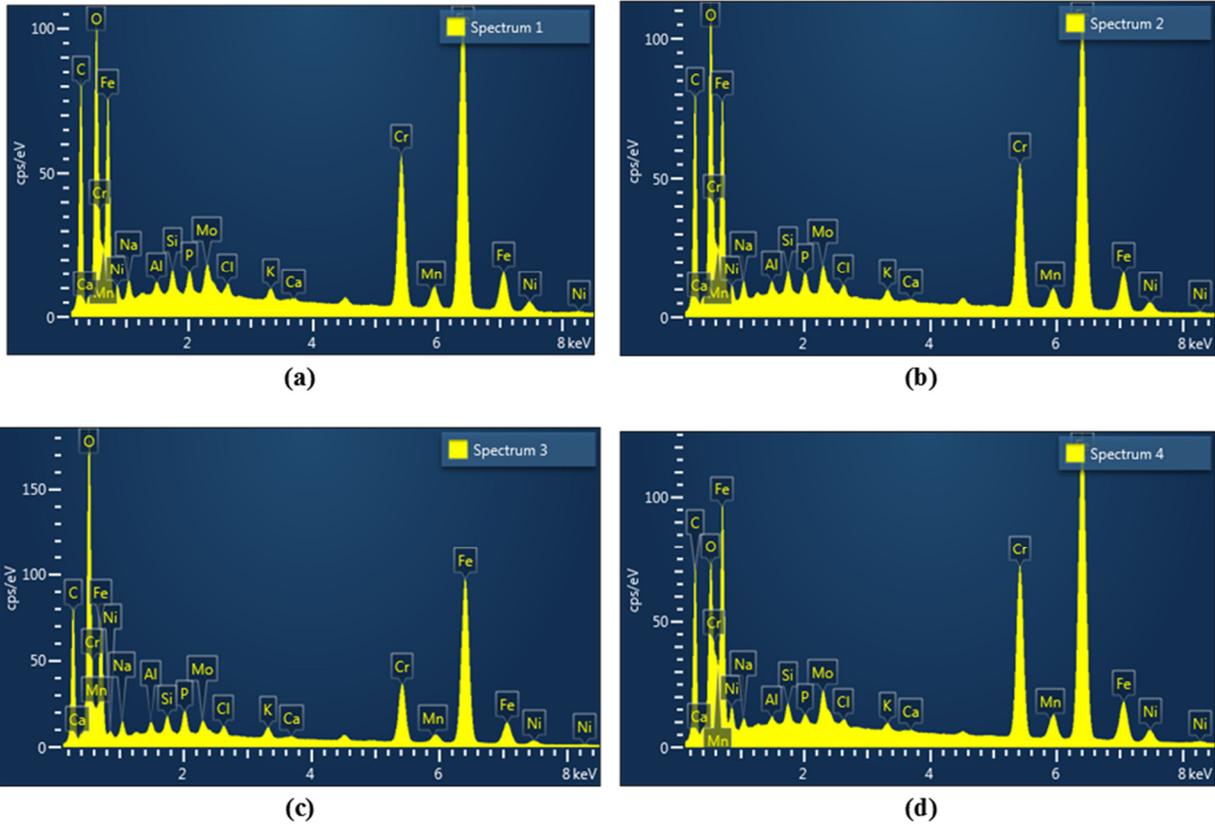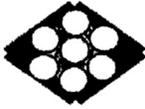
Figure E2. Evaluation Using EDS of Different Locations Shown in Figure E1. EDS = energy dispersive spectroscopy.

APPENDIX F

MILL REPORT FOR THE NIMMO PARKWAY BRIDGE STAINLESS STEEL PRESTRESSED CONCRETE STRANDS

SUMIDEN WIRE PRODUCTS CORPORATION

710 Marshall Stuart Drive   (615) 446-3199

Dickson, TN 37055   Fax (615) 740-1518

SWPC

*** MILL CERTIFICATE OF INSPECTION ***   PAGE 1 OF 1

ORDER NUMBER :   ISSUE DATE :   9/3/2013

COMMODITY : STAINLESS STEEL STRAND, UNCOATED SEVEN-WIRE
                  FOR PRESTRESSED CONCRETE

SPECIFICATION : ASTM A416-LATEST
                  SIZE 1/2" LOW RELAXATION

CUSTOMER : BAYSHORE CONCRETE PRODUCTS

P.O.NUMBER :

MANUFACTURER : SUMIDEN WIRE PRODUCTS CORPORATION

DESTINATION :

PACK NUMBER CERTIFIED :

| NO.	PACK#	HEAT#	GRADE (ksi)	B.S. (lb)	EL (%)	Y.P. (lb)	CURVE#	AREA (sq. in.)	ELASTIC MODULUS (M psi)
1	Pack #3	533311	250	38736	1.47	34686	pack #4	0.1527	24.5
2	Pack #6	533311	250	38736	1.47	34686	pack #4	0.1527	24.5
3	Pack #7	533311	250	38736	1.47	34686	pack #4	0.1527	24.5

Note: Total elongation under load does not meet the ASTM A416 section 6.4 minimum requirement of 3.5%

We hereby certify that:
* We have accurately carried out the inspection of commodity as described above in accordance with all applicable specification of the contract.

* The material described above will bond to concrete of a normal strength and consistency in conformance with the prediction equations for transfer and development length given in the ACI / AASHTO specifications.

Quality Assurance Section

75

Strain (in/in)
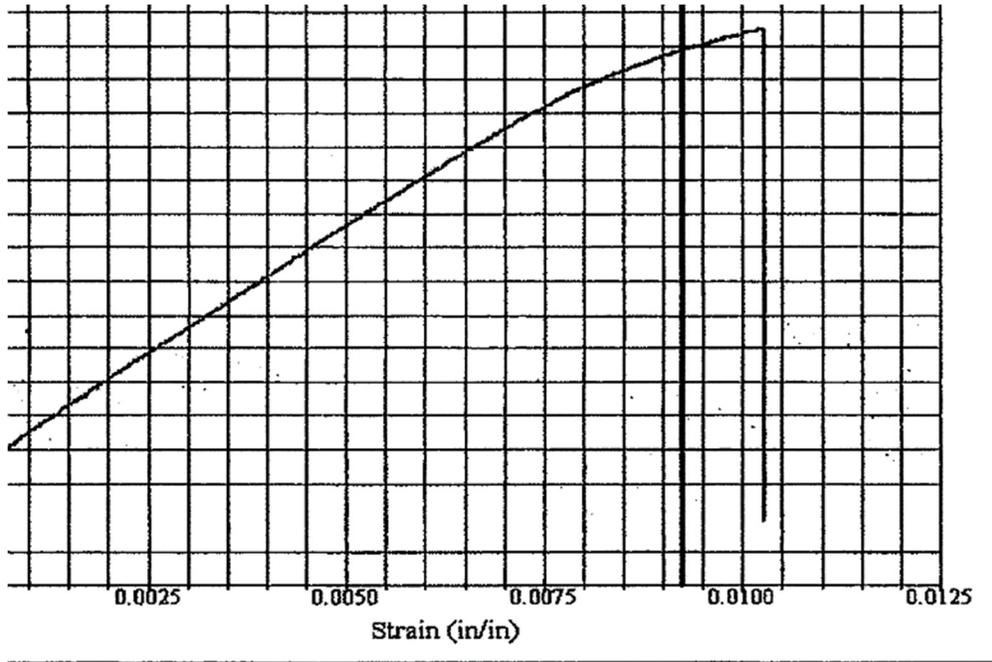
* Vertical Line is drawn at 1% Extension Under Load
* Tested to ASTM A1061 Standards

irve Number	**Pack #4**		
Size	**1/2"**		
Grade	**250k**		
Yield Point	**34,686**	**lbf**	
Actual Area	**0.1527**	**in²**	
ominal Area	**0.144**	**in²**	
ted Modulus	**24.5**	**Msi**	
Diameter OW 1	4.19	mm	
Diameter OW 2	4.18	mm	
Diameter OW 3	4.18	mm	
Diameter OW 4	4.18	mm	
Diameter OW 5	4.18	mm	
Diameter OW 6	4.18	mm	
Diameter CW	4.40	mm	
Date Tested	12/10/2012		
Tested By	Darryl		

SWPC

Approval

Curve Pack #4

Sumiden Wire Products Corporation

Relaxation Curve of PC Strand

Strand Size	0.50" x 250K	Initial Load	80% GUTS = 28,800lbf
Pack Number	SS Strand	Area in^2	0.1527
Heat Number		Relax % @ 1000hrs	1.00%
		Extrapolated from 200 hrs.	
Specification	ASTM A416		
		Tested by	Don Hiranaga
Test Method	ASTM E328	02/06/13-02/15/13	

Jack Toda Chief Engineer

Time (hours)

Relaxation (%)

1.00%

SUMIDEN WIRE PRODUCT